Towards embryonic scaffolds for regenerative medicine

Glycosaminoglycans, effector molecules and collagen

P.J.E. Uijtdewilligen

Towards embryonic scaffolds for regenerative medicine

Glycosaminoglycans, effector molecules and collagen

Peter Uijtdewilligen

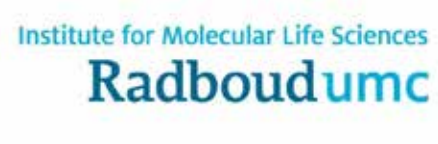

Research presented in this thesis was performed at the Department of Biochemistry, Radboud Institute for Molecular Life Sciences (RIMLS), formely known as Nijmegen Centre for Molecular Life Sciences, Radboud university medical centre, and funded by the Dutch Program for Tissue Engineering.

Towards embryonic scaffolds for regenerative medicine - Glycosaminoglycans, effector molecules and collagen

Uijtdewilligen, Peter Johannus Evert

Thesis, Radboud university medical centre, Nijmegen, The Netherlands

Cover image: mouse embryo at fourteen days post conception on a background of an artistic modification of a scanning electron microscopical picture of a type I collagen scaffold.

Cover design and lay-out: P.J.E. Uijtdewilligen

Printend by: Printservice Ede te Ede.

ISBN: 978-94-92896-00-1

Towards embryonic scaffolds for regenerative medicine

Glycosaminoglycans, effector molecules and collagen

Proefschrift

ter verkrijging van de graad van doctor
aan de Radboud Universiteit Nijmegen
op gezag van de rector magnificus prof. dr. J.H.J.M. van Krieken,
volgens besluit van het college van decanen
in het openbaar te verdedigen op maandag ***19 februari 2018***
om ***10.30*** uur precies

door

Peter Johannus Evert Uijtdewilligen

geboren op 5 augustus 1980
te Utrecht

Promotor

Prof. dr. R.E. Brock

Copromotoren

Dr. A.H.M.S.M. van Kuppevelt

Dr. ir. W.F. Daamen

Manuscriptcommissie

Prof. dr. W.F.J. Feitz (voorzitter)

Prof. dr. R.A. Bank (UMCG)

Dr. ir. F.A.D.T.G. Wagener

Paranimfen:

Kasper Boers

Elly Versteeg

Table of contents

Chapter 1

General introduction, aims and outline of this thesis

Abstract

Regenerative medicine aims to develop medical devices, cell therapy and materials, *e.g.* tissue engineered constructs, to aid and enhance the treatment of damaged tissues and organs. The ultimate goal of these treatments is regeneration without the formation of scar tissue. A strategy that could lead to this goal is the use of principles found in embryonic development. In this thesis, we aimed to design an embryonic-like scaffold that may be used for the treatment of human skin defects resulting in improved skin regeneration. In the process leading to the design of an embryonic-like scaffold we studied effector molecules, *e.g.* growth factors and morphogens, and components of the embryonic ECM with a focus on glycosaminoglycans.

This chapter commences with an overview of adult skin anatomy of both mouse and human skin. Subsequently skin development will be described predominantly for mouse skin. Next, human wound repair will be discussed and the principles of this process are compared to scarless healing as found during embryonic development based on examples from multiple animal model systems. Relevant principles of tissue engineered constructs are discussed and the main components of these constructs described. Glycosaminoglycan (GAG) biosynthesis is described as GAGs are expected to be one of the important building blocks of the embryonic-like scaffold and as Chapters 5 and 6 will focus on GAGs in development and disease. Finally, the aims and outline of this thesis are described.

1.1 Skin

Skin is considered the largest organ of the human body. It protects us from the environment both physically and through signalling mechanisms [1,2]. In this section, an overview is given of the anatomy and development of skin.

1.1.1 Anatomy of mature skin

Murine skin can be subdivided in four layers, *i.e.* the epidermis, dermis, panniculus adiposus and panniculus carnosus (Figure 1) [3]. Human skin contains essentially the same layers except for the panniculus carnosus, a subdermal muscle layer [1]. The epidermis is a keratinized stratified squamous epithelium [4], which protrudes into the dermis by rete ridges and appendages, such as hair follicles, sweat glands and sebaceous glands. Epidermal rete ridges are suggested to provide a microenvironment for epidermal stem cells, which additionally reside in the bulge area of hair follicles [1,5] and may also be present in sebaceous glands [6]. Stem cells are involved in the constant renewal of the epidermal barrier, skin homeostasis, hair follicle regeneration and wound repair [2,6]. The epidermis rests upon the dermis, which consists of connective tissue containing fibrillar collagens. Both layers are separated by a basement membrane produced predominantly by the epidermal basal cell layer. In mature dermis, two layers can be distinguished, *i.e.* the papillary dermis close to the epidermis and the reticular dermis near the panniculus adiposus [5]. Both layers of the dermis contain various cell types, *e.g.* fibroblasts, macrophages, mast cells, immune cells, and structures such as blood vessels, lymphatics and nerves [5], all resting within a matrix which, in addition to collagen, contains elastic fibers, fibronectin and glycosaminoglycans. Glycosaminoglycans are thought to regulate molecular trafficking in the dermis by binding and modulating extracellular molecules [1].

1.1.2 Development of the epidermis

The epidermis is formed after gastrulation from ectoderm under the influence of Wnt signalling. Wnt signalling stimulates the expression of bone morphogenetic markers and inhibits cells to react to fibroblast growth factors, which stimulate a neural fate [6,7]. The epidermal-fated ectodermal cells will form a periderm layer 9 days post conception in mice and after 4 to 8 weeks of gestation in humans. The periderm is an embryo-specific stratified cell layer separating the embryo from the amniotic fluid [1,8,9]. The development of the epidermis continues 12 days post conception in mice and 9 weeks of gestation in humans by regional stratification under the control of Hox genes and the transcription factor P63, a homolog of P53 [1]. P63 knockout mice show a lack of stratification of the epidermis and die, amongst others, due to dehydration [10]. Stratification is a process in which cells of the basal cell layer, resting upon the basement membrane, divide asymmetrically causing terminal differentiation and resulting in three histological distinguishable layers on top of the stratum basale, *i.e.* the stratum spinosa, stratum granulosum and the stratum corneum (Figure 2). Depending on the thickness of skin, a stratum lucidum is present between the stratum granulosum and stratum corneum. Cells are shedded at the end of terminal differentiation [2,11].

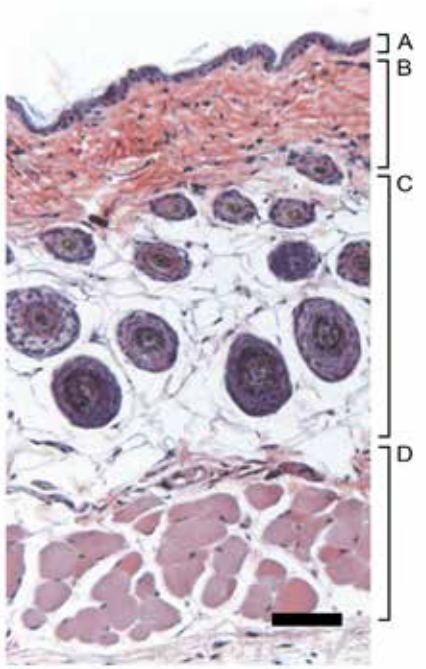

Figure 1 – Anatomy of murine skin. Mouse skin consists of an epidermis (A) resting upon the dermis (B). Beneath the dermis the panniculus adiposus (C), a fat layer, and the panniculus carnosus (D), a muscle layer, can be found. Bar is 50 µm.

1.1.3 Development of the dermis

The dermis (Figure 3) originates from different sources of mesoderm depending on the location on the embryo. Dorsal dermis is derived from the dermamyotome, a compartment of somites. Lateral plate mesoderm is the origin for ventral and limb dermis, while neural crest cells are the origin of cranial dermis [1,12]. The dermis is thought to have a crucial role in the development of the epidermis through various cell signalling processes by which epidermal cell differentiation and appendage formation is initiated [1,6]. In adult skin the dermis provides nutrients to the epidermis [1].

The development of the dermis will be discussed for mice. The structural development of the dermis in mice starts 14 days post conception when the undifferentiated mesenchymal cells adopt a fibroblast-like phenotype and start producing extracellular matrix components. At 16 days post conception the fibroblasts have matured into dermal fibroblasts and extracellular matrix production is increased. The dermal matrix subsequently matures further by the thickening of the collagen fibers [1].

1.1.4 Development of the basement membrane

The basement membrane separates the epidermis and the dermis. It contains, amongst other components, type IV and VII collagen, fibronectin, entactin, heparan sulfate (HS) and laminin 5. The basal cell layer of the epidermis supplies and organises type IV collagen and laminin. Fibronectin is supplied by both dermis and epidermis [4]. The composition of these components may vary due to spatiotemporal development of skin [5]. The importance of the basement membrane has been shown in type IV collagen knockout mice, which die 10 to 11 days post conception due to lack of integrity, stability and functionality of basement membranes [13].

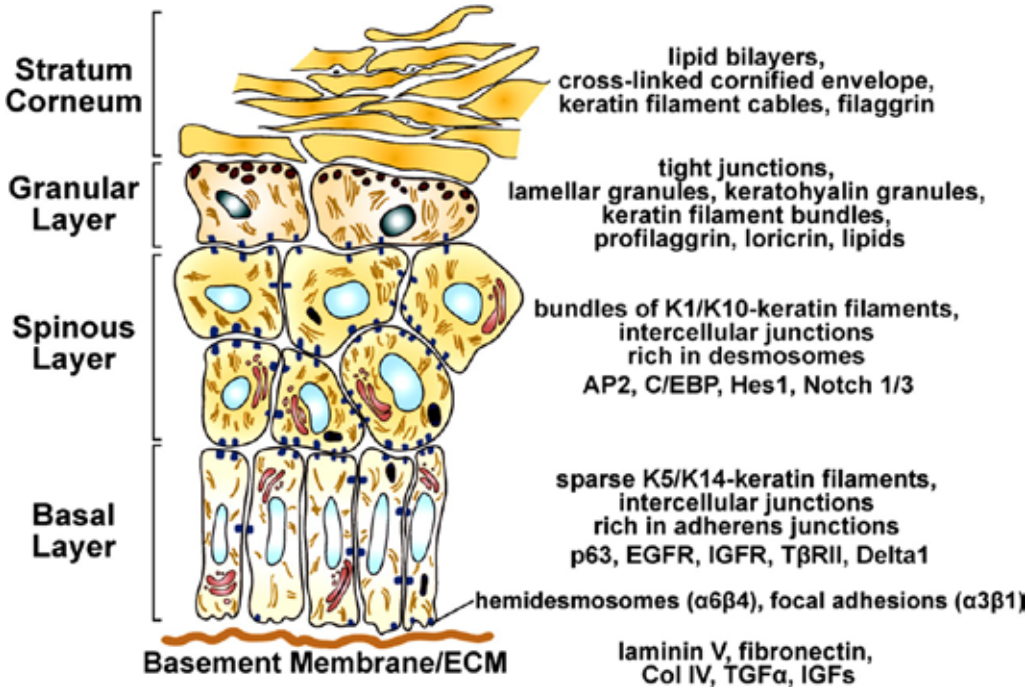

Figure 2 – Terminal differentiation of skin adapted from Fuchs 2008 [2]. Terminal differentiation is started upon asymmetrical differentiation of cells in the basal layer resulting in four distinct layers upon the basement membrane, i.e. the basal layer, the spinous layer, the granuluar layer and the stratum corneum.

1.1.5 Development of skin appendages

Appendages are formed by a complex but organized interplay between epidermal and dermal cells and can be seen in the mouse embryo 16 days post conception and in human embryos around 16 weeks of gestation [1,8]. It is thought that the dermis provides the first signal to form a cluster of ectodermal cells, under which mesenchymal cells in the dermis assemble into a dermal papilla [1,6]. To illustrate the formation of skin appendages we focus on the development of hair follicles in mice (Figure 4) [14]. During hair follicle development Wnt signalling molecules, fibroblast growth factors and BMP inhibitory factors are important for the formation of the ectodermal placodes [6].

In the second stage the dermal papilla moves downward to form a hair germ which develops in a hair peg in stage three [14]. The leading front of the downward growing hair follicle is highly proliferative and interacts constantly with the dermal papilla [6]. The inner cell layers of the hair peg develop in an inner rooth sheath cone in stage four and the dermal papilla becomes enclosed in the growing hair follicle as part of the bulb region [6,14]. Cells above the root in the outer root sheath stay in contact with the basement membrane [6]. In the next stage the bulge area and sebaceous gland are becoming apparent by a local thickening of cells in the hair follicle near the epidermis and the

presence of sebocytes, respectively. At stage six, a growing hair becomes visible in the hair shaft and melanin is produced. At 18.5 days post conception in mouse, hairs can be found hidden in the hair shafts, corresponding to stage seven according to Paus et al. (1999) [14]. Stage eight of hair follicle morphogenesis is visible after birth when hairs emerge out of the skin [14].

1.2 Skin defects and wound repair

Skin is the first line of defence against physical harm, *e.g.* burns, cuts and abrasions. Depending on the size and depth of the wound, skin heals with or without a scar. In comparison with healthy undamaged skin, a scar is characterized by disorganized extracellular matrix [15] or a macroscopic fibrous disturbance [9]. It is the aim of this project to take the first steps towards fully regenerated damaged skin, resembling scarless healing as found in dermal wounds in early embryonic development [8,16].

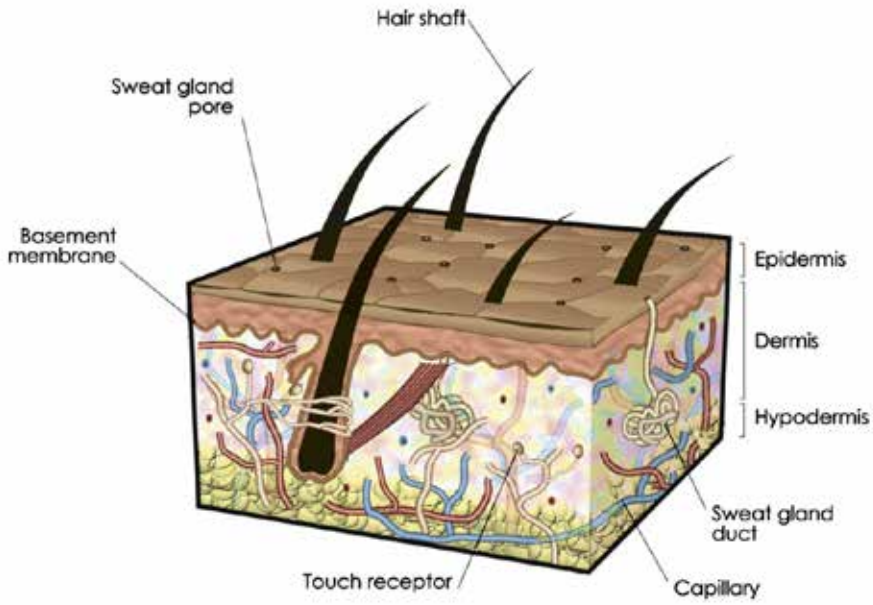

Figure 3 – Schematic representation of the human dermis adapted from Kamel et al. 2013 [36]. The dermis consists of connective tissue in which fibroblasts reside. In addition sweat glands, blood vessels (capillaries) and touch receptors can be found in skin. The dermis rests upon the panniculus adiposus or hypodermis.

1.2.1 Wound healing

Wound healing can be subdivided into four stages, *i.e.* haemostasis, inflammation, proliferation and remodelling (Figure 5). Upon wounding the haemostasis stage is initiated and is characterized by the formation of a fibrin clot, which serves as a temporal barrier to protect the wounded area. In addition it serves as a provisional matrix for cells during the repair process and as a reservoir of signalling molecules, which are released to start the next stage of wound healing, the inflammation stage. This stage is started by the release of chemotactic cues recruiting inflammatory cells, which remove death tissue and prevent infections [8,15,17].

In the subsequent proliferation stage, 2 to 10 days after injury, new tissue formation is started by proliferation of cells in the epidermal cell layer at the wound edges, which migrate over the injured dermis and mature by stratification, restoring the barrier function of skin. In the dermis the formed fibrin clot is replaced by granulation tissue accompanied by the formation of new blood vessels. In addition, fibroblasts proliferate, deposit collagen and are recruited into the granulation tissue. Part of the recruited fibroblasts differentiate into myofibroblasts to contract the edges to close the wound and deposit collagen [8,15,17]. In the final stage of wound healing (remodelling), the extracellular matrix is remodelled to restore skin integrity [8,15].

The ECM of healthy skin consist of a basket-weaven collagen network. The new collagen fibrils formed during the proliferation and remodelling phase, however, are deposited as densely packed bundles, which is typical for the ECM of a scar [18].

1.2.2 Scarless healing or regeneration

In contrast to adult wound healing, skin wounds in early gestation heal rapidly and scarlessly [8,9]. In general, the phases of wound healing are suggested to be equal to adult wound healing. Differences which may explain the outcome of wound healing in early gestational embryos and adult skin can be found in mechanical aspects, environmental aspects, the inflammatory response, ECM content and cellular characteristics [9,19,20].

One of the major mechanical differences between adult and embryonic wound healing is the method of wound closure. Wound closure in embryonic wound healing is facilitated by the formation of an actin ring in the leading edge of basal marginal cells of the epidermis surrounding the wound. This actin ring pulls the wound edges together to close the wound [19,21]. In adult wound healing the wound is closed by contraction of the dermis due to the action of myofibroblasts. The epidermis is reepithelized by proliferation and migration through lamellipodial crawling [19].

The environment of a mammalian embryo is filled with amniotic fluid, which is rich in hyaluronic acid and growth factors [9], which are suggestively beneficial for scarless wound healing [22]. Experiments with opossums, however, showed that scarless healing can also take place outside the uterus [8,23]. Experiments in sheep and subcutaneous transplantation of human foetal skin in athymic mice suggest that the environment may not be key for scarless and adult healing, resulting in a scar [9,24,25].

Inflammatory processes are important for adult wound healing. In foetal wound healing, however, differences can be found in the number and type of inflammatory cells present

in comparison to the same process in an adult [9]. Differences include the lack of polymorphonuclear leukocytes and the number of macrophages entering the wound [8,26]. In general, during scarless healing inflammation is reduced or even absent [9]. These observations are supported by experiments in which the inflammatory response was suggestively reduced during normal wound healing, leading to a reduction in scar formation [9,27].

Another difference between adult wound healing and early gestational wound healing is the content of the ECM. For proper development, the undamaged foetal ECM promotes migration and proliferation. These characteristics of the foetal ECM are beneficial during wound repair and could explain the phenomenon of scarless healing [9]. The main collagen in foetal skin contains type I and III collagen. The percentage of type III collagen in skin is higher in foetal skin than in adult skin, *i.e.* 30-60% versus 10-20%, respectively [8]. The high content of type III collagen is thought to be an important factor for the scarless nature of foetal wound healing [8]. Another component of the ECM found in the foetal ECM and less in adult ECM is hyaluronic acid [9,28,29]. Hyaluronic acid stimulates fibroblast migration [8], probably resulting is rapid regeneration of the damaged dermis in comparison to adult wound healing.

In addition to the fast migration of fibroblasts, foetal fibroblasts are shown to be different in comparison to their adult counterparts. The main difference is the increased production of collagen and the percentage of type III and IV collagen produced [8,9]. Foetal fibroblasts produce collagen while proliferating [9], possibly via an alternative translationatory machinery using IRES sites [30]. In addition, foetal fibroblasts produce more hyaluronic acid and display more receptors for hyaluronic acid [9]. The fibroblasts important for adult wound healing are myofibroblasts, which have a role in wound closure by contraction and production of collagen. The produced collagen is laid down in a parallel pattern resulting in a scar. In wounds made in early gestation, myofibroblasts were almost absent [9].

In mammals the ability to heal without a scar is age-dependent [9]. In human embryos scarring can be observed after 24 weeks of gestation and in mice after 18.5 days post conception [9]. Within the transition period between scarless healing and healing with a scar, the size of the wound determines the outcome of wound healing [9].

1.2.3 Wound types

In this thesis, we focus on the development of a tissue engineered construct for burn wounds [31,32]. Burn wound healing is essentially the same as normal wound healing, although the degree of systemic inflammation is more pronounced [31]. Burn wounds can be classified on the depth of the wound. In first degree burns only the epidermis is damaged, while in second degree burns the epidermis and part of the dermis are affected. First and second degree wounds heal within 2 to 3 weeks, optionally facilitated by local wound care, and the damaged tissue is fully regenerated [32].

Full-thickness burn wounds are classified as third or higher degree wounds, depending on the number of tissues affected underneath the skin [32]. Large second degree, third

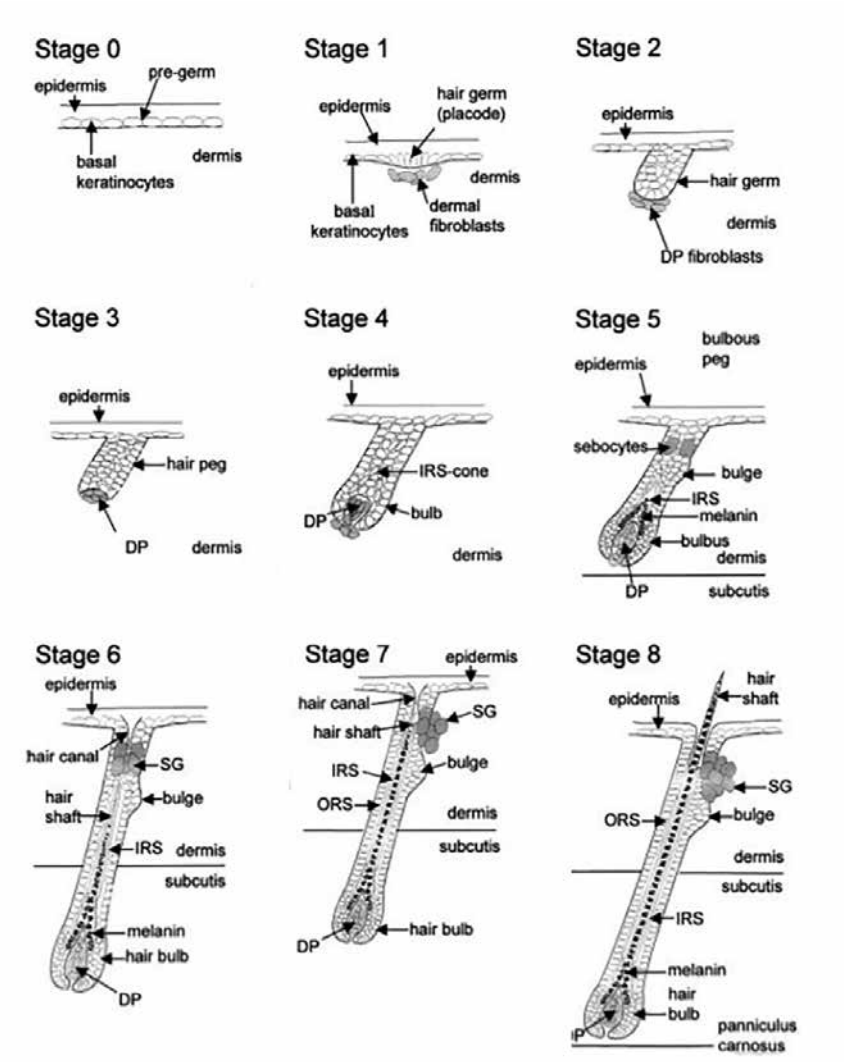

Figure 4 – The 8 stages of hair follicle development according to Paus et al. [14]. Hair follicle development start after an interplay in stage 0 between epidermal and dermal cells forming a dermal papilla (DP) in stage 1. The dermal papilla will move downward and will form a hair germ in stage 2, which will develop into a hair peg in stage 3. In stage 4 the inner cell layers of the hair peg differentiate into the inner root sheath cone (IRS cone) and the dermal papilla becomes enclosed in the bulb region. Specific hair follicle structures start to develop at stage five (5), in which a the bulge area and a sebaceous gland become apparent. The first growing hair becomes visible in stage six (6) in the formed hair shaft. Stage seven (7) hairs can be found hidden in the hair shafts, which become visible in stage eight (8) after birth when hairs emerge out of the skin [14]. For a more detailed figure of hair follicle development the reader is referred to the original publication by Paus et al. [14].

and higher degree burn wounds are treated by excision of the damaged tissue and grafting using an autologous split-thickness skin graft [31]. If the patients do not have a suitable donor site for the split-thickness skin graft, an allograft or xenograft is used to temporarily cover the damaged skin area [31,33]. The temporary cover can be removed when a suitable skin graft or tissue engineered skin construct is placed.

1.3 Skin tissue engineering

Constructs for the treatment of full-thickness wounds can be made from natural or synthetic materials and aim to mimick normal skin anatomy, thereby stimulating regeneration [34–36]. The design and function of the constructs, however, needs to be improved. In essence a functional skin construct should control fluid loss, prevent or reduce infection, reduce contraction and reduce scarring [36]. Some examples of building blocks for scaffolds will be given. In addition, tissue engineered skin constructs used in the clinic or under development will be discussed.

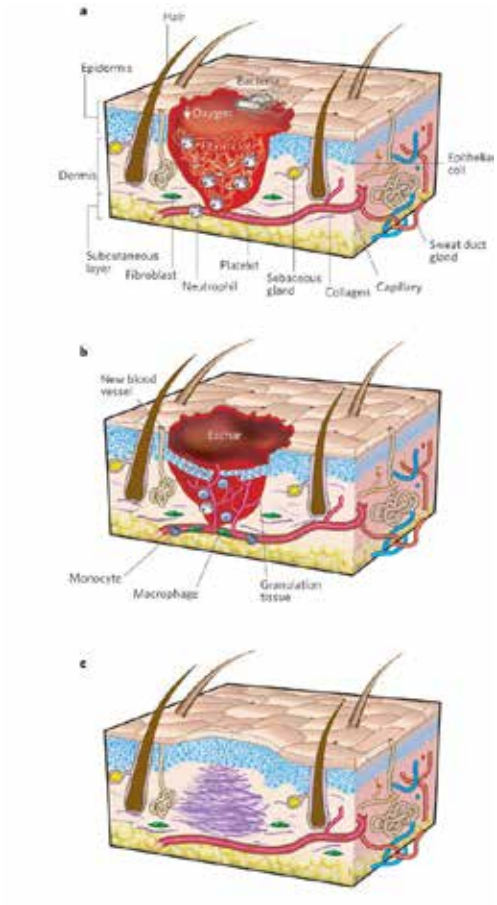

Figure 5 – Stages of wound repair (adapted from Gurtner et al. (2008) [15]).

Wound healing can be characterized by four stages, i.e. haemostasis (a), inflammation (a), proliferation (b) and remodelling (c). In the first stage, haemostasis (a), a fibrin clot is formed as a provisional matrix and a reservoir of signalling molecules. In the inflammation stage (a), death tissue is removed and infection reduced by inflammatory cells. In the third stage, proliferation (b), new tissue formation is started by migration of epidermal cells over the injured dermis and subsequent terminal differentiation of the newly formed epidermal barrier. The formed fibrin clot is replaced by granulation tissue in the dermis accompanied by the formation of new blood vessels. In the final stage of wound healing (c), remodelling of the extracellular matrix restores skin integrity.

For many years the gold standard for the treatment of full thickness wounds has been an autologous split-thickness skin graft [37]. A split skin graft, *i.e.* epidermis with a thin layer of dermis, is taken from a donor site on the same patient and transplanted to the wounded area. A split skin graft may be combined with a dermal substitute, *e.g.* the combination of an Integra dermal substitute and a split skin graft [38,39]. The main advantage of a split skin graft is a high percentage of graft acceptance. The main disadvantages of this method, however, are the formation of scar tissue and wound contraction [40]. Tissue engineered constructs may offer a better alternative to reduce scar tissue and wound contraction by the addition of specific effector molecules.

Three types of tissue engineered skin substitutes exist, *i.e.* epidermal substitues, dermal substitutes and full-thickness skin substitutes [31]. Epidermal substitutes consist of cultured epidermal cells, but lack dermal components. Dermal substitues are generally acellular matrices [31], although examples with cells exist, *e.g.* denovoderm [41]. A full-thickness skin substitute replaces both epidermis and dermis. In general, tissue-engineered skin constructs contain three elements, *i.e.* cells, a scaffold mimicking skin ECM and signalling molecules [36]. The scaffold that will be designed in this thesis will be acellular, so we will focus mainly on the scaffold and signalling molecules (Figure 5). Acellular constructs are designed to simulate the natural ECM and are based on either natural materials, *e.g.* collagen and glycosaminoglycans, or synthetic materials, *e.g.* silicone, polyvinylalcohol and polylactide [36]. The major benefit for natural materials is biocompatibility, while synthetic materials tend to have better handling [36]. In Kamel et al. (2013) [36] an overview is given of skin constructs used in the clinic and under development.

1.3.1 Collagen

Type I collagen is a widely used material as the basic material for natural-based skin tissue engineering due to its biocompatibility, low antigenicity, biodegradability and availability [34,36,42–45]. It is a member of a large family of more than 28 different collagens [46]. As normal skin consists mainly of type I collagen, a type I collagen-based construct is probably suitable to mimic the ECM during tissue engineered aided wound closure [1]. For the design of an embryonic-like collagen-scaffold, however, it may be essential to incorporate type III collagen, since it has been shown that embryonic skin contains a higher percentage of this collagen compared to adult skin. Isolation of type III collagen is not possible as for type I collagen [47]. There are reports, however, that suggest that type III collagen can be produced in the yeast *Pichia pastoris* [48]. The higher percentage of type III collagen is thought to be an important factor for the scarless nature of foetal wound healing [8].

1.3.2 Glycosaminoglycans in skin constructs

Glycosaminoglycans (GAGs) are added to a tissue engineered construct as they regulate signalling molecules [8,34,49] and increase the water-binding capacity [50]. The molecules can be attached to the tissue engineered construct via crosslinking [51]. In section 1.4 an overview is given on glycosaminoglycans. This section will focus on examples of glycosaminoglycans in tissue engineering.

Heparan sulfate (HS) is known for its interaction with signalling molecules and its specific modifications, may regulate tissue specific growth factor binding and release [52–55]. In this research project heparin will be incorporated into the scaffold as described in earlier publications of our research group [56]. Chondroitin sulfate has been used for incorporation into tissue engineered constructs as well [51]. An example of a commercially available skin construct, containing shark chondroitin sulfate, is Integra® [57].

Hyaluronic acid, a non-sulfated GAG, has been reported to be present in the embryonic ECM [9,28,29], and therefore it is of interest for the aim of this research project, *i.e.* mimicking embryonic development in a skin construct. Hyaluronic acid is used in commercially available constructs such as Laserskin®, Hyalomatrix® and Hyalograft® [36].

1.3.3 Effector molecules

A tissue engineered construct can be combined with effector molecules, like growth factors, morphogens, cytokines and other cells signalling molecules. The effector molecules trigger cellular responses of cells transplanted with the construct or cells migrating into the construct. Depending on the aim of the treatment, the signalling molecules incorporated into the construct can promote migration, proliferation or differentiation. In case of a temporary construct, used to protect the wounded area, one can postulate on the addition of anti-inflammatory effector molecules [36].

Based on studies done on the transforming growth factor beta family (TGFβ), it was proposed that addition of TGFβ isoform 3 (TGFβ3) could lead to scarless healing in an adult wound [16]. This was based on the observation that the effector molecule profile in foetal wound healing showed increased levels of TGFβ3 and decreased levels of platelet-derived growth factors, TGFβ1 and TGFβ2 [58]. Experiments using TGFβ3, however, did not result in scarless healing [59].

Another growth factor family with a possible role in scarless healing is the fibroblast growth factor (FGF) family, which is a large family of 21 isoforms involved in various cellular processes. Within this family FGF2, FGF7 and FGF10 are suggested to be important for adult wound healing [36]. It has been shown that during scarless wound healing FGF2 is important as well [60], while FGF7 and FGF10 are downregulated [61].

1.4 Glycosaminoglycan synthesis and degradation

Glycosaminoglycans (GAGs) have been shown to be important for normal development, since it has been suggested that glycosaminoglycans (GAG), such as heparan sulfate (HS), chondroitin sulfate (CS) and dermatan sulfate (DS), play a role in binding, guiding and modulating growth factors and morphogens during various cell signaling processes [53,62,63] and are involved in the development of the ECM [64,65]. In addition GAGs

have been shown to be involved in the formation of effector molecule gradients, which are essential for the developmental processes [66–68]. GAGs can be found in different structures within skin, *e.g.* heparan sulfate in the basement membrane [69], chondroitin sulfate and dermatan sulfate in the dermis [70] and hyaluronic acid during skin development [8].

1.4.1 GAG synthesis

To synthesize GAGs UDP-activated sugar monomers are made including UDP-acetylglucosamine (UDP-GlcNAc), UDP-acetylgalactosamine (UDP-GalNAc) and UDP-glucuronic acid (UDP-GlcA). The UDP-activated monomers are transported from the cytoplasm to the Golgi system. In the Golgi system proteoglycan are formed consisting of a proteoglycan core protein (PG) and one or more sugar chains, *i.e.* HS, CS and DS [71].

1.4.2 Proteoglycans and the linkage region

Proteoglycan (PG) core proteins display GAGs and are classified on the type of sugar chain attached, *i.e.* HSPG, CSPG or DSPG for HS, CS and DS, respectively. The sugar chain is bound to specific serine residues on the core protein via a linkage region [72]. The linkage region is formed by the addition of a xylose sugar (Xyl) to the serine residue, followed by the addition of two galactose (Gal) and one glucuronic acid residue (GlcA) [72].

1.4.3 Initiation and elongation

The subsequent sugar added to the linkage region determines if the sugar chain will be a HS chain or a CS/DS chain. Addition of N-acetylglucosamine (GlcNAc) to the linker region will initiate the synthesis of heparan sulfate (HS) and the sugar chain is elongated by alternating addition of GlcA and GlcNAc monomers (Figure 6) [53,72]. CS and DS chains are initiated by the addition of N-acetylgalactosamine (GalNAc) and elongated by alternating addition of GlcA and GalNAc monomers [72].

1.4.4 Modification

The HS and CS/DS chain will be further processed in the Golgi system during and after polymerization by modifications of the individual saccharide units. The modification of HS can be described in several steps (Figure 6). The first step is the N-deacetylation and N-sulfation of GlcNAc residues by N-acetylglucosaminyl-N-deacetylase/N-sulfotransferases (*i.e.* Ndst1, 2, 3 and 4). The GlcA residues are epimerized into iduronic acid (IdoA) residues by glucuronyl C5 epimerase (Glce). The IdoA residues, and in a lesser extent the remaining GlcA residues, are subsequently sulfated at the 2-O position by heparan sulfate 2-O sulfotransferase (Hs2st).

The GlcNS and sporadically the GlcNAc residues are sulfated at the 6-O position by three heparan sulfate 6-O sulfotransferases (Hs6st1, 2 and 3) and/or sulfated at the 3-O position by seven heparan sulfate 3-O sulfotransferases (Hs3st1, 2, 3A, 3B, 4, 5 and 6). After secretion the modifications continue by the action of two sulfatases (Sulf1 and 2) aided by their cofactors (sulfate-modifying factor 1 and 2) which specifically remove

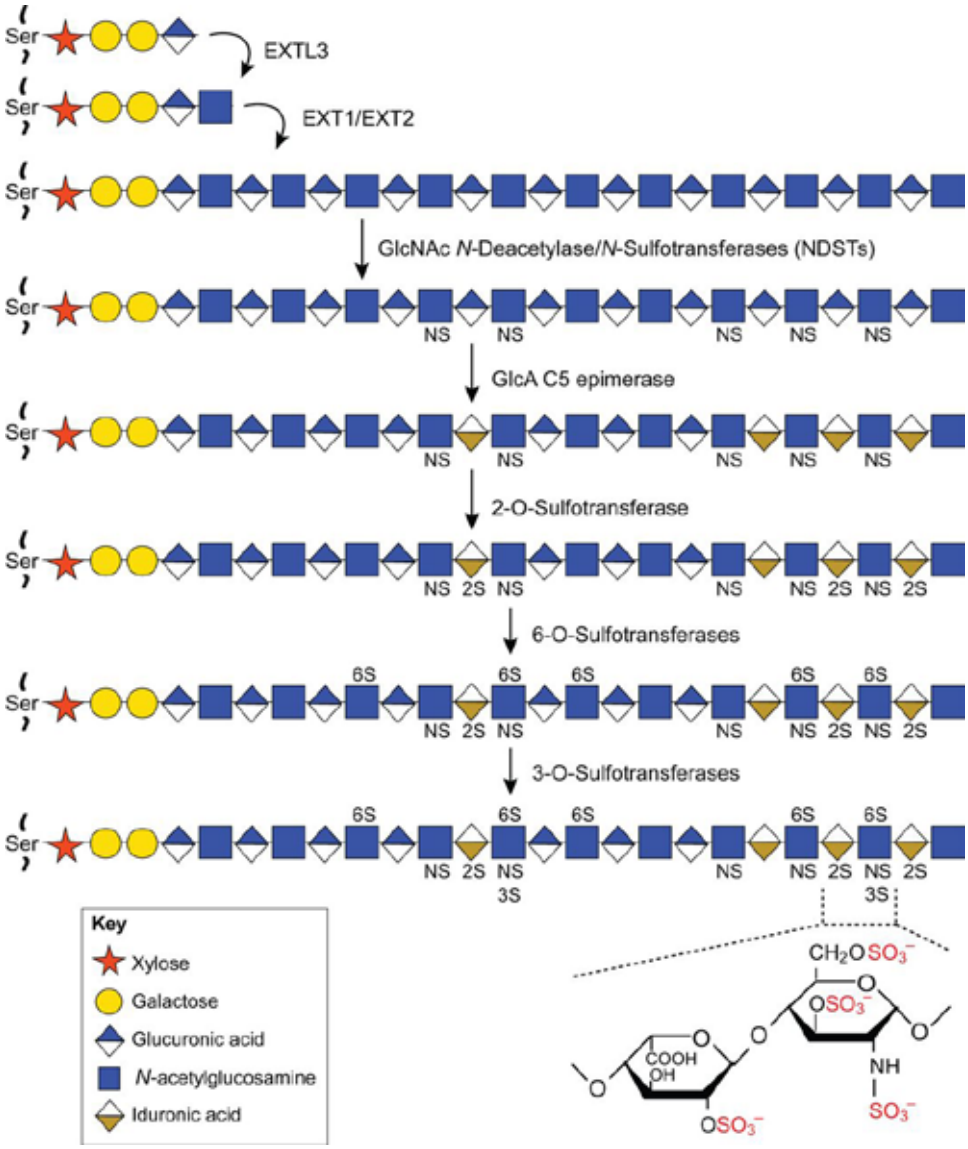

Figure 6 – Heparan sulfate synthesis. After initation of heparan sulfate (HS) synthesis by the addition of N-acetlylated-glucosamine (GlcNAc) to the xylose-galactose-galactose-glucuronic acid (Xyl-Gal-Gal-GlcA) linker region, the chain is elongated. GlcNAc units can be deacetylated and N-sulfated. Subsequently the GlcA units can be epimerized into iduronic acid (IdoA) units and sulphated at the 2-O position. The GlcNS units can be sulphated at the 6-O and 3-O position. This figure is adapted from Poulain and Yost [80].

sulfate groups at the 6-O position of the GlcNS and GlcNAc residues [53,73,74].

The CS and DS chain can be modified at the 2-O and 3-O position of the GlcA unit and at the 4-O and 6-O positon of the GalNAc unit [75]. The main difference between CS and DS is, that DS contains epimerized GlcA units [72].

1.4.5 GAG degradation

Glycosaminoglycan chains are generally degraded in smaller sugar polymers outside the cell, internalized via endocytosis and subsequently processed to monomeric sugar units in lysosomes. The sugar monomers can be recycled to form new sugar chains [72]. Heparanase is an enzyme important for HS degradation that is also involved in wound healing, as overexpression of heparanase resulted in accelerated wound healing [76].

1.5 Aims and outline of the research

The major aims of the PhD project were: 1) construction and evaluation of type I collagen based constructs crosslinked with glycosaminoglycans and loaded with effector molecules to mimic embryonic scaffolds, and 2) the study of glycosaminoglycan metabolism during skin formation.

In **Chapter 2**, an overview is given of gene expression analysis of embryonic skin based on EXON array data, resulting in a selection of twenty growth factors. Two of these growth factors, *i.e.* insulin-like growth factor 2 and sonic hedgehog, were incorporated into a type I collagen-heparin construct. In addition, **Chapter 2** also describes the creation of type I collagen-hyaluronan scaffolds.

Chapter 3 presents a new method to analyse the outcome of collagen construct treated wounds, where newly synthesized collagen can be discriminated from the collagen in the construct. This method is based on the detection of dermatan sulfate with the single-chain antibody GD3A12 [77].

In **Chapter 4** research is presented towards the development of an effector molecule gradient. The approach described uses a gradient of glycosaminoglycans, which resulted in a gradient of the effector molecule fibroblast growth factor 2.

In **Chapter 5** the role of glycosaminoglycans in skin is discussed based on a gene expression study using EXON arrays and custom designed taqman low density arrays (TLDA cards). In addition the expression in two mouse models is analysed, *i.e.* an glucuronic acid epimerase knockout mouse model [78] and a heparanase overexpression model [79].

Chapter 6 focusses on another organ (lung) and describes that a lack of heparan sulfate/overexpression of heparanase is associated with destruction of lung tissue.

1.6 References

[1] J. Rossant, P.P.L. Tam, Mouse Development: Patterning, Morphogenesis, and Organogenesis, First edit, Academic Press, London, UK, 2002.

[2] E. Fuchs, Skin stem cells: rising to the surface, J Cell Biol. 180 (2008) 273–284.

[3] J.A. McGrath, R.A.J. Eady, F.M. Pope, Anatomy and Organization of Human Skin, Rook's Textb. Dermatology. (2004) 45–128.

[4] E. Fuchs and Raghavan, S., Getting under the skin of epidermal morphogenesis, Nat. Rev. Genet. 3 (2002) 199–209.

[5] F.M. Watt, H. Fujiwara, Cell-extracellular matrix interactions in normal and diseased skin, Cold Spring Harb. Perspect. Biol. 3 (2011) 1–14.

[6] E. Fuchs, Scratching the surface of skin development, Nature. 445 (2007) 834–842.

[7] P. Sengel, Pattern formation in skin development, Int J Dev Biol. 34 (1990) 33–50.

[8] K.M. Bullard, M.T. Longaker, H.P. Lorenz, Fetal wound healing: Current biology, World J. Surg. 27 (2003) 54–61.

[9] B.J. Larson, M.T. Longaker, H.P. Lorenz, Scarless fetal wound healing: a basic science review., Plast. Reconstr. Surg. 126 (2010) 1172–80.

[10] M.I. Koster, D.R. Roop, The role of p63 in development and differentiation of the epidermis, J Dermatol Sci. 34 (2004) 3–9.

[11] T. Lechler and Fuchs, E., Asymmetric cell divisions promote stratification and differentiation of mammalian skin, Nature. 437 (2005) 275–280.

[12] I. Olivera-Martinez Viallet, J.P., Michon, F., Pearton, D.J., and Dhouailly, D., The different steps of skin formation in vertebrates, Int. J. Dev. Biol. 48 (2004) 107–115.

[13] E. Pöschl, U. Schlötzer-Schrehardt, B. Brachvogel, K. Saito, Y. Ninomiya, U. Mayer, Collagen IV is essential for basement membrane stability but dispensable for initiation of its assembly during early development., Development. 131 (2004) 1619–1628.

[14] R. Paus Müller-Röver, S., van der Veen, C., Maurer, M., Eichmüller, S., LIng, G., Hofmann, U., Foitzik, K., Mecklenburg, L., and Handjiski, B., A Comprehensive Guide for the Recognition and Classification of Distict Stages of Hair Follicle Morphogenesis, J. Invest. Dermatol. 113 (1999) 523–532.

[15] G.C. Gurtner, S. Werner, Y. Barrandon, M.T. Longaker, Wound repair and regeneration, Nature. 453 (2008) 314–321.

[16] M.W. Ferguson, S. O'Kane, Scar-free healing: from embryonic mechanisms to adult therapeutic intervention, Philos Trans R Soc L. B Biol Sci. 359 (2004) 839–850.

[17] P. Martin, Wound healing--aiming for perfect skin regeneration, Science. 276 (1997) 75–81.

[18] P. Martin, S.M. Parkhurst, Parallels between tissue repair and embryo morphogenesis, Development. 131 (2004) 3021–3034.

[19] P. Martin, J. Lewis, Actin cables and epidermal movement in embryonic wound healing, Nature. 360 (1992) 179–183.

[20] S. Nodder and Martin, P., Wound healing in embryos: a review, Anat Embryol. 195 (1997) 215–228.

[21] M.J. Redd, L. Cooper, W. Wood, B. Stramer, P. Martin, Wound healing and inflammation: embryos reveal the way to perfect repair., Philos. Trans. R. Soc. Lond. B. Biol. Sci. 359 (2004) 777–84.

[22] W.Y. Chen, M.E. Grant, a M. Schor, S.L. Schor, Differences between adult and foetal fibroblasts in the regulation of hyaluronate synthesis: correlation with migratory activity., J. Cell Sci. 94 (Pt 3) (1989) 577–584.

[23] J.R. Armstrong, M.W. Ferguson, Ontogeny of the skin and the transition from scar-free to scarring phenotype during wound healing in the pouch young of a marsupial, Monodelphis domestica., Dev. Biol. 169 (1995) 242–60.

[24] M.T. Longaker, D.J. Whitby, M.W. Ferguson, H.P. Lorenz, M.R. Harrison, N.S. Adzick, Adult skin wounds in the fetal environment heal with scar formation, Ann Surg. 219 (1994) 65–72.

[25] H.P. Lorenz, M.T. Longaker, L. a Perkocha, R.W. Jennings, M.R. Harrison, N.S. Adzick, Scarless wound repair: a human fetal skin model., Development. 114 (1992) 253–259.

[26] N. Scott Adzick, M.R. Harrison, P.L. Glick, J.H. Beckstead, R.L. Villa, H. Scheuenstuhl, W.H. Goodson, Comparison of fetal, newborn, and adult wound healing by histologic, enzyme-histochemical, and hydroxyproline determinations, J. Pediatr. Surg. 20 (1985) 315–319.

[27] M.W. Ferguson and O'Kane, S., Scar-free healing: from embryonic mechanisms to adult therapeutic intervention, Philos Trans R Soc L. B Biol Sci. 359 (2004) 839–850.

[28] S.M. Alaish, D. Yager, R.F. Diegelmann, I.K. Cohen, Biology of fetal wound healing: Hyaluronate receptor expression in fetal fibroblasts, J. Pediatr. Surg. 29 (1994) 1040–1043.

[29] M.T. Longaker, E.S. Chiu, M.R. Harrison, T.M. Crombleholme, J.C. Langer, B.W. Duncan, N.S. Adzick, E.D. Verrier, R. Stern, Studies in fetal wound healing. IV. Hyaluronic acid-stimulating activity distinguishes fetal wound fluid from adult wound fluid., Ann. Surg. 210 (1989) 667–672.

[30] M. López-Lastra, A. Rivas, M.I. Barría, Protein synthesis in eukaryotes: The growing biological relevance of cap-independent translation initiation, Biol. Res. 38 (2005) 121–146.

[31] M.P. Rowan, L.C. Cancio, E. a Elster, D.M. Burmeister, L.F. Rose, S. Natesan, R.K. Chan, R.J. Christy, K.K. Chung, Burn wound healing and treatment: review and advancements., Crit. Care. 19 (2015) 243.

[32] G.M. Kagan, R.J.; Peck, M.D.; Ahrenholz, D.H.; Hickerson, W.L.; Holmes, J.H.; Korentager, R.A.; Kraatz, J.J.; Kotoski, Surgical Management of the Burn Wound and Use of Skin Substitutes, J. Burn Care Res. 34 (2013) e60-79.

[33] Isbi Practice Guidelines Committee, Steering Subcommittee, Advisory Subcommittee, ISBI Practice Guidelines for Burn Care., Burns. 42 (2016) 953–1021.

[34] A.N. Renth, M.S. Detamore, Leveraging “raw materials” as building blocks and bioactive signals in regenerative medicine., Tissue Eng. Part B. Rev. 18 (2012) 341–62. .

[35] M.S. Hu, Z.N. Maan, J.-C. Wu, R.C. Rennert, W.X. Hong, T.S. Lai, A.T.M. Cheung, G.G. Walmsley, M.T. Chung, A. McArdle, M.T. Longaker, H.P. Lorenz, Tissue engineering and regenerative repair in wound healing., Ann. Biomed. Eng. 42 (2014) 1494–507.

[36] R.A. Kamel, J.F. Ong, E. Eriksson, J.P.E. Junker, E.J. Caterson, Tissue engineering of skin, J. Am. Coll. Surg. 217 (2013) 533–555.

[37] S. MacNeil, Progress and opportunities for tissue-engineered skin., Nature. 445 (2007) 874–880.

[38] D.Q.A. Nguyen, T.S. Potokar, P. Price, An objective long-term evaluation of Integra (a dermal skin substitute) and split thickness skin grafts, in acute burns and reconstructive surgery, Burns. 36 (2010) 23–28.

[39] E.N. Lamme, H.J. de Vries, H. van Veen, G. Gabbiani, W. Westerhof, E. Middelkoop, Extracellular matrix characterization during healing of full-thickness wounds treated with a collagen/elastin dermal substitute shows improved skin regeneration in pigs., J. Histochem. Cytochem. 44 (1996) 1311–1322.

[40] R. Rudolph, The effect of skin graft preparation on wound contraction., Surg. Gynecol. Obstet. 142 (1976) 49–56.

[41] C. Oostendorp, P.J.E. Uijtdewilligen, E.M. Versteeg, T.G. Hafmans, E.H. van den Bogaard, P.K.J.D. de Jonge, A. Pirayesh, J.W. Von den Hoff, E. Reichmann, W.F. Daamen, T.H. van Kuppevelt, Visualisation of newly synthesised collagen in vitro and *in vivo*., Sci. Rep. 6 (2016) 18780.

[42] S.T. Boyce, Design principles for composition and performance of cultured skin substitutes, in: Burns, 2001: pp. 523–533.

[43] J. Glowacki, S. Mizuno, Collagen scaffolds for tissue engineering, Biopolymers. 89 (2008) 338–344.

[44] M. Chvapil, R. Kronenthal, Medical and surgical applications of collagen, Int Rev Connect Tissue. (1973).

[45] J.M. Pachence, Collagen-based devices for soft tissue repair, J. Biomed. Mater. Res. 33 (1996) 35–40.

[46] S. Ricard-Blum, The Collagen Family, Cold Spring Harb. Perspect. Biol. 3 (2011) 1–19.

[47] J.S. Pieper, a. Oosterhof, P.J. Dijkstra, J.H. Veerkamp, T.H. Van Kuppevelt,

Preparation and characterization of porous crosslinked collagenous matrices containing bioavailable chondroitin sulphate, Biomaterials. 20 (1999) 847–858.

[48] J. Myllyharju, M. Nokelainen, A. Vuorela, K.I. Kivirikko, Expression of recombinant human type I–III collagens in the yeast Pichia pastoris, Biochem. Soc. Trans. 28 (2000) 353.

[49] M. Bernfield, M. Gotte, P.W. Park, O. Reizes, M.L. Fitzgerald, J. Lincecum, M. Zako, Functions of cell surface heparan sulfate proteoglycans, Annu Rev Biochem. 68 (1999) 729–777.

[50] W.F. Daamen, H.T.B. Van Moerkerk, T. Hafmans, L. Buttafoco, a. a. Poot, J.H. Veerkamp, T.H. Van Kuppevelt, Preparation and evaluation of molecularly-defined collagen-elastin-glycosaminoglycan scaffolds for tissue engineering, Biomaterials. 24 (2003) 4001–4009.

[51] J.S. Pieper, T. Hafmans, J.H. Veerkamp, T.H. Van Kuppevelt, Development of tailor-made collagen-glycosaminoglycan matrices: EDC/NHS crosslinking, and ultrastructural aspects, Biomaterials. 21 (2000) 581–593.

[52] J.S. Pieper, T. Hafmans, P.B. Van Wachem, M.J.A. Van Luyn, L.A. Brouwer, J.H. Veerkamp, T.H. Van Kuppevelt, Loading of collagen-heparan sulfate matrices with bFGF promotes angiogenesis and tissue generation in rats, J. Biomed. Mater. Res. 62 (2002) 185–194.

[53] S. Sarrazin, W.C. Lamanna, J.D. Esko, Heparan sulfate proteoglycans, Cold Spring Harb. Perspect. Biol. 3 (2011) 1–33.

[54] S. Yamada, M. Onishi, R. Fujinawa, Y. Tadokoro, K. Okabayashi, M. Asashima, K. Sugahara, Structural and functional changes of sulfated glycosaminoglycans in Xenopus laevis during embryogenesis, Glycobiology. 19 (2009) 488–498.

[55] J.D. Esko, S.B. Selleck, Order out of chaos: assembly of ligand binding sites in heparan sulfate, Annu. Rev. Biochem. 71 (2002) 435–471.

[56] S.T.M. Nillesen, G. Lammers, R.G. Wismans, M.M. Ulrich, E. Middelkoop, P.H. Spauwen, K.A. Faraj, J. Schalkwijk, W.F. Daamen, T.H. Van Kuppevelt, Design and in vivo evaluation of a molecularly defined acellular skin construct: Reduction of early contraction and increase in early blood vessel formation, Acta Biomater. 7 (2011) 1063–1071.

[57] N.S. Moiemen, E. Vlachou, J.J. Staiano, Y. Thawy, J.D. Frame, Reconstructive surgery with Integra dermal regeneration template: histologic study, clinical evaluation, and current practice, Plast Reconstr Surg. 117 (2006) 160S–174S.

[58] A. Leung, T. Crombleholme, S. Keswani, Fetal wound healing: implications for minimal scar formation., Curr Opin Pediatr. 24 (2012) 371–378.

[59] M.T. Longaker, R.J. Rohrich, L. Greenberg, H. Furnas, R. Wald, V. Bansal, H. Seify, A. Tran, J. Weston, J.M. Korman, R. Chan, D. Kaufman, V.R. Dev, J. a Mele, M. Januszyk, C. Cowley, P. McLaughlin, B. Beasley, G.C. Gurtner, A Randomized Controlled Trial of the embrace® Device to Reduce Incisional Scar Formation., Plast. Reconstr. Surg. 1399099 (2014) 536–546.

[60] G.E. Spyrou, I.L. Naylor, The effect of basic fibroblast growth factor on scarring, Br. J. Plast. Surg. 55 (2002) 275–282.

[61] C.M. Dang, S.R. Beanes, C. Soo, K. Ting, P. Benhaim, M.H. Hedrick, H.P. Lorenz, Decreased expression of fibroblast and keratinocyte growth factor isoforms and receptors during scarless repair, Plast. Reconstr. Surg. 111 (2003) 1969–1979.

[62] H.E. Bülow, O. Hobert, The Molecular Diversity of Glycosaminoglycans Shapes Animal Development, Annu. Rev. Cell Dev. Biol. 22 (2006) 375–407.

[63] U. Häcker, K. Nybakken, N. Perrimon, Heparan sulphate proteoglycans: the sweet side of development., Nat. Rev. Mol. Cell Biol. 6 (2005) 530–541.

[64] C.C. Reed and Iozzo, R.V., The role of decorin in collagen fibrillogenesis and skin homeostasis, Glycoconj. J. 19 (2003) 249–255.

[65] K.G. Danielson, H. Baribault, D.F. Holmes, H. Graham, K.E. Kadler, R. V. Iozzo, Targeted disruption of decorin leads to abnormal collagen fibril morphology and skin fragility, J. Cell Biol. 136 (1997) 729–743.

[66] L. Hufnagel, J. Kreuger, S.M. Cohen, B.I. Shraiman, On the role of glypicans in the process of morphogen gradient formation, Dev Biol. 300 (2006) 512–522.

[67] D. Yan, X. Lin, Shaping morphogen gradients by proteoglycans., Cold Spring Harb. Perspect. Biol. 1 (2009) 1–17.

[68] O. Wartlick, A. Kicheva, M. González-Gaitán, Morphogen gradient formation., Cold Spring Harb. Perspect. Biol. 1 (2009) 1-22.

[69] E. Zcharia, D. Philp, E. Edovitsky, H. Aingorn, S. Metzger, H.K. Kleinman, I. Vlodavsky, M. Elkin, Heparanase Regulates Murine Hair Growth, Am. J. Pathol. 166 (2005) 999–1008.

[70] J.M. Trowbridge, J.A. Rudisill, D. Ron, R.L. Gallo, Dermatan sulfate binds and potentiates activity of keratinocyte growth factor (FGF-7), J Biol Chem. 277 (2002) 42815–42820.

[71] J.E. Silbert, G. Sugumaran, Biosynthesis of Chondroitin / Dermatan Sulfate, IUBMB Life. 54 (2002) 177–186.

[72] A. Imamura, H. Ando, S. Korogi, G. Tanabe, O. Muraoka, H. Ishida, M. Kiso, Essentials of glycobiology, Second Edi, 2009.

[73] J.D. Esko, U. Lindahl, Molecular diversity of heparan sulfate, J. Clin. Investig. 108 (2001) 169–173.

[74] M. Buono, I. Visigalli, R. Bergamasco, A. Biffi, M.P. Cosma, Sulfatase modifying factor 1-mediated fibroblast growth factor signaling primes hematopoietic multilineage development., J. Exp. Med. 207 (2010) 1647–60.

[75] M. Guerrini, D. Beccati, Z. Shriver, A. Naggi, K. Viswanathan, A. Bisio, I. Capila, J.C. Lansing, S. Guglieri, B. Fraser, A. Al-Hakim, N.S. Gunay, Z. Zhang, L. Robinson, L. Buhse, M. Nasr, J. Woodcock, R. Langer, G. Venkataraman, R.J. Linhardt, B. Casu, G. Torri, R. Sasisekharan, Oversulfated chondroitin sulfate is a contaminant in heparin associated with adverse clinical events, Nat. Biotechnol. 26 (2008) 669–675.

[76] E. Zcharia, R. Zilka, A. Yaar, O. Yacoby-Zeevi, A. Zetser, S. Metzger, R. Sarid, A. Naggi, B. Casu, N. Ilan, I. Vlodavsky, R. Abramovitch, Heparanase accelerates wound angiogenesis and wound healing in mouse and rat models., FASEB J. 19 (2005) 211–21.

[77] G.B. Ten Dam, S. Yamada, F. Kobayashi, A. Purushothaman, E.M.A. Van De Westerlo, J. Bulten, A. Malmström, K. Sugahara, L.F. Massuger, T.H. Van Kuppevelt, Dermatan sulfate domains defined by the novel antibody GD3A12, in normal tissues and ovarian adenocarcinomas, Histochem. Cell Biol. 132 (2009) 117–127.

[78] J.P. Li, F. Gong, K. El Darwish, M. Jalkanen, U. Lindahl, Characterization of the D-Glucuronyl C5-epimerase Involved in the Biosynthesis of Heparin and Heparan Sulfate, J. Biol. Chem. 276 (2001) 20069–20077.

[79] E. Zcharia, S. Metzger, T. Chajek-Shaul, H. Aingorn, M. Elkin, Y. Friedmann, T. Weinstein, J.P. Li, U. Lindahl, I. Vlodavsky, Transgenic expression of mammalian heparanase uncovers physiological functions of heparan sulfate in tissue morphogenesis, vascularization, and feeding behavior, Faseb J. 18 (2004) 252–263.

[80] F.E. Poulain, H.J. Yost, Heparan sulfate proteoglycans: a sugar code for vertebrate development?, Development. 142 (2015) 3456–3467.

Chapter 2

Towards embryonic-like scaffolds for skin tissue engineering: identification of effector molecules and construction of scaffolds

P.J.E. Uijtdewilligen[1]*, E.M.M. Versteeg*[1]*, C. Gilissen*[2]*, S.V. van Reijmersdal*[2]*, R. Schoppmeyer*[1]*, R.G. Wismans*[1]*, W.F. Daamen*[1] *and T.H. van Kuppevelt*[1]

[1]Department of Biochemistry, NCMLS, Radboud university medical centre, The Netherlands

[2]Department of Human Genetics, Radboud university medical centre, The Netherlands

This chapter has been published in *Journal of Tissue Engineering and Regenerative Medicine 2016;* ***10;*** *E34-E44*

Abstract

Autologous skin grafts are the gold standard for the treatment of burn wounds. In a number of cases, treatment with autologous tissue is not possible and skin substitutes are used. The outcome, however, is not optimal and improvements are needed. Inspired by scarless healing in early embryonic development, we here set out a strategy for the design and construction of embryonic-like scaffolds for skin tissue engineering. This strategy may serve as a general approach in the construction of embryonic-like scaffolds for other tissues/organs. As a first step, key effector molecules upregulated during embryonic and neonatal skin formation were identified using a comparative gene expressing analysis. A set of 20 effector molecules was identified, from which insulin-like growth factor 2 (IGF2) and sonic hedgehog (SHH) were selected for incorporation into a type I collagen–heparin scaffold. Porous scaffolds were constructed using purified collagen fibrils and 6% covalently bound heparin (to bind and protect the growth factors), and IGF2 and SHH were incorporated either individually (~0.7 and 0.4 μg/mg scaffolds) or in combination (combined ~1.5 μg/mg scaffolds). In addition, scaffolds containing hyaluronan (up to 20 μg/mg scaffold) were prepared, based on the up- or downregulation of genes involved in hyaluronan synthesis/degradation and its suggested role in scarless healing. In conclusion, based on a comprehensive gene expression analysis, a set of effector molecules and matrix molecules was identified and incorporated into porous scaffolds. The scaffolds thus prepared may create an 'embryonic-like' environment for cells to recapitulate embryonic events and for new tissues/organs.

Introduction

Third-degree and chronic wounds covering large areas need to be treated to aid the natural process of wound healing. Full- and split-thickness skin grafts are the golden standards. Treatment with a full-thickness skin graft will lead to maximal functionality and minimal scar formation. Treatment with meshed split-thickness skin grafts, however, may result in scar formation, since the graft is meshed to cover a larger wound area and contains only part of the dermis in comparison to full-thickness skin grafts (Adams and Ramsey, 2005). Both treatments create a secondary wound at the donor site, which is limited in patients with large burn wounds. In addition, both treatments are generally not used for patients with vascular disease (Adams and Ramsey, 2005; Metcalfe and Ferguson, 2007; Wood and Davies, 1995). Tissue engineered skin grafts offer an alternative in such cases (Macri and Clark, 2009). Different types of skin grafts are commercially available, including those based on decellularized cadaveric skin (*e.g.* Alloderm), those based on natural materials, such as type I collagen (*e.g.* Apligraf and Integra) and those based on synthetic materials (*e.g.* Dermagraft). Constructs are either acellular (Alloderm and Integra) or cellular (Apligraf and Dermagraft) (Supp and Boyce, 2005; van der Veen *et al.*, 2010). The current skin grafts all have their own advantages and disadvantages but share common problems, such as poor graft take due to inadequate vascularization, scarring due to improper collagen deposition and reduced functionality due to lack of appendages (Metcalfe and Ferguson, 2007). Most importantly, the outcome of tissue-engineered skin grafts is generally worse than that of full- or split-thickness skin grafts (Gurtner *et al.*, 2008), and improvements are needed. In this study, we take an alternative approach to constructing skin grafts, emanating from processes taking place during embryonic skin development.

It has long been known that embryonic wounds can heal without the formation of scar tissue (Bullard *et al.*, 2003), depending on the gestational age and size of the wound. The major differences of early embryonic scarless healing in comparison to late embryonic/adult scar healing are the lack of a fibrin clot, a reduced inflammatory response and elevated levels of effector molecules (growth factors/morphogens) important for skin morphogenesis (Bullard *et al.*, 2003; Metcalfe and Ferguson, 2007). In addition, the extracellular matrix depositions of early embryonic dermal fibroblasts and late embryonic/adult fibroblasts differ (Metcalfe and Ferguson, 2007). Addition of embryonic effector molecules and extracellular matrix components may induce embryonic-like processes leading to better wound healing, such as less contraction, less scar tissue formation, improved mechanical properties and regeneration of appendages. Mouse skin is formed from endoderm and mesoderm 7.5–17.5 days postconception (E7.5–E17.5). After birth, skin matures further, *e.g.* by the outgrowth of hairs (Rossant and Tam, 2002). Several effector molecules have been reported to be important for embryonic skin development, including members of the wingless-type MMTV integration site (WNT) family, the transforming growth factor (TGF) family, the fibroblast growth factor (FGF) family and the epidermal growth factor (EGF) family (McElwee and Hoffmann, 2000).

In this study we set out a design strategy to identify (effector) molecules associated with skin embryonic processes, and construct scaffolds containing such molecules, thereby creating an ’embryonic-like’ microenvironment. The methodology may be adopted for the construction of embryonic-like scaffolds for other tissue/organs.

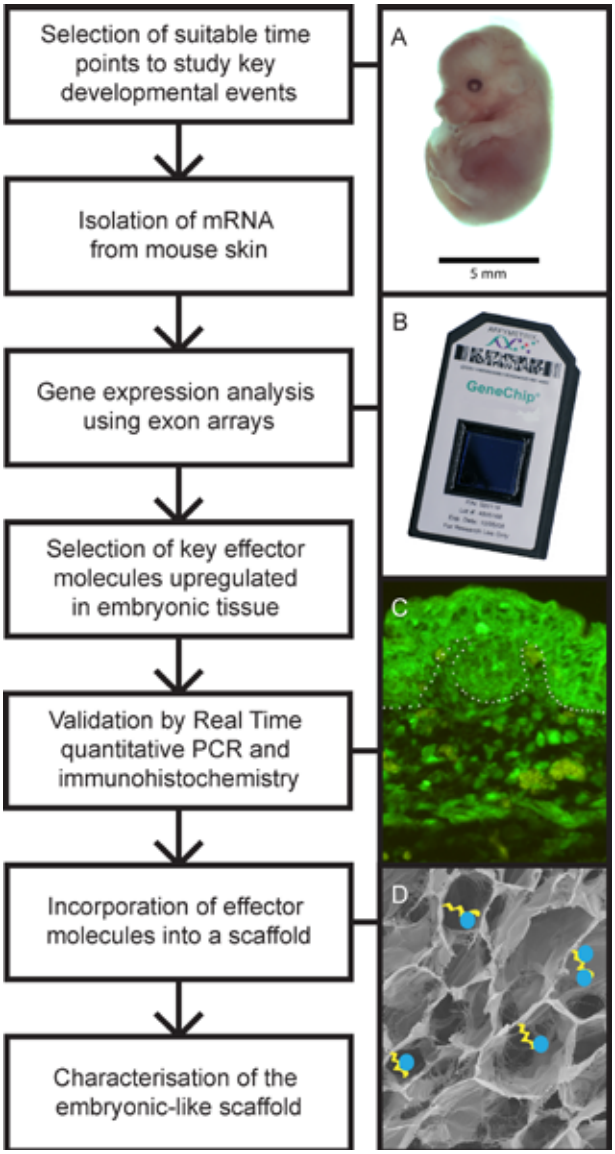

Figure 1. General design for the construction of embryonic-like scaffolds. Time points were selected, based on the literature, of important events during embryonic skin development. The picture shows an E14 embryo (A). At the selected time points, E14, E16, P1 and P90, mRNA of mouse skin was isolated and used for expression analysis with GeneChip exon arrays (B). Data were screened for differential expression of effector molecules (growth factors/morphogens). The expression of the selected molecules was validated using real-time quantitative PCR and immunohistochemistry (C); E16 skin stained for IGF2 (white dotted line depicts the basal membrane separating the epidermis and dermis). Selected effector molecules were incorporated into a type I collagen–heparin scaffold (D); SEM image of collagen scaffold with heparin (yellow lines) and effector molecules (blue spheres) schematically shown.

Materials and methods

An overview of the experimental set-up of this study is given in Figure 1.

Animals

NIH guidelines for the care and use of laboratory animals (NIH publication 85–23 Rev. 1985) were observed. The study was approved by the Ethics Committee of the Radboud University Nijmegen. C57BL6/j mice were obtained from Elevage Janvier (Le Genest Saint Isle, France). Mice 90 days of age (90 days post birth [P90]) were used for timed matings and embryos were isolated at 14 days post conception (E14), 16 days post conception (E16), and 1 day post birth (P1).

RNA isolation

For E14, skin from seven embryos (one litter) was pooled for RNA isolation. For E16, two litters of seven embryos were used for two samples (each sample from a separate litter). For P1, two litters of three pups were used for two samples (each sample from a separate litter). For P90, two individual mice were used for two samples. Dorsal-lateral skin was snap-frozen in liquid nitrogen and stored at -80^{o}C. For the E14 embryos, dorsal–lateral skin was scraped using a cryomicrotome at -20^{o}C to minimize contamination with other tissues, which was checked by haematoxylin and eosin (H&E) staining (Bancroft and Stoeltzing, 1990) (results not shown). The frozen samples were ground in a microdismembrator (Sartorius, Bunnik, The Netherlands) and RNA was isolated using the TRIZOL method (Invitrogen, Paisley, UK) in combination with RNeasy Mini kit with DNAse step (Qiagen, Hilden, Germany). RNA quality was checked using the Bioanalyser system (Agilent Technologies, Amstelveen, The Netherlands). The RNA integrity numbers and the rRNA ratios (see Supporting information, Table S1) were sufficient for gene expression analysis, based on criteria described by Schroeder *et al.* (2006).

GeneChip mouse exon 1.0 ST array

GeneChip Mouse Exon 1.0 ST arrays (exon arrays; Affymetrix, High Wycombe, UK) were used to analyse expression, using 1 µg RNA/chip. The quality of the expression data was checked based on Kadota *et al.* (2009) (see Supporting information, Table S1). Gene level expression data were calculated for the CORE transcripts (probe sets supported by RefSeq mRNAs), using Affymetrix Expression Console software with quantile normalization (all arrays are considered to have an equal intensity distribution), GC content background correction (probes with high GC content hybridize better, corrected for with built-in probes with different known GC contents) and summarization with the RMA algorithm (Lammers *et al.*, 2010). Data were imported into GeneSpring GX 7.3 (Agilent Technologies), duplicates were averaged and the expression of each transcript was normalized to the median per array. Statistical significance was tested using ANOVA and Benjamini-Hochberg multiple testing correction (Benjamini and Hochberg, 1995).

cDNA synthesis and real-time quantitative PCR (qPCR)

cDNA was made from RNA samples using the Superscript III First-Strand Synthesis system (Invitrogen) with random hexamers. cDNA was tested by conventional PCR (Fast start Taq polymerase, Roche, Almere, The Netherlands), using primers against GAPDH (forward 5`- TGATGGGTGTGAACCACGAG-3`, reverse 5`-GGGCCATCCACAGTCTTCTG-3`). The 7000 Sequence Detection System (Applied Biosystems, Warrington, UK) and the Power SYBR Green PCR Master Mix from Applied Biosystems were used for Real-time quantitative PCR (qPCR) validation with custom-designed primers (for IGF2, forward 5`-TGTGCTGCATCGCTGCTTAC-3`, reverse 5`-CGGCCTGAGAGGTAGACACG-3`; for SHH, forward 5`-GCGGCAGATATGAAGGGAAG-3`, reverse 5`-CTCCAGGCCACTGGTTCATC-3`). Primers (Isogen Bioscience, Maarssen, The Netherlands) were tested for qPCR usage based on the slope and linear regression of a standard curve (Wong and Medrano, 2005).

Expression was analysed based on the threshold cycle (CT), which was obtained using SDS 2.3 software and RQ Manager 1.2 (Applied Biosystems). The CT values were further processed using Microsoft Excel and the $2^{-\Delta\Delta CT}$ method, using GAPDH as the reference gene and P90 as the calibrator point (Livak and Schmittgen, 2001). Statistical significance was tested with an unpaired t-test (two-tailed) using SPSS 18.0 (SPSS/ IBM, Chicago, IL, USA).

Immunohistology

For paraffin sections, specimens were fixed in 4% paraformaldehyde in 0.1M phosphate buffer (PB), pH 7.4 (Sigma-Aldrich, Zwijndrecht, The Netherlands), for 4 h, stored in 70% ethanol (Royal Nedalco, Bergen op Zoom, The Netherlands) and subsequently embedded in paraffin. Paraffin sections (5 µm) were stained with H&E (Bancroft and Stoeltzing, 1990). For immunohistochemistry, sections were deparaffinized, hydrated and treated for antigen retrieval, using 0.1% trypsin (DIFCO Laboratories, Detroit, USA) for 15min at 37°C (0.1% trypsin containing 0.1% calcium chloride, pH 7.4) and subsequently in 0.01M sodium citrate buffer, pH 6.0, for 2 h at room temperature.

For cryo-sections, samples were snap-frozen in liquid nitrogen-cooled isopentane (Sigma-Aldrich, Zwijndrecht, The Netherlands); 4 µm sections were cut, mounted on Superfrost slides (Menzel-Gläser, Braunschweig, Germany) and air-dried. Before staining, the sections were fixed for 10 min in 4% paraformaldehyde. The sections were blocked with phosphate-buffered saline (PBS) containing 1% bovine serum albumin (BSA) and 0.1% Tween (PBS–T–BSA), incubated with primary antibodies in PBS–T–BSA (Table 1) and subsequently with the appropriate secondary and tertiary antibodies. After a short dehydration step with 100% ethanol, the sections were embedded in MOWIOL (Calbiochem, Darmstadt, Germany).

Table 1. Antibodies used for immunohistochemistry and Western blotting

Antibody	Supplier and catalogue no.	Secondary antibody/third antibody	Supplier and catalogue no.
Goat anti-mouse IGF2 (western blot)	R&D systems AF792	Donkey anti-goat IgG Alexa 488 conjugated	Molecular Probes A11055
Rabbit anti-mouse IGF2 (paraffin and cryo sections)	Abcam AB9574	Goat anti-rabbit IgG Alexa 488	Molecular Probes A11078
Rabbit anti-mouse SHH	Santa Cruz SC-0024	Goat anti-rabbit IgG Alexa 488	Molecular Probes A11078
Rabbit anti-rat Col1	Chemicon AB755P	Goat anti-rabbit IgG Alexa 488	Molecular Probes A11078
HA binding protein	Calbiochem 385911	Streptavidin Alexa 488	Molecular Probes S11223
HS4C3	(van Kuppevelt *et al*., 1998)	Rabbit anti-VSV/goat anti-rabbit IgG Alexa 594	Rockland Immunochemicals 600-401-386/Molecular Probes A11037

Scaffold preparation and analysis

Collagen–heparin scaffolds

Collagen scaffolds were prepared from type I collagen fibrils isolated from bovine Achilles tendon (Pieper *et al.*, 1999) and prepared by freezing and lyophilizing a 0.8% suspension in 0.25 M acetic acid (Merck) at -20°C (Pieper *et al.*, 2002). Scaffolds were crosslinked with 0.05% heparin in the crosslinking solution [33mM 1-ethyl-3-dimethyl aminopropyl carbodiimide (EDC) and 6mM N-hydroxysuccinimide (NHS) in 50mM 2-morpholinoethane sulphonic acid, pH 5.0, containing 40% ethanol (Merck)]. The crosslinking reaction was stopped by washings in 0.1M Na_2HPO_4, 1M NaCl, 2M NaCl and demineralized water. The scaffolds were frozen at -80°C using dry-ice/ethanol and lyophilized. The scaffolds used in the experiment were approximately 1mg.

Collagen–heparin–effector molecule(s) scaffolds

To incorporate the effector molecules, collagen–heparin scaffolds were incubated in 200 µl PBS containing 20 µg/ml carrier-free mouse recombinant IGF2 (792-MG, R&D Systems, Oxon, UK) and/or 10 µg/ml carrier-free mouse recombinant SHH (461-SH/CF, R&D Systems) per mg scaffold for 1 h at room temperature. The scaffolds were washed once with PBS and twice with demineralized water for 15 min.

The morphology of the scaffolds was analysed using scanning electron microscopy (SEM), using a JEOL JSM-6310 SEM at 15 kV (Daamen *et al.*, 2005). The degree of crosslinking was analysed using 2,4,6-trinitrobenzene sulphonic acid (TNBS) (Olde Damink *et al.*, 1996) and the amount of bound heparin using a hexosamine assay (Pieper *et al.*, 1999). The amount of bound growth factor was analysed using western blotting with antibodies against SHH (1:5000) and against IGF2 (1:500) (Table 1), using peroxidase-conjugated secondary antibodies and visualization using a chemiluminescent detection kit (ECL Kit, GE Healthcare, Diegem, Belgium) (Nillesen *et al.*, 2007). The amount of bound growth factor was determined in triplicate, based on a standard curve present on the gel.

Collagen–hyaluronan scaffolds

0.0125%, 0.025% or 0.05% hyaluronic acid sodium salt (Fluka, MW 1.63 x 10^3 kDa) was suspended in 0.25M acetic acid and type I collagen fibrils were added. The suspension was mixed and was allowed to swell overnight at 4°C. The swollen suspension was homogenized and lyophilized. Scaffolds were crosslinked as described above. The amount of bound hyaluronan was analysed using a modified Stains-All DPTC

(4,5,4`5`-dibenzo-3,3`-diethyl-9-methyl-thiacarbocyanine; Sigma) colorimetric assay (Edstrom, 1969). The scaffolds were digested for 1 h in a papain solution (2.5 U/ml; Sigma) in phosphate buffer (50mM Na_3PO_4, 2mM EDTA, 2mM cysteine, pH 6.5). For the calibration curve, 100 µl standards were used containing 0–5 µg hyaluronic acid sodium salt. To 100 µl of the digested scaffolds, 900 µl staining solution was added [2.8 mg Stains-all in 5ml 50% isopropanol (Merck), 42.5ml demineralized water, 100 ml 1M acetic acid (Merck) and 2.5 ml 0.01M ascorbic acid (Sigma)]. Hyaluronan contentwas measured at 650 nm. For immunohistochemistry, paraffin sections were used. Specimens were fixed and stored in Kryofix [48% ethanol (Royal Nedalco) and 7%PEG300 (Sigma)] and embedded in paraffin before use. Paraffin sections (5µm) were stained as described under *histochemistry*, but without the antigen retrieval step.

Results

Histology of developing mouse skin

Embryonic skin development was studied at four time points. At E14 the epidermis of dorsal-lateral skin was only a few cell layers thick, the dermis consisting of loosely organized cells (Figure 2A). Literature data indicate that hair follicle development is initiated at E14 by the formation of a dermal condensation (Rossant and Tam, 2002), out of which appendages are formed at E16. Appendages were found at E16 in addition to stratification of the epidermis and an organized dermis (Figure 2B). Skin at 1 day post-birth (P1) is more organized than at E16 (Figure 2C) and resembles adult skin at P90 (Figure 2D).

Selection of effector molecules

Gene expression was analysed using GeneChip Mouse Exon 1.0 ST arrays (Affymetrix). The expression data were screened for key effector molecules in embryonic skin development, using several selection steps. In the first step of the screening, we selected genes that showed significant two-fold differential expression ($p<0.05$; ANOVA) (see Supporting information, Table S2). In the second step, the resulting list was screened for effector molecules which were upregulated during embryonic

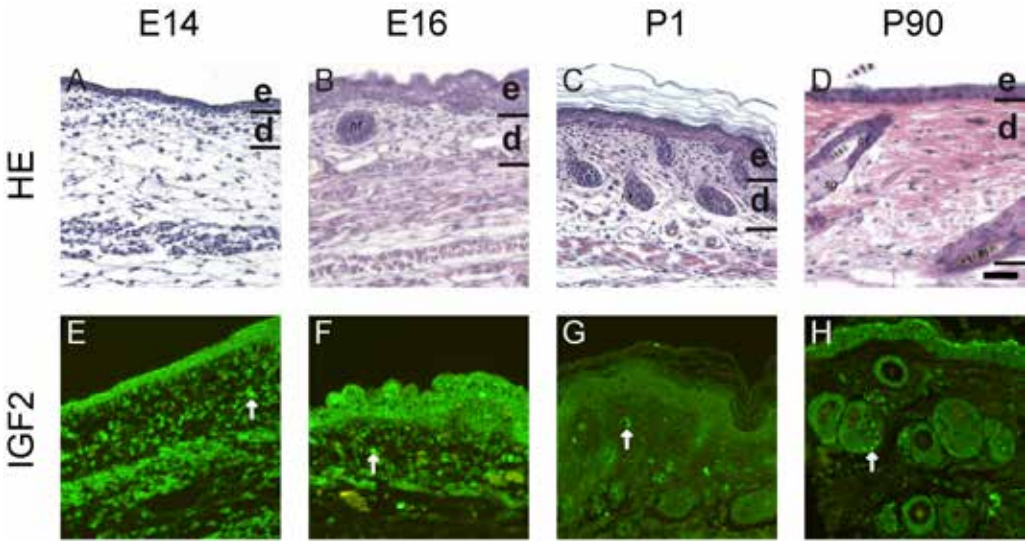

Figure 2. H&E (A–D) and immunohistochemical stainings (E–H) of various stages of mouse skin development. (A) At E14 the epidermis (e) is 2–5 cell layers thick and the dermis (d) consists of undifferentiated mesenchymal cells and dermal fibroblasts. (B) Appendages, e.g. hair follicles (hf), are clearly visible at E16. Epidermis and dermis development is well under way. (C) One day post-birth (P1), the skin is stratified and hair growth has started. (D) Adult P90 skin; a sebaceous gland is shown (sg). (E–H) Cellular staining of IGF2 was seen at E14 and E16. At P1 and P90 staining is decreased in comparison to the other time points. Scale bar=50 μm

Table 2. Gene expression data of differentially expressed effector molecules

Affymetrix transcript ID	Gene symbol	Mean E14	Mean E16	Mean P1	Mean P90	E14 vs P90		E16 vs P90		P1 vs P90	
		(arbitrary units)				$p^{\dagger}$	Fold change	$p^{\dagger}$	Fold change	$p^{\dagger}$	Fold change
6932718	*BMP3*	83.56	142.9	142.0	60.04	0.280 (0.130)	1.392	0.067 (0.008)	2.381	0.100 (0.008)	2.365
6990569	*BMP5**	94.59	15.54	13.80	13.05	0.001 (0.000)	7.247	0.141 (0.031)	1.191	0.688 (0.355)	1.057
6819442	*FGF9**	107.2	57.98	49.58	44.87	0.004 (0.000)	2.390	0.079 (0.010)	1.292	0.468 (0.151)	1.105
6810592	*FGF10*	59.26	87.66	83.48	38.97	0.138 (0.048)	1.521	0.057 (0.005)	2.250	0.094 (0.007)	2.142
7017134	*FGF13**	111.5	67.82	51.70	37.18	0.012 (0.001)	2.998	0.075 (0.009)	1.824	0.296 (0.062)	1.391
6787174	*FGF18**	205.8	88.97	88.78	74.50	0.014 (0.001)	2.763	0.445 (0.241)	1.194	0.590 (0.246)	1.192
6981854	*FGF20*	39.54	79.95	39.28	32.20	0.659 (0.471)	1.228	0.125 (0.024)	2.483	0.777 (0.485)	1.220
6818153	*GDF10**	527.9	245.6	239.7	226.2	0.028 (0.004)	2.334	0.757 (0.605)	1.086	0.894 (0.713)	1.060
6972317	*IGF2**	2025	1897	1778	33.96	0.001 (0.000)	59.61	0.002 (0.000)	55.86	0.002 (0.000)	52.36
6942654	*PDGFa**	325.3	379.2	377.7	161.6	0.028 (0.004)	2.013	0.035 (0.002)	2.347	0.057 (0.002)	2.338
6898686	*PDGFc**	334.2	342.8	161.9	155.3	0.019 (0.002)	2.152	0.035 (0.002)	2.207	0.902 (0.731)	1.042
6936889	*SHH*	32.41	115.4	249.2	54.51	0.448 (0.256)	0.595	0.308 (0.129)	2.117	0.152 (0.018)	4.571
6802449	*TGFβ3**	331.2	195.4	288.3	138.8	0.026 (0.004)	2.386	0.238 (0.081)	1.408	0.100 (0.008)	2.077
6951974	*WNT2*	91.27	97.65	96.41	29.95	0.057 (0.014)	3.047	0.082 (0.011)	3.260	0.122 (0.012)	3.219
6907887	*WNT2b**	66.61	61.78	48.39	30.43	0.009 (0.001)	2.189	0.024 (0.001)	2.030	0.077 (0.004)	1.590
6750567	*WNT6**	116.0	97.73	86.16	36.63	0.011 (0.001)	3.166	0.032 (0.002)	2.668	0.064 (0.003)	2.352
6955539	*WNT7a*	41.24	36.32	28.36	19.48	0.060 (0.015)	2.117	0.131 (0.027)	1.865	0.395 (0.108)	1.456
6837582	*WNT7b**	128.3	202.4	106.8	55.86	0.072 (0.019)	2.297	0.050 (0.004)	3.623	0.237 (0.041)	1.912
6838399	*WNT10b*	70.83	155.6	128.7	55.33	0.629 (0.438)	1.280	0.120 (0.023)	2.812	0.240 (0.042)	2.325
6944581	*WNT16**	28.66	58.35	41.52	24.29	0.358 (0.185)	1.180	0.026 (0.001)	2.402	0.093 (0.007)	1.710

Twenty growth factors were found with significant two-fold differential expression using ANOVA ($p < 0.05$).
*Using the more stringent Benjamini–Hochberg multiple testing correction, the expression of only 13 growth factors was found to be significant ($p < 0.05$).
†The p value given within brackets is the value obtained using ANOVA.

development. These molecules, *e.g.* growth factors and morphogens, were identified on the basis of their assigned function (growth factor, morphogen, mitogen), as available in the Gene database of NCBI (www.ncbi.nlm.nih. gov) and the database of Ensembl (www.ensembl.org). In the third and last step, the expression data of the effector molecules was studied for upregulation at the embryonic and/or early postnatal time points (E14, E16 and/or P1) in comparison to P90.

The search resulted in a list of 20 growth factors (Table 2) significantly upregulated ($p<0.05$; ANOVA) at one or more of the time points in comparison to P90. Additional statistical validation of the results using Benjamini–Hochberg multiple testing correction (Benjamini and Hochberg,1995), shortened the list to 13 growth factors. It was decided to keep the seven genes in the selection, since literature data suggested an important role in embryonic development (Bayle *et al.*, 2008; Kalinina *et al.*, 2009; Kettunen *et al.*, 2006; Nanba *et al.*, 2003; Tao *et al.*, 2002; Wang and Shackleford, 1996; Woods *et al.*, 2006). From the list of 20, two growth factors were selected for incorporation into scaffolds, IGF2 and SHH. IGF2 was>50-fold upregulated during embryonic development (E14 and E16) and at P1. These results were validated by real-time qPCR and immunohistochemistry. Validation of IGF2 expression by qPCR confirmed the data observed with the exon array (*e.g.* fold change E16 vs P90: 342 ± 47, $p<0.05$). Immunohistochemistry showed a strong staining of IGF2 at E14 and E16 both in the dermis and epidermis (Figure 2E–H). Staining at P1, however, was less intense and more comparable to staining at P90. These results suggested that IGF2 protein is primarily present in the embryonic stages, despite the high level of mRNA expression at P1 in the microarray.

SHH was selected because, next to IGF2, its mRNA was upregulated when comparing neonatal to adult skin (about 4.6-fold at P1; Table 2), which was confirmed by qPCR (fold change P1 vs P90: 6.4 ± 2.5, $p<0.05$). SHH plays a prominent role in appendage development (St-Jacques *et al.*, 1998). In addition, it is a heparin-binding protein (Zhang *et al.*, 2007). Several attempts were made to stain SHH using tissue sections, but were unsuccessful.

Table 3. Characteristics of type I collagen–heparin scaffolds with bound IGF2 and SHH, and of type I collagen–hyaluronan scaffolds

	Crosslinking efficiency (%) (mean ± sd)	Amount of bound heparin (µg/mg scaffold) (mean ± sd)	Amount of bound hyaluronan (µg/mg scaffold) (mean ± sd)	Amount of bound IGF2 (µg/mg scaffold) (mean ± sd)	Amount of bound SHH (µg/mg scaffold) (mean ± sd)
Col-Hep-IGF2	49 ± 1	59 ± 9	–	0.7 ± 0.2	–
Col-Hep-IGF2-SHH	49 ± 1	59 ± 9	–	0.8 ± 0.1	0.7 ± 0.1
Col-Hep-SHH	49 ± 1	59 ± 9	–	–	0.4 ± 0.1
Col-Ha-0.0500	36 ± 8	–	20 ± 8	–	–
Col-Ha-0.0250	35 ± 8	–	13 ± 4	–	–
Col-Ha-0.0125	35 ± 10	–	8 ± 3	–	–

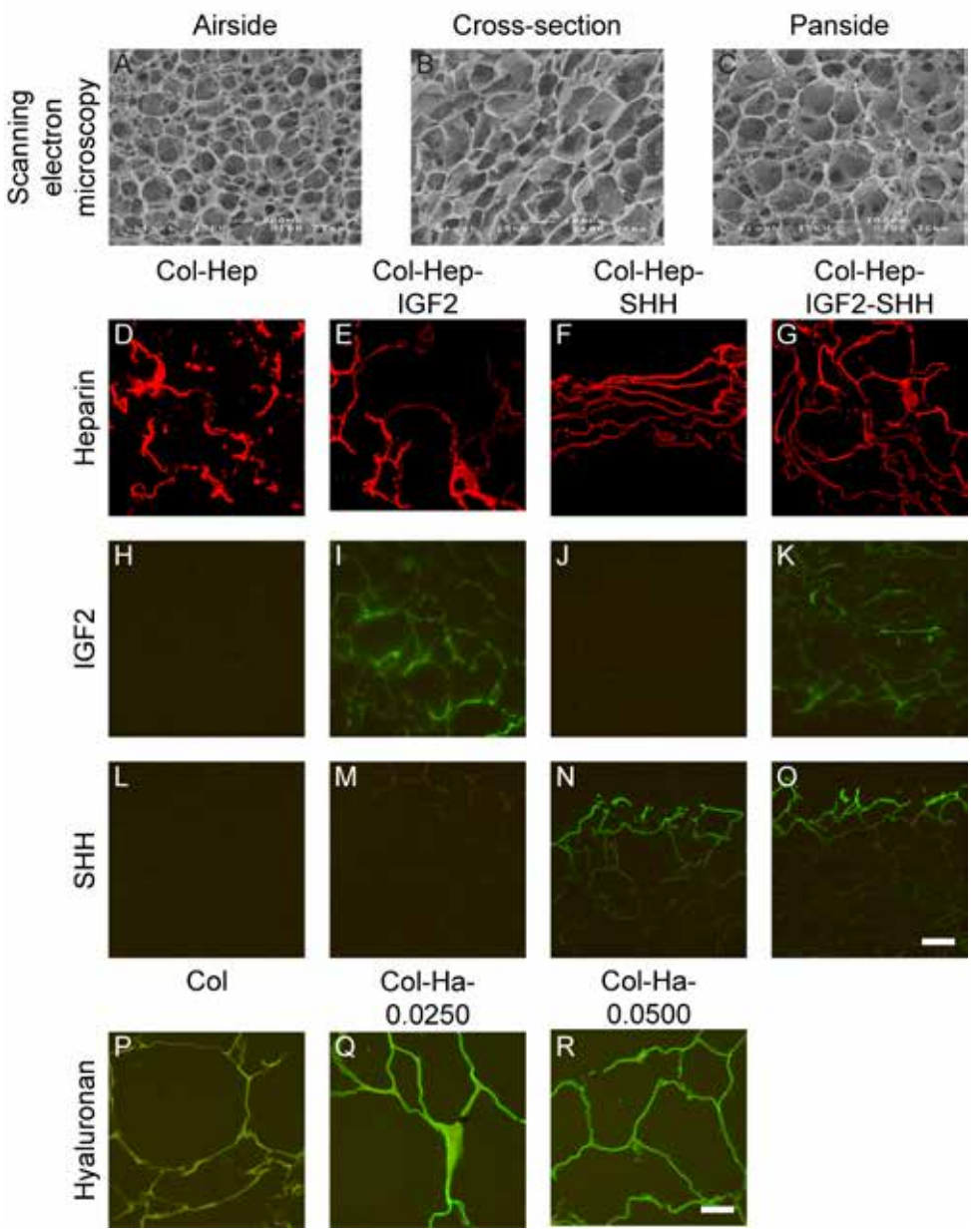

Figure 3. Scaffold structure and distribution of heparin, IGF2, SHH and hyaluronan in the prepared embryonic-like scaffolds. (A–C) SEM images show the porous structure of type I collagen–heparin scaffolds. (D–G) Staining of heparin was found in the scaffold crosslinked with heparin. (H–K) IGF2 and (L–O) SHH staining was found in the scaffold loaded with one or both of the growth factors. (P–S) Hyaluronan staining showed it was successfully incorporated using a concentration of 0.0250% (Col–Ha-0.0250, Q) or 0.0500% (Col–Ha-0.0500, R). Hyaluronan staining was not observed in the control (CX, P; note that the control shows yellow background staining). Scale bar=100 μm (A–O); 50 μm (P–R)

Preparation and evaluation of embryoniclike scaffolds

Scaffolds containing effector molecules

To study the possibility of incorporation of the growth factors into collagen constructs, we made type I collagen–heparin scaffolds and loaded them with IGF2 and SHH. Heparin was added because it binds growth factors (*e.g.* SHH), and may promote their sustained release (Geutjes *et al.*, 2006). Sonic hedgehog was added to the scaffolds since it was significantly upregulated at P1 vs P90 (ANOVA analysis), plays a crucial role in development, and because of its favourable heparin-binding properties (Nanba *et al.*, 2003; St-Jacques *et al.*, 1998; Zhang *et al.*, 2007). Type I collagen is used in our scaffold design since it is the main collagen in skin (Rossant and Tam, 2002) and shows various favourable properties for scaffold design, *e.g.* low immunogenicity and good handling (Geutjes *et al.*, 2006; Pieper *et al.*, 1999).

Type I collagen scaffolds were crosslinked with an EDC/NHS solution in the presence of 0.05% heparin, resulting in 49 ± 1% (mean ± SD, n=3) reduction in primary amine groups indicating crosslinking (Table 3). The amount of heparin bound to the scaffold was 59 ± 9 µg heparin/mg scaffold (mean ± SD, n=3) (Table 3). The incorporation of heparin was also evaluated by immunohistochemistry (Figure 3D–G). Heparin staining was found predominantly at the edges of the scaffold. The scaffolds had a porous structure, as visualized using SEM (Figure 3A–C).

The scaffolds were loaded with IGF2 and SHH. Growth factor incorporation was studied by western blotting and immunohistochemistry. A collagen–heparin crosslinked scaffold loaded with IGF2 (Col–Hep–IGF2) contained 0.7 ± 0.2 µg IGF2/mg scaffold (mean ± SD, n=3). Loading of SHH (Col–Hep–SHH) resulted in 0.4 ± 0.1 µg SHH/mg scaffold. A scaffold loaded with both growth factors (Col–Hep–IGF2–SHH) contained 0.8 ± 0.1 µg IGF2 and 0.7 ± 0.1 µg SHH/mg scaffold (Table 3, Figure 4). Results are given as average ± SD (n=3). Immunohistochemistry was used to visualize the distribution of IGF2 and SHH. Both SHH and IGF2 were found predominantly at the edge of the scaffold, similar to heparin (Figure 3H–O).

Table 4. Gene expression data of enzymes involved in hyaluronan synthesis/degradation

Affymetrix transcript ID	Gene symbol	Mean E14	Mean E16	Mean P1	Mean P90	E14 vs P90		E16 vs P90		P1 vs P90	
		(arbitrary units)				$p^{\dagger}$	Fold change	$p^{\dagger}$	Fold change	$p^{\dagger}$	Fold change
6854042	*HAS1*	15.78	30.80	32.40	19.90	0.465 (0.271)	0.793	0.226 (0.074)	1.548	0.278 (0.055)	1.628
6835856	*HAS2*	208.9	195.3	139.1	99.16	0.095 (0.028)	2.107	0.157 (0.038)	1.969	0.537 (0.202)	1.403
6978932	*HAS3*	46.78	162.6	151.7	40.72	0.861 (0.746)	1.149	0.128 (0.026)	3.994	0.202 (0.030)	3.726
6992224	*HYAL1*	40.99	59.02	106.7	265.8	0.003 (0.000)	0.154	0.011 (0.000)	0.222	0.041 (0.001)	0.402
6992221	*HYAL2*	126.5	99.45	124.5	108.4	0.410 (0.224)	1.167	0.653 (0.470)	0.918	0.610 (0.266)	1.149
6992228	*HYAL3*	23.52	35.03	29.98	26.36	0.499 (0.303)	0.892	0.166 (0.042)	1.329	0.599 (0.254)	1.137

$^{\dagger}p$ values are calculated using Benjamini–Hochberg multi-testing correction. *p* values within brackets are obtained using ANOVA

Scaffolds containing hyaluronan

Literature data indicate an increased content of hyaluronate (HA) in embryonic skin (Metcalfe and Ferguson, 2007). Trends observed in the gene expression data on embryonic skin development are in line with this observation, since hyaluronan synthase 2 (HAS2) was 2.1-fold upregulated at E14 and the expression of HAS3 was >3.5-fold upregulated at E16 and P1. The gene expression for HYAL1 (hyaluronidase, involved in breakdown of HA) was 6.5-, 4.5- and 2.5-fold downregulated with respect to P90 at E14, E16 and P1, respectively (Table 4).

Collagen scaffolds with covalently bound hyaluronan were constructed by mixing the collagen suspension with hyaluronate, freezing, lyophilization and crosslinking. This method is different from the construction of type I collagen–heparin scaffolds, where heparin is added to the scaffold during the crosslinking step. Crosslinking resulted in 36 ± 8%, 35 ± 8% and 35 ± 10% (mean ± SD, n=3) of reduction in primary amine groups in scaffolds to which 0.0500% (Col–Ha-0.0500), 0.0250% (Col–Ha-0.0250) or 0.0125% (Col–Ha-0.0125) of hyaluronan was added, respectively (Table 3).

The amount of hyaluronan bound to the scaffolds was determined using a modified Stains-All colorimetric assay (Edstrom, 1969). The scaffolds contained 20 ± 8, 13 ± 4 and 8 ± 3 µg (mean ± SD, n=3) of hyaluronan/mg scaffold for Col–Ha-0.0500, Col–Ha-0.0250 and Col–Ha-0.0125, respectively (Table 3). Immunohistochemistry showed that hyaluronan was distributed throughout the scaffold (Figure 3P–R). The scaffold morphology was similar to that observed for collagen–heparin scaffolds (data not shown).

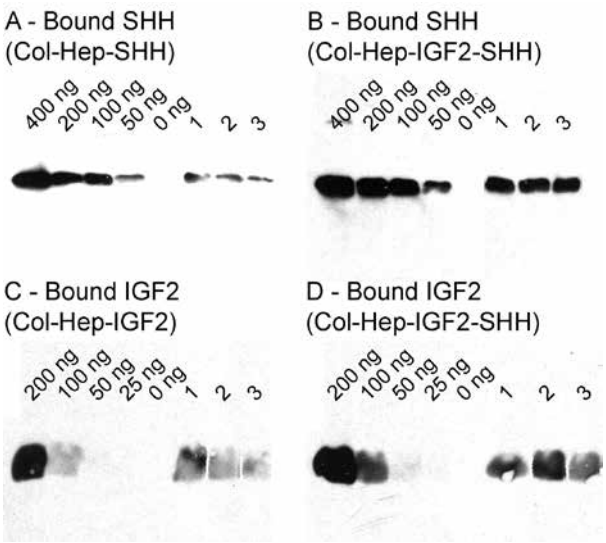

Figure 4. Growth factors bound to scaffolds analysed by western blot. SHH bound to the collagen–heparin scaffold is shown in blot A and SHH bound in combination with IGF2 is shown in blot B. In blots C andD, IGF2 bound to the collagen–heparin scaffold is shown without or in combination with SHH. Three separate growth factor incubations were analysed (samples 1–3). Based on the calibration curve, the amount of growth factor is estimated and corrected for the volume used and the amount of scaffold in the initial sample.

Discussion

In this study we laid down a general strategy to construct embryonic-like skin constructs as an alternative to current skin grafts. It is our hypothesis that incorporation of effector molecules, upregulated in embryonic skin development, can stimulate embryonic-like processes in the adult wound and may ultimately lead to better skin regeneration, *e.g.* without contraction or scar formation (Metcalfe and Ferguson, 2007).

Selection of effector molecules

Using high-density gene expression arrays, 20 candidate effector molecules were found upregulated during skin development. Six of them have been reported to play an important role in skin development, underscoring the validity of the selection procedure used here. FGF10 and IGF2 are involved in epidermal development (Bennett *et al.*, 2003; Tao *et al.*, 2002) and platelet-derived growth factor-a (PDGFa) in dermal development (Betsholtz *et al.*, 2001). WNT10b and SHH have been reported to regulate appendage formation, *e.g.* hair follicles (Nanba *et al.*, 2003; Ouji *et al.*, 2008). TGFb3 is expressed in the epidermis, dermis and hair follicles during skin development, but its specific function remains to be elucidated (Pelton *et al.*, 1991). FGF10 is suggested to have a role in the early stages of adult wound healing, since expression is upregulated 1 day after wounding (Tagashira *et al.*, 1997).

In addition to the six genes with a described/proposed function, we found 14 genes with an unknown function in skin development but a reported function in other developmental processes. Additional research is needed to elucidate their role during skin development, especially because some genes show favourable properties. FGF9, for instance, could be involved in dermal and appendage development via stimulation of SHH and FGF10 (White *et al.*, 2006). Another example is WNT2 and WNT2b, which could have a function in dermal development, based on a fibrillin-1 skin fibrosis model in which WNT2 and WNT2B are upregulated after an in-frame duplication of the fibrillin-1 gene (Bayle *et al.*, 2008). Thus, 14 new effector molecules were identified using the strategy taken, in addition to the confirmation of six genes with a known role in skin development. The novel effector molecules may be important for the construction of new biomaterials.

Scaffolds containing effector molecules

The basic scaffold for incorporation of effector molecules was based on collagen fibrils to which heparin was covalently attached. Heparin binds, protects and modulates a large number of effector molecules, including a number of the molecules identified in this study, such as FGF9 and FGF20 (Kalinina *et al.*, 2009), FGF10 (Izvolsky *et al.*, 2003), FGF18 (Chuang *et al.*, 2010), PDGFa (Feyzi *et al.*, 1997), SHH (Zhang *et al.*, 2007) bone morphogenetic protein 3 (BMP3), BMP5, growth differentiation factor 10 (GDF10) (Cunningham *et al.*, 1995) and the WNT proteins (Lin 2004). TGFb3 and IGF2, however, are reported not to bind to heparin (Arai *et al.*,1996; Lyon *et al.*,1997), although the latter could be incorporated in a collagen–heparin-based construct.

To test whether it is possible to make an embryonic-like construct, we decided to make a collagen–heparin scaffold containing IGF2 and SHH. IGF2 induces proliferation of

transient amplifying cells or stem cells in the basal epidermal layer (Bennett *et al.*, 2003) and stimulates angiogenesis via VEGF in the dermis (Kim and Kim, 2005). Stimulation of angiogenesis may lead to better graft take through faster vascularization (Metcalfe and Ferguson, 2007). SHH induces proliferation of cells in both the basal epidermal layer and the dermal layer and potentially even induces appendage formation (Nanba *et al.*, 2003; St-Jacques *et al.*, 1998; Zhou *et al.*, 2006). Restoring appendages could increase the functionality of the repaired/regenerated skin (Metcalfe and Ferguson, 2007). Both effector molecules could be successfully incorporated in the scaffolds, either individually or in combination, and at a concentration high enough to exert a biological effect. Although functional testing of the embryonic-like scaffold remains to be carried out, we showed that the construction of a scaffold that may induce an embryonic-like microenvironment is feasible.

Scaffolds containing specific matrix molecules

Literature data suggested that hyaluronan is an important extracellular matrix component during embryonic scarless wound healing (Metcalfe and Ferguson, 2007; Toole, 2001). This observation was confirmed by the gene expression data of hyaluronan synthesis-related genes. Therefore, we decided to incorporate hyaluronan in our scaffolds and we were able to create collagen–hyaluronan scaffolds that contained up to 20 µg hyaluronan/mg scaffold. Hyaluronan has an important role in late embryonic and adult wound healing. It regulates the inflammatory response, organizes the granulation tissue matrix and facilitates cell proliferation and migration (Chen and Abatangelo, 1999). Based on the role of hyaluronan during embryonic development and embryonic/adult wound healing, we suggest that incorporation of hyaluronan into a tissue-engineered skin graft may accelerate and improve wound healing. Currently, one hyaluronan-based skin graft, Hyalomatrix (Price *et al.*, 2007), is commercially available and is reported to promote neodermis formation (Myers *et al.*, 2007). Based on the described effects of Hyalomatrix and the properties of hyaluronan, addition of hyaluronan to a type I collagen construct may lead to better neodermis formation (Myers *et al.*, 2007) and enhanced cell proliferation and migration in the dermal compartment (Chen and Abatangelo, 1999). Combined with effector molecules, such a scaffold may recapitulate early events of skin generation and thus contribute to proper regeneration of skin tissue.

Conclusion

In this study we propose a general strategy to design and construct 'embryonic-like' scaffolds targeted to create a microenvironment which may stimulate cells to take an embryonic-like approach to regenerate tissues and organs. We have shown the feasibility of the identification of effector molecules upregulated during development by gene expression microarrays, and of the subsequent construction of scaffolds containing such molecules. The approach may be generally applicable for the design of embryonic-like scaffolds for other tissues/organs. *In vitro*/*in vivo* testing should be the next step to evaluate the functionality of the scaffolds.

Acknowledgements

This study was financially supported by the Dutch Programme for Tissue Engineering (Grant No. DPTE6735). We would like to thank the Microarray Facility Nijmegen of the Radboud university medical centre, The Netherlands, for carrying out the array experiments and assistance with the data analysis. We would also like to thank the Department of Rheumatology, Radboud university medical centre, for help in setting up the real-time qPCR validation. The Central Animal Laboratory of Radboud university medical centre is acknowledged for assistance with the animal experiments.

Conflict of interest

The authors have declared that there is no conflict of interest.

Author contributions

P.J.E.U., Ph.D. student responsible for project; E.M.M.V., technician responsible for tissue-engineering protocols; C.G., bioinformatician responsible for microarray analysis; S.V.v.R., technician responsible for microarray runs; R.S., student responsible for hyaluronan part; R.G.W., technician responsible for histology; W.F.D., project leader; T.H.v.K., group leader.

Supporting information on the internet

The following supporting information may be found in the online version of this article:

Table S1. RNA quality and accuracy of expression data

Table S2. Expression data of genes with significant two-fold differential expression in comparison to P90 ($p<0.05$, based on ANOVA)

References

Adams DC, Ramsey ML. 2005; Grafts in dermatologic surgery: review and update on full- and split-thickness skin grafts, free cartilage grafts, and composite grafts. Dermatol Surg 31: 1055–1067.

Arai T, Busby W Jr, Clemmons DR. 1996; Binding of insulin-like growth factor (IGF) I or II to IGF-binding protein-2 enables it to bind to heparin and extracellular matrix. Endocrinology 137: 4571–4575.

Bancroft JD, Stoeltzing O. 1990; Theory and Practice of Histological Techniques. Churchill Livingston: Edinburgh, UK.

Bayle J, Fitch J, Jacobsen K, *et al.* 2008; Increased expression of Wnt2 and SFRP4 in Tsk mouse skin: role of Wnt signaling in altered dermal fibrillin deposition and systemic sclerosis J Invest Dermatol 128: 871–881.

Benjamini Y, Hochberg Y. 1995; Controlling the false discovery rate: a practical and powerful approach to multiple testing. J R Statist Soc B 57: 289–300.

Bennett WR, Crew TE, Slack JM, *et al.* 2003; Structural-proliferative units and organ growth: effects of insulin-like growth factor 2 on the growth of colon and skin. Development 130: 1079–1088.

Betsholtz C, Karlsson L, Lindahl P. 2001; Developmental roles of platelet-derived growth factors. Bioessays 23: 494–507.

Bullard KM, Longaker MT, Lorenz HP. 2003; Fetal wound healing: current biology. World J Surg 27: 54–61.

Chen WY, Abatangelo G. 1999; Functions of hyaluronan in wound repair. Wound Repair Regen 7: 79–89.

Chuang CY, Lord MS, Melrose J, *et al.* 2010; Heparan sulfate-dependent signaling of fibroblast growth factor 18 by chondrocyte-derived perlecan. Biochemistry 49: 5524–5532.

Cunningham NS, Jenkins NA, Gilbert DJ, *et al.* 1995; Growth/differentiation factor-10: a new member of the transforming growth factor-b superfamily related to bone morphogenetic protein-3. Growth Factors (Chur, Switzerland) 12: 99–109.

Daamen WF, Hafmans T, Veerkamp JH, *et al.* 2005; Isolation of intact elastin fibers devoid of microfibrils. Tissue Eng 11: 1168–1176.

Edstrom RD. 1969; A colorimetric method for the determination of mucopolysaccharides and other acidic polymers. Anal Biochem 29: 421–432.

Feyzi E, Lustig F, Fager G, *et al.* 1997; Characterization of heparin and heparan sulfate domains binding to the long splice variant of platelet-derived growth factor A chain. J Biol Chem 272: 5518–5524.

Geutjes PJ, Daamen WF, Buma P, *et al.* 2006; From molecules to matrix: construction and evaluation of molecularly defined bioscaffolds. Adv Exp Med Biol 585: 279–295.

Gurtner GC, Werner S, Barrandon Y, *et al.* 2008; Wound repair and regeneration. Nature 453: 314–321.

Izvolsky KI, Shoykhet D, Yang Y, *et al.* 2003; Heparan sulfate–FGF10 interactions during lungmorphogenesis. Dev Biol 258: 185–200.

Kadota K, Nakai Y, Shimizu K. 2009; Ranking differentially expressed genes from Affymetrix gene expression data: methods with reproducibility, sensitivity, and specificity. Algorithm Mol Biol 4: 7.

Kalinina J, Byron SA, Makarenkova HP, *et al.* 2009; Homodimerization controls the fibroblast growth factor 9 subfamily's receptor binding and heparan sulfatedependent diffusion in the extracellular matrix. Mol Cell Biol 29: 4663–4678.

Kettunen P, Nie X, Kvinnsland IH, *et al.* 2006; Histological development and dynamic expression of Bmp2–6 mRNAs in the embryonic and postnatal mouse cranial base. Anat Rec 288: 1250–1258.

Kim HJ, Kim TY. 2005; Regulation of vascular endothelial growth factor expression by insulin-like growth factor-II in human keratinocytes, differential involvement of mitogen-activated protein kinases and feedback inhibition of protein kinase C. Br J Dermatol 152: 418–425.

Lammers G, Gilissen C, Nillesen ST, *et al.* 2010; High density gene expression microarrays and gene ontology analysis for identifying processes in implanted tissue engineering constructs. Biomaterials 31:8299–8312.

Lin X. 2004; Functions of heparan sulfate proteoglycans in cell signaling during development. Development 131: 6009–6021.

Livak KJ, Schmittgen TD. 2001; Analysis of relative gene expression data using realtime quantitative PCR and the 2–ΔΔCT method. Methods 25: 402–408.

Lyon M, Rushton G, Gallagher JT. 1997; The interaction of the transforming growth factor-bs with heparin/heparan sulfate is isoform-specific. J Biol Chem 272:18000–18006.

Macri L, Clark RA. 2009; Tissue engineering for cutaneous wounds: selecting the proper time and space for growth factors, cells and the extracellular matrix. Skin Pharmacol Physiol 22: 83–93.

McElwee K, Hoffmann R. 2000; Growth factors in early hair follicle morphogenesis. Eur J Dermatol 10: 341–350.

Metcalfe AD, Ferguson MW. 2007; Tissue engineering of replacement skin: the crossroads of biomaterials, wound healing, embryonic development, stem cells and regeneration. J R Soc Interface 4: 413–437.

Myers SR, Partha VN, Soranzo C, *et al.* 2007; Hyalomatrix: a temporary epidermal barrier, hyaluronan delivery, and neodermis induction system for keratinocyte stem cell therapy. Tissue Eng 13: 2733–2741.

Nanba D, Nakanishi Y, Hieda Y. 2003; Role of Sonic hedgehog signaling in epithelial and mesenchymal development of hair follicles in an organ culture of embryonic mouseskin. Dev Growth Differ 45: 231–239.

Nillesen ST, Geutjes PJ, Wismans R, *et al.* 2007; Increased angiogenesis and blood vessel maturation in acellular collagen– heparin scaffolds containing both FGF2 and VEGF. Biomaterials 28: 1123–1131.

Olde Damink LH, Dijkstra PJ, van Luyn MJ, *et al.* 1996; Cross-linking of dermal sheep collagen using a water-soluble carbodiimide. Biomaterials 17: 765–773.

Ouji Y, Yoshikawa M, Moriya K, *et al.* 2008; Wnt-10b, uniquely among Wnts, promotes epithelial differentiation and shaft growth. Biochem Biophys Res Commun 367: 299–304.

Pelton RW, Saxena B, Jones M, *et al.* 1991; Immunohistochemical localization of TGFb1, TGFb2 and TGFb3 in the mouse embryo: expression patterns suggest multiple roles during embryonic development. J Cell Biol 115: 1091–1105.

Pieper JS, Hafmans T, van Wachem PB, *et al.* 2002; Loading of collagen–heparan sulfate matrices with bFGF promotes angiogenesis and tissue generation in rats. J Biomed Mater Res 62: 185–194.

Pieper JS, Oosterhof A, Dijkstra PJ, *et al.* 1999; Preparation and characterization of porous crosslinked collagenous matrices containing bioavailable chondroitin sulphate. Biomaterials 20: 847–858.

PriceRD, BerryMG,Navsaria HA; 2007;Hyaluronic acid: the scientific and clinical evidence. J Plast Reconstr Aesthet Surg 60: 1110–1119.

Rossant J, Tam PPL. 2002; Mouse Development: Patterning, Morphogenesis and Organogenesis. Academic Press: London, UK.

Schroeder A, Mueller O, Stocker S, *et al.* 2006; The RIN: an RNA integrity number for assigning integrity values to RNA measurements. BMC Mol Biol 7: 3.

St-Jacques B, Dassule HR, Karavanova I, *et al.* 1998; Sonic hedgehog signaling is essential for hair development. Curr Biol 8: 1058–1068.

Supp DM, Boyce ST. 2005; Engineered skin substitutes: practices and potentials. Clin Dermatol 23: 403–412.

Tagashira S, Harada H, Katsumata T, *et al.* 1997; Cloning of mouse FGF10 and upregulation of its gene expression during wound healing. Gene 197: 399–404.

Tao H, Yoshimoto Y, Yoshioka H, *et al.* 2002; FGF10 is a mesenchymally derived stimulator for epidermal development in the chick embryonic skin. Mech Dev 116: 39–49.

Toole BP. 2001; Hyaluronan in morphogenesis. Semin Cell Dev Biol 12: 79–87. van der Veen VC, van derWalMB, van Leeuwen MC, *et al.* 2010; Biological background of dermal substitutes. Burns 36: 305–321.

van Kuppevelt TH, Dennissen MA, van Venrooij WJ, *et al.* 1998; Generation and application of type-specific anti-heparan sulfate antibodies using phage display technology. Further evidence for heparan sulfate heterogeneity in the kidney. J Biol Chem 273: 12960–12966.

Wang J, Shackleford GM. 1996; Murine Wnt10a and Wnt10b: cloning and expression in developing limbs, face and skin of embryos and in adults. Oncogene 13: 1537–1544.

White AC, Xu J, Yin Y, *et al.* 2006; FGF9 and SHH signaling coordinate lung growth anddevelopment through regulation of distinct mesenchymal domains. Development 133: 1507–1517.

Wong ML, Medrano JF. 2005; Real-time PCR for mRNA quantitation. Biotechniques 39:75–85.

Wood MK, Davies DM. 1995; Use of split-skin grafting in the treatment of chronic leg ulcers. Ann R Coll Surg Engl 77: 222–223.

Woods CG, Stricker S, Seemann P, *et al.* 2006; Mutations in WNT7A cause a range of limb malformations, including Fuhrmann syndrome and Al-Awadi–Raas- Rothschild–Schinzel phocomelia syndrome. Am J Hum Genet 79: 402–408.

Zhang F, McLellan JS, Ayala AM, *et al.* 2007; Kinetic and structural studies on interactions between heparin or heparan sulfate and proteins of the hedgehog signaling pathway. Biochemistry 46: 3933–3941.

Zhou JX, Jia LW, Liu WM, *et al.* 2006; Role of sonic hedgehog in maintaining a pool of proliferating stem cells in the human fetal epidermis. Hum Reprod 21: 1698–1704.

Chapter 3

Visualisation of newly synthesised collagen *in vitro* and *in vivo*

*Corien Oostendorp[1#], **Peter J.E. Uijtdewilligen[1#]**, Elly M. Versteeg[1], Theo G. Hafmans[1], Ellen H. van den Bogaard[2], Paul K.J.D. de Jonge[3], Ali Pirayesh[4], Johannes W. Von den Hoff[5], Ernst Reichman[6], W.F. Daamen[1] and T.H. van Kuppevelt[1]*

[1]Radboud university medical center, Radboud Institute for Molecular Life Sciences, Department of Biochemistry, Nijmegen, The Netherlands.

[2]Radboud university medical center, Radboud Institute for Molecular Life Sciences, Department of Dermatology, The Netherlands.

[3]Radboud university medical center, Radboud Institute for Molecular Life Sciences, Department of Urology, Nijmegen, The Netherlands.

[4]Ghent University Hospital, Burn Center, Department of Plastic and Reconstructive Surgery, Ghent, Belgium.

[5]Radboud university medical center, Department of Orthodontics and Craniofacial Biology, Nijmegen, The Netherlands.

[6]University Children's Hospital Zurich, Department of Surgery, Tissue Biology Research Unit, Zurich, Switzerland

 # These authors contributed equally to this work.

This chapter has been published in *Scientific reports 2016; **6**; 18780*

Abstract

Identifying collagen produced *de novo* by cells in a background of purified collagenous biomaterials poses a major problem in for example the evaluation of tissue-engineered constructs and cell biological studies to tumor dissemination. We have developed a universal strategy to detect and localize newly deposited collagen based on its inherent association with dermatan sulfate. The method is applicable irrespective of host species and collagen source.

Introduction

Collagen, the most abundant protein family in the human body, plays a pivotal role in the organization of tissues and organs, and is a major determinant during organogenesis. In the field of tissue engineering and regenerative medicine, type I collagen is a key biomaterial[1] whereas in other fields, notably cancer research, collagen gels are frequently used in 3D studies to the migrational behavior of cells[2].

A common challenge in the field is to make a distinction between the collagen synthesized by cells and the (abundant) pre-existing collagen present in the biomaterial. Antibodies raised against collagens are of limited use due to the highly conserved nature of collagens[3] and the associated cross reactivity between collagen from different species. Other methods like metabolic radiolabeling and mass spectrometry[4] are laborious and do not provide information about the topography and organization of the newly synthesized collagen fibers.

In this study we evaluated newly synthesized fibrillar collagen (*e.g.* type I collagen), by making use of the inherent and intrinsic association of the glycosaminoglycan dermatan sulfate with collagen fibrils. Dermatan sulfate is the glycosaminoglycan part of the proteoglycans decorin and biglycan, which are both collagen fibril-associated molecules that play a role in the regulation of collagen fibril diameter. These proteoglycans remain present on the mature collagen fibril (Fig. 1a, cartoon), and therefore dermatan sulfate is associated with collagen fibrils[5,6]. The technique described here is based on the selective detection of dermatan sulfate using the single chain variable fragment antibody GD3A12[7], combined with the absence of dermatan sulfate in experimentally or commercially produced biomaterials. We tested the technique both *in vivo* and *in vitro* using a number of collagenous biomaterials including gels cultured with human fibroblasts with or without keratinocytes (denovoSkin and denovoDerm respectively)[8], experimental and commercially available scaffolds, and glycerol preserved acellular human dermis (Glyaderm®)[9].

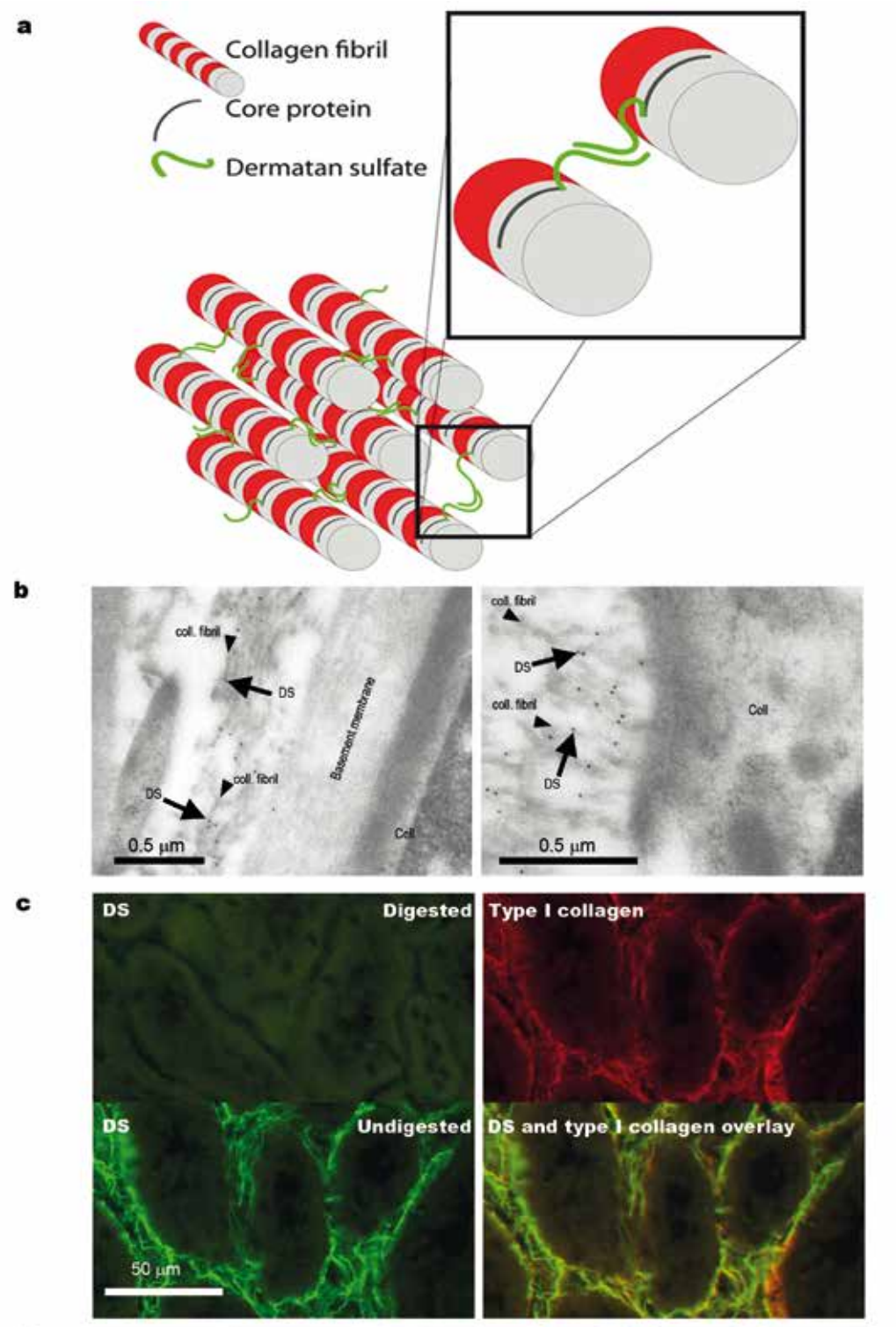
a
Collagen fibril
Core protein
Dermatan sulfate
b
coll. fibril
DS
Basement membrane
coll. fibril
DS
Cell
0.5 µm
coll. fibril
DS
coll. fibril
DS
Cell
0.5 µm
c
DS
Digested
Type I collagen
DS
Undigested
DS and type I collagen overlay
50 µm

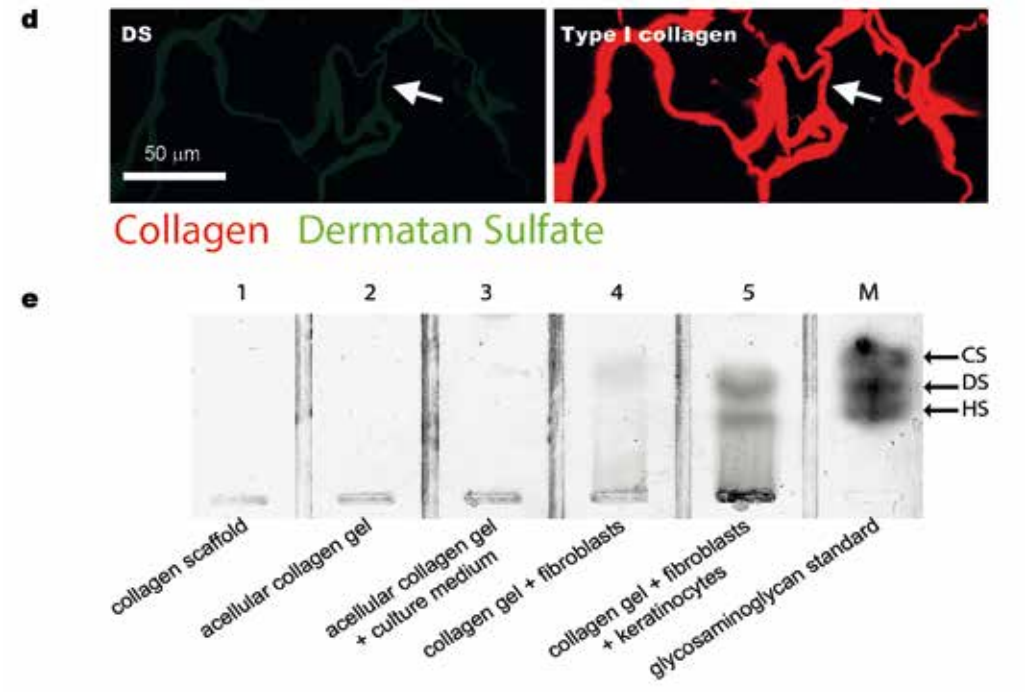

Figure 1. Overview and validation of strategy to identify newly synthesized collagen by dermatan sulfate. (a) Cartoon illustrating the intrinsic association of dermatan sulfate with collagen fibrils. (b) Identification of collagen fibrils using the anti-dermatan sulfate single chain antibody GD3A12. Arrows indicate immunogold labeling on collagen fibrils (rat kidney tissue, Bowman's capsule), but not on other structures such as cells and basement membranes. (c) Specificity of the anti-dermatan sulfate antibody as evidenced by loss of immunostaining after digestion of dermatan sulfate by chondroitinase B (rat kidney tissue). Note co-localization of dermatan sulfate and type I collagen. (d,e) Absence of dermatan sulfate in pre-seeded/pre-implanted collagenous biomaterials as indicated by (d) immunostaining for dermatan sulfate (antibody GD3A12), (e) biochemical analysis of dermatan sulfate (agarose gel electrophoresis). In (d) arrows indicate identical areas stained for dermatan sulfate and type I collagen. In (e), lanes 1–3 represent acellular collagen gels/scaffolds, whereas lanes 4 and 5 represent cellularized gels. M, marker containing 5 ng each of chondroitin sulfate (CS), dermatan sulfate (DS) and heparan sulfate (HS). coll.fibril: collagen fibril.

Results

To evaluate the potential of the anti-dermatan sulfate antibody to identify collagen fibrils we applied immuno-electron microscopy using rat kidney cryosections. Antibody reactivity, as visualized by gold sphere-labeled protein A, was confined to collagen fibrils whereas other structures like cells and basement membranes did not stain (Fig. 1b). Using immunofluorescence, antibody staining for dermatan sulfate was shown to co-localize with type I collagen, and was abolished by pretreatment of the sections with chondroitinase B, which specifically digests dermatan sulfate (Fig. 1c).

Absence of dermatan sulfate in the biomaterials

All collagenous biomaterials used were tested for the presence of dermatan sulfate, using immunohistochemical and/or biochemical techniques. Using immunofluorescence, dermatan sulfate could not be detected in any of the biomaterials (Fig. 1d, and supplementary Figure S1). In addition, using a highly sensitive silver staining method, dermatan sulfate could not be observed in collagen scaffolds (Fig. 1e, lane 1) or in collagen gels (Fig. 1e, lane 2 and 3).

Collagen deposition in vitro and in vivo

Having demonstrated the capacity of the antibody to detect collagen fibrils by virtue of its association with dermatan sulfate, and having established the absence of dermatan sulfate in collagenous biomaterials, we studied newly synthesized collagen fibrils produced by cells both *in vitro* and *in vivo*, using dermatan sulfate staining. Fibroblasts cultured *in vitro* in a collagenous gel produced collagen as evidenced by the presence of dermatan sulfate, which co-localized with type I collagen. Use of anti-type I collagen antibody did not discriminate between bovine collagen from the scaffold and the human collagen produced by the fibroblasts (Fig. 2a1–3). Dermatan sulfate staining, however, indicated the location of newly synthesized human collagen and was not present in the bovine scaffold collagen. Dermatan sulfate was also identified biochemically, and was detected only in cellularized collagen gels, and not in gels without cells (Fig. 1e, lane 4). The location of newly synthesized collagen was time dependent, and initially present only at the perimeter of the fibroblasts (Fig. 2b1). At later stages (*e.g.* 12 days of culturing) collagen was also located further away from the cells, and eventually most of the original gel contained newly synthesized collagen (Fig. 2b4). These results were confirmed biochemically, showing increased amounts of dermatan sulfate as a function of time (Fig. 1e).

Glycosaminoglycans are evolutionary highly conserved structures that are found throughout vertebrates as well as invertebrates[10]. It may therefore be expected that the anti-dermatan sulfate antibody can be used irrespective of the species that deposits the collagen. To evaluate this we stained collagen scaffolds implanted in different animal species and in humans. The following samples were used: 1) a flat collagen scaffold implanted subcutaneously in mice, 2) a tubular collagen scaffold implanted in the ureter of pigs, 3) a commercial collagen-chondroitin sulfate skin substitute (Integra®) implanted in a full-thickness skin defect in rats[11], 4) Integra® implanted in a soft tissue palatal defect in dogs[12], 5) Glyaderm® (acellular human dermis) implanted in a full-thickness skin defect

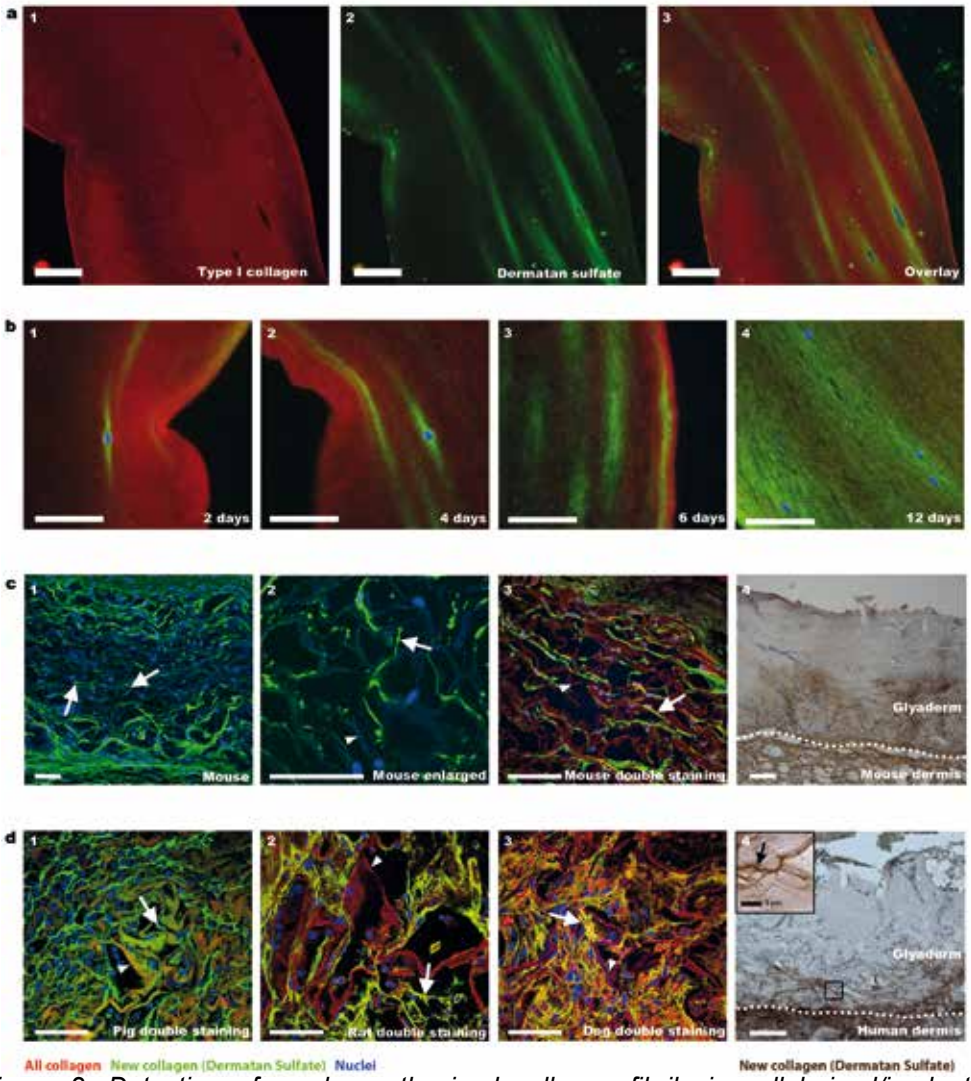

Figure 2. Detection of newly synthesized collagen fibrils in cellularized/implanted collagenous biomaterials. (a) Collagen gel cultured for 6 days with human fibroblasts. Newly deposited collagen is indicated by green dermatan sulfate staining (a2,a3), whereas all collagen is indicated by red type I collagen staining (a1,a3). (b) Location of newly deposited collagen in collagen gels cultured in time with fibroblasts/keratinocytes. Note increase of new collagen over time (b1-4). (c) Newly deposited collagen fibrils (arrows) in a collagen scaffold (arrowhead), two weeks after subcutaneous implantation in mice (c1-3) (for clarity, autofluorescence of background collagen was enhanced). For Glyaderm® (acellular human dermis), new collagen is indicated by brown staining (c4). (d) Newly deposited collagen fibrils (arrow) in various species (d1-4) after implantation of a collagen scaffold (arrowhead) in pig (1 month) (d1), Integra® (arrow head) in rat (1 week) (d2), Integra® (arrow head) in dog (4 weeks) (d3), and Glyaderm® in human (inset shows fibrillar structure) (d4). Scale bars are 50 µm unless indicated otherwise.

in mice13 and 6) Glyaderm® clinically applied in full-thickness skin defects in humans[14]. We were able to visualize the dermatan sulfate (and hence newly deposited collagen) in all species tested, indicating the robustness and species independency of the procedure (Fig. 2c,d). In line with the ingrowth of cells from the surrounding tissue into the scaffold, newly deposited collagen fibers were most prominent at the border of the scaffold, whereas deeper in the scaffold they were thinner and less abundant (Fig. 2c1). Small collagen deposits could easily be identified (Fig. 2c2). The newly formed collagen was generally oriented in the same direction as the fibers from the original scaffold (*e.g.* in a parallel orientation, see Fig. 2c3). In the pig model (Fig. 2d1), newly formed collagen was clearly present alongside the collagen fibers of the original implanted tubular collagen scaffold. Newly formed collagen fibers could also be easily identified in rats and dogs after implantation (7 and 28 days respectively) with Integra® (Fig. 2d2,d3). Integra® itself was not stained by the anti-dermatan sulfate antibody (supplementary Figure S1), even though the closely related glycosaminoglycan chondroitin sulfate is abundantly present in this commercially available skin substitute. The method was also applicable using the human skin derived Glyaderm®. Full-thickness wounds in mice treated with Glyaderm®[13] showed deposition of new collagen 8 days after implantation (Fig. 2c4). Please note that due to the strong autofluorescence of elastic fibers in Glyaderm® we used bright field instead of fluorescence microscopy. Finally, the method was probed in a clinical setting in which burn patients were treated using Glyaderm®[14]. Biopsies taken 7 days after implantation clearly show new collagen in the dense collagenous environment of Glyaderm® at the border of the wound bed (Fig. 2d4). Collagen fibers of the surrounding native tissue (*i.e.* in tissue not formed within the biomaterial) were also positive for dermatan sulfate in all species tested, as expected.

Discussion

The results presented above indicate that the anti-dermatan sulfate antibody GD3A12 is suitable to species independently detect newly formed collagen. Previously, analysis has been hampered by the inability to (immuno)histologically distinguish newly formed collagen from biomaterial/scaffold collagen. The technique described here offers a solution to this problem. However, it is not without potential pitfalls. Although the vast majority of dermatan sulfate is associated with collagen as part of the proteoglycans decorin and biglycan[5], a small fraction may be present associated with other structures such as elastin and fibrillin-containing microfibrils[15]. In addition, dermatan sulfate may be part of the proteoglycan versican[16] associated with elastic fibers[17]. However, in this study we did not observe any association of dermatan sulfate with elastic fibers detected either by autofluorescence or by anti-elastin antibodies (see double staining with dermatan sulfate, supplementary Figure S2), indicating that such an association was not present in the tissues studied here.

Next to the obvious use in regenerative medicine, the proposed method may be applied to other fields of research including cancer biology. Tumor cells spread and invade into the surrounding tissues while remodeling the extracellular matrix. It has been suggested that in doing so tumor cells make use of newly deposited collagen fibrils[18]. A widely used 3D model to study the migrational behavior of tumor cells is the use of collagen gels. The technique described here may be of value in further defining the role of newly formed collagen fibrils in tumor biology using such models[2].

In conclusion, the detection of newly synthesized collagen based on its association with dermatan sulfate and applying the single chain antibody GD3A12 represents an inexpensive, fast and easy technique to evaluate the presence and orientation of de novo synthesized collagen fibrils in collagen based biomaterials. As such it can be applied in many research areas including tissue engineering and tumor biology.

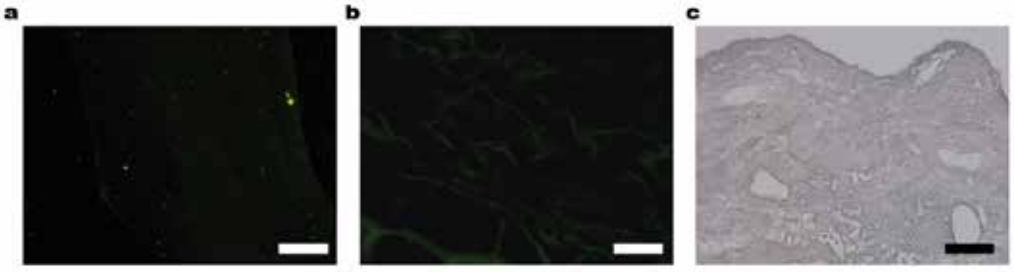

Supplementary Figure S1. Absence of dermatan sulfate in collagenous biomaterials before implantation/cell seeding. Immunostaining for dermatan sulfate (green) on (a) acellular bovine type I collagen hydrogel, (b) Integra® before implantation and (c) Glyaderm® before implantation. Note lack of staining. Scale bars are 50 µm.

Materials and methods

Materials

Papain, barium acetate, paraformaldehyde, 3,3′-diaminobenzidine tetrahydrochloride (DAB), 4′,6-diamidino-2-phenylindole dihydrochloride (DAPI) and protein A were from Sigma, St. Louis MO, USA. Chondroitinase B was from IBEX, Montreal, Quebec, Canada. Agarose and gel bond film were from Lonza, Rockland, USA, and Tissue Tek from Sakura Finetek Europe BV, Alphen aan den Rijn, The Netherlands. Tris-HCl was from Invitrogen, Carlsbad, CA, USA. Sodium chloride and magnesium acetate were from Merck, Darmstadt, Germany. Lowicryl HM20 was from Aurion, Wageningen, The Netherlands and Mowiol 4-88 mounting medium was from Calbiochem, San Diego, CA, USA. Bovine serum albumin (BSA) was from PAA laboratories, Pasching, Austria. The following antibodies were used: rabbit anti-bovine type I collagen IgG from Millipore, Cambridge, UK; mouse anti-bovine elastin IgG from Sigma; rabbit anti-VSV IgG from Rockland, Gilbertsville, PA, USA; mouse anti-VSV IgG from mouse hybridoma cell line P5D4 from the American Type Culture Collection, Rockville, MD, USA; peroxidase labeled mouse anti-VSV IgG from Sigma and mouse anti-Penta-His IgG from QIAGEN GmbH, Hilden, Germany; goat anti-mouse IgG Alexa Fluor 488 conjugated and goat anti-rabbit IgG Alexa Fluor 594 conjugated from Invitrogen, Eugene, OR, USA. The single chain variable fragment antibody GD3A12 selective for dermatan sulfate was obtained as described[7,19]. As a source of this antibody, periplasmic fractions isolated from bacteria expressing the antibody were used[20]. The antibody contains a VSV and a HIS tag.

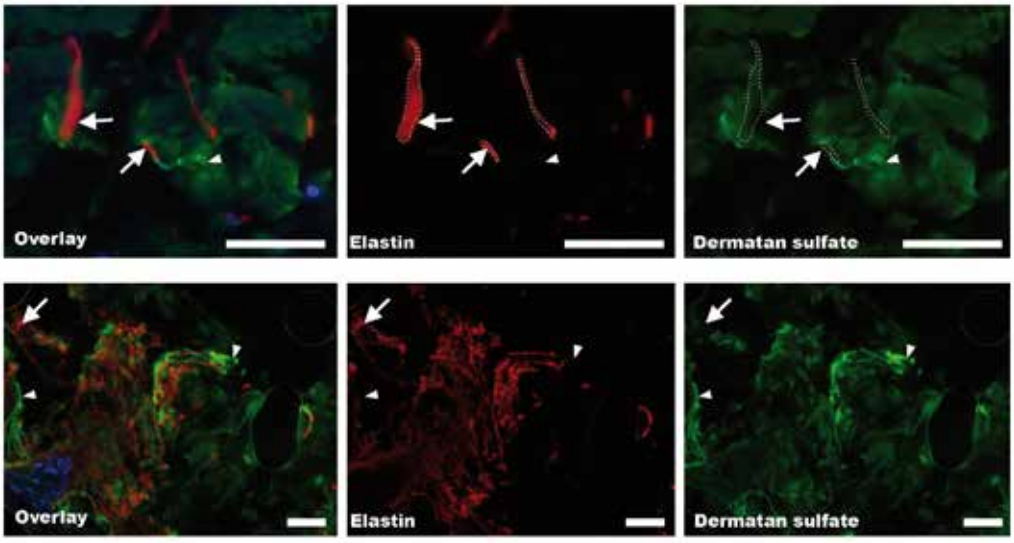

Supplementary Figure S2. Absence of dermatan sulfate on elastic fibers shown by double immunostaining of cryosections of sheep skin for elastin (red) and dermatan sulfate (green). Elastic fibers (red, arrow) are negative for dermatan sulfate (green, arrow head), and dermatan sulfate is negative for elastin staining. Scale bars are 50 µm.

Histology

Paraffin-embedded and frozen tissues were sectioned at 5 µm thickness. Paraffin sections were deparaffinized in xylene for 3 × 5 min, followed by a descending series of ethanol and processed for immunohistochemistry. Cryosections were air-dried before staining.

Immunofluorescence stainings

To stain for dermatan sulfate, deparaffinized sections were blocked for 15 min with 1% BSA in Tris buffered saline (TBS, 50 mM Tris-HCl pH 7.0 containing 150 mM NaCl). All further incubations were performed at ambient temperatures for 45 min and sections were washed 3 × 5 min with TBS in between incubations. Antibodies were diluted in 1% BSA in TBS. Paraffin sections were incubated with antibody GD3A12 (1:5 - 1:20), followed by incubation with mouse anti-VSV antibody P5D4 (1:10) and an Alexa Fluor 488-conjugated goat anti mouse antibody. For double staining with type I collagen, antigen retrieval using citrate buffer was applied. Paraffin sections were pretreated with citrate (10 mM sodium citrate, pH 6.0) for 20 min at either 95 °C (tissues) or ambient temperature (cultured gels). In one occasion boiling temperature was used, but this caused damage to the sections. Sections were extensively washed with TBS to remove the citric acid buffer and blocked with TBS/BSA. Anti-type I collagen antibody (1:500–1:1500) was applied and visualized using an Alexa Fluor 594-conjugated goat anti-rabbit antibody. For detection of dermatan sulfate in implanted collagen scaffolds in mice, a rabbit anti-VSV antibody (1:500) was used and visualized using goat anti-rabbit IgG Alexa Fluor 488. In the case of double staining of dermatan sulfate and type I collagen in mice, dermatan sulfate was visualized using Alexa Fluor 488 conjugated mouse anti-Penta-His antibody.

For double staining of sheep skin cryosections for elastin and dermatan sulfate, the sections were air-dried for 30 min. Hereafter, the procedure as described above was applied. Mouse anti-bovine elastin antibody was diluted 1:200 and visualized using goat anti-mouse IgG Alexa Fluor 594. Dermatan sulfate was visualized using rabbit anti-VSV IgG and goat anti-rabbit IgG Alexa Fluor 488.

For visualization of the nuclei, sections were incubated for 15 min with DAPI (10 µ g/ml in PBS). After extensive washings with PBS, the sections were enclosed with Mowiol mounting medium.

For detection of dermatan sulfate in the human skin substitute Glyaderm®, containing autofluorescent elastic fibers, peroxidase conjugated mouse anti-VSV IgG (1:100) and DAB were used.

Omission of the antibody GD3A12 was taken as a control, and was negative in all cases.

Digestion of dermatan sulfate to evaluate specificity of GD3A12

To evaluate the specificity of the antibody GD3A12 for dermatan sulfate, cryosections were digested overnight at 37 °C with 20 mU/ml chondroitinase B in 25 mM Tris-HCl pH 8.0 containing 2 mM magnesium acetate. The next day, the digestion was repeated with 20 mU/ml chondroitinase B for another 2 h. As a control, sections were incubated in buffer without enzyme.

Microscopic imaging, equipment and settings

Images of the *in vitro* cultured collagen gels were taken with a Leica DM6000 B microscope equipped with a Leica DFC 480 camera (20x objective), using Leica Application suite V4.3.0. The exposure time was kept constant for all measurements. DAPI, Alexa Fluor 488 and 594 were excited with a mercury HBO100 lamp using the excitation filters BP410/15 nm BP490/20 nm and BP562/40 nm respectively, and the emission was collected after filtering with 430, 500, 593 dichroic mirrors respectively.

All other images were captured with the Olympus FV1000 Confocal Laser Scanning Microscope. Photos wereimaged using a 20× objective and a 60× objective. DAPI, Alexa Fluor 488 and Alexa Fluor 594 were excited at 405 nm, 488 nm and 559 nm, respectively. Using a combination of the beam splitters SMD490 and SDM560, the emission was collected with the emission filters BA430-470, BA505-540 and BA575-675 for DAPI, Alexa Fluor 488 and Alexa Fluor 594, respectively.

For Figs 1c and 2a,b and supplementary Figure S1a, the microscope settings were as follows: space resolution 2560 × 1920, pixel dimension 0.012 pixels/μm, image depth 32 (RGB), excitation filters: 410/15 (DAPI), 490/20 (AF488), 562/20 (AF594) and gamma correction was set at 1. For Figs 1d and 2c,d, the settings were as follows: space resolution 1024 × 1024, pixel dimension 1.61 pixels/μ m, image depth 32 (RGB), excitation filters 405 (DAPI), 488 (AF488), 559 (AF594), emission filters BA430-470 (DAPI), BA505-540 (AF488), BA575-675 (AF594). Dichroic beam splitters 490 9DAPI) and 560 (AF488) were used. No gamma correction was applied.

Image processing was performed using ImageJ 1.48v (National Institutes of Health, USA). Before merging, both brightness and contrast were adjusted similarly for all photos including the controls.

Immuno-electron microscopy

To evaluate the reactivity of the antibody for dermatan sulfate on collagen fibrils, immuno-electron microscopy was performed on lowicryl HM20 embedded rat kidney samples[21]. The tissue was incubated for 3 h in Somogyi solution [0.1 M phosphate buffer (pH 7.3) containing 4% formaldehyde, 0.05% glutaraldehyde and 0.2% picric acid] [22]. After cutting, 200 μ m sections were frozen in liquid propane at − 190 °C. Using freeze-substitution (Leica-KF80) the sections were embedded in lowicryl HM20. Ultrathin sections were mounted on nickel grids. For immunostaining sections were blocked with 0.25% BSA in phosphate buffered saline (BSA/PBS), followed by an overnight incubation at 4 °C with antibody GD3A12 (5× diluted periplasmic fraction in BSA/PBS). After washing, bound GD3A12 was visualized using 10 nm gold-sphere labeled protein A (1:400 in BSA/PBS) prepared according to Slot *et al.*[23]. Subsequently, sections were washed in PBS, post-fixed for 5 min in 2.5% glutaraldehyde in 0.1 M phosphate buffer (pH 7.4), washed with distilled water, and post-stained with uranyl acetate. Sections were examined using a JEOL 1010 electron microscope.

Agarose gel electrophoresis

To analyze the presence of glycosaminoglycans including dermatan sulfate in collagen scaffolds/gels, agarose gel electrophoresis was performed. To 40 mg dry weight of the samples, 2.5 U/ml papain was added to a total volume of 500 μ l in order to digest

proteins. 0.5 µl of the samples was loaded on a 1 mm thick 1% agarose gel in 50 mM $Ba(Ac)_2$, pH 5.0, casted on a gel bond film. A marker was included containing 5 ng of chondroitin sulfate (CS), 5 ng dermatan sulfate (DS) and 5 ng heparan sulfate. The gel was run at 30 mA in electrophoresis buffer (50 mM $Ba(Ac)_2$, pH 5.0) until the front of the loading dye had moved about 8 cm into the agarose gel. Subsequently, the agarose gel was stained with silver as described by Van de Lest *et al.*[24].

Gels and scaffolds

All experimental protocols described by Sun *et al.*[25], Nillesen *et al.*[11], van Kilsdonk *et al.*[13], de Jonge *et al.*[26], and Ophof *et al.*[12] were approved by the Institutional Animal Welfare Committee (DEC) of the Radboud university medical center, Nijmegen, The Netherlands. The experimental procedures described by Braziulis *et al.*[8] were approved by the Ethics Committee of the Canton Zürich (KEK), Switzerland. The study protocol as described by Pirayesh *et al.*[14] was approved by the Ghent University Hospital Ethics Committee.

All experiments were carried out in accordance with the guidelines of the Institute of Laboratory Animal Research[27] and the declaration of Helsinki principles.

Cellularized collagen gels

The dermal (denovoDerm) and dermal-epidermal (denovoSkin) collagen gels were prepared using bovine type I telocollagen seeded either with primary fibroblasts only (denovoDerm), or with a combination of primary fibroblasts and keratinocytes (denovoSkin), isolated from skin biopsies from 3 individuals who had given informed consent, as described by Braziulis *et al.*[8]. 50,000 fibroblasts were cultured in DMEM supplemented with 10% fetal bovine serum (FBS), 10 mM 4-(2-hydroxyethyl)-1-piperazineethanesulfonic acid buffer (HEPES), 90 µ g/ml streptomycin and 90 U/ml penicillin (all compounds from Invitrogen, Basel, Switzerland) for 2, 4 or 6 days in compressed collagen gels at 37 °C and 5% CO_2. For the dermal-epidermal skin substitute, 500,000 keratinocytes were seeded on top of the dermal substitute and cultured for another 6 days (12 days in total) in serum free keratinocyte medium. Samples were fixed in 4% paraformaldehyde and embedded in paraffin.

Acellular collagen scaffolds implanted in mice

Flat porous collagen scaffolds were prepared as described by Sun *et al.*[25] from a 0.4% (w/v) type I collagen suspension in 0.25 M acetic acid. After homogenization, the suspension was pipetted in a polystyrene mold, frozen and lyophilized resulting in porous collagen scaffolds. Hereafter, the collagen scaffolds were pre-incubated in 50 mM 2-(N-morpholino)ethanesulphonic acid pH 5.0 (MES) and crosslinked using 33 mM 1-ethyl-3-(3-dimethylaminopropyl) carbodiimide (EDC) and 6 mM N-hydroxysuccinimide (NHS) in 50 mM MES buffer containing 40% ethanol for 4 h. After multiple washing steps with subsequently 0.1 M Na_2HPO_4, 1 M NaCl, 2 M NaCl, and water, the scaffolds were frozen at − 20 °C and lyophilized, followed by sterilization by γ -irradiation (25 kGy, Synergy Health, the Netherlands). Collagen scaffolds were incubated in sterile 0.9% NaCl and subcutaneously implanted in 7-weeks-old Balb/cByj mice. After two weeks, mice were sacrificed and tissue was dissected around the site of implantation, fixed in 4% paraformaldehyde and embedded in paraffin.

Tubular acellular collagen scaffolds implanted in pigs

Tubular collagen constructs of 6 cm in length and an inner diameter of 6 mm were prepared as described using a 0.5% (w/v) collagen suspension in 0.25 M acetic acid[28]. After lyophilization the tubes were crosslinked followed by extensive washing, as described above. Tubular scaffolds were kept in 70% ethanol before γ -sterilization. Sterilized tubular collagen scaffolds were implanted in the ureter of 4-months-old pigs, dissected after one month, fixed in 4% paraformaldehyde and embedded in paraffin[26]. Integra® implanted in rat and dog. In rats, Integra®, a commercially available collagen-chondroitin sulfate scaffold[29], was implanted in a full thickness wound[11]. After 7 days, rats were sacrificed, the wound area dissected, fixed in 4% paraformaldehyde and embedded in paraffin[11]. In dogs, Integra® was implanted according to the Von Langenbeck procedure for palatal repair[12]. Samples were taken 28 days post implantation. Tissue was fixed in 4% formaldehyde, decalcified in 20% formic acid and 5% sodium citrate[12] and imbedded in paraffin.

Glyaderm® implanted in mouse and human

Glyaderm®, a glycerol preserved acellular human dermis containing native collagen and elastic fibers[9] was produced by the Euro Skin Bank, Beverwijk, The Netherlands. Full thickness wounds at the back of 8-week-old mice were implanted with Glyaderm®. After 8 days, mice were sacrificed, fixed in 4% paraformaldehyde and embedded in paraffin[13].

Application of Glyaderm® to a human wound bed was performed and described by Pirayesh *et al.*[14]. Informed consent was given by all patients. Full-thickness defects were engrafted with Glyaderm®. After 1 week, biopsies were fixed in 4% paraformaldehyde and embedded in paraffin.

Acknowledgements

This work was supported by the European Union (EuroSkinGraft: FP7 grant 279024) and the Dutch program for Tissue Engineering (grant DPTE 6735).

Author Contributions

C.O. and P.U. wrote the main manuscript text. P.U. prepared Figure 1a, C.O. Figure 1a–d, and 2 and supplementary Figures S1 and S2. E.V. prepared Figures 1e and 2c1. T.H. prepared 1b. E.B., P.J., A.P., J.H. and E.R. were responsible for the performance of the *in vitro* and *in vivo* experiments and collected the tissue samples. W.D. and T.K. were involved in study design, manuscript text and design of the figures. All authors have given approval for the final version of the manuscript.

References

1. Renth, A. N. & Detamore, M. S. Leveraging “raw materials” as building blocks and bioactive signals in regenerative medicine. Tissue Eng., Part B 18, 341–362 (2012).

2. Meyer, A. S. *et al.* 2D protrusion but not motility predicts growth factor-induced cancer cell migration in 3D collagen. J. Cell Biol. 197, 721–729 (2012).

3. Kielty, C. M. & Grant, M. E. In Connective tissues and its heratible disorders (ed. Inc. Wiley-Liss) Ch. 2, 159–221 (2002).

4. Pan, S. *et al.* Mass Spectrometry Based Targeted Protein Quantification: Methods and Applications. J. Proteome Res. 8, 787–797 (2008).

5. Orgel, J. P., Eid, A., Antipova, O., Bella, J. & Scott, J. E. Decorin core protein (decoron) shape complements collagen fibril surface structure and mediates its binding. PLoS One 4, e7028 (2009).

6. Miyake, N. *et al.* Loss-of-function mutations of CHST14 in a new type of Ehlers-Danlos syndrome. Hum. Mutat. 31, 966–974 (2010).

7. Ten Dam, G. B. *et al.* Dermatan sulfate domains defined by the novel antibody GD3A12, in normal tissues and ovarian adenocarcinomas. Histochem. Cell Biol. 132, 117–127 (2009).

8. Braziulis, E. *et al.* Modified plastic compression of collagen hydrogels provides an ideal matrix for clinically applicable skin substitutes. Tissue Eng., Part C 18, 464–474 (2012).

9. Richters, C. D. *et al.* Development of a dermal matrix from glycerol preserved allogeneic skin. Cell Tissue Banking 9, 309–315 (2008).

10. Yamada, S., Sugahara, K. & Ozbek, S. Evolution of glycosaminoglycans: Comparative biochemical study. Commun. Integr. Biol. 4, 150–158 (2011).

11. Nillesen, S. T. *et al.* Design and *in vivo* evaluation of a molecularly defined acellular skin construct: reduction of early contraction and increase in early blood vessel formation. Acta Biomater. 7, 1063–1071 (2011).

12. Ophof, R., van der Loo, L. M., Maltha, J. C., Kuijpers-Jagtman, A. M. & Von den Hoff, J. W. Dentoalveolar development in beagle dogs after palatal repair with a dermal substitute. Am. J. Orthod. 138, 58–66 (2010).

13. van Kilsdonk, J. W. *et al.* An *in vitro* wound healing model for evaluation of dermal substitutes. Wound Rep. Reg. 21, 890–896 (2013).

14. Pirayesh, A., Hoeksema, H., Richters, C., Verbelen, J. & Monstrey, S. Glyaderm dermal substitute: Clinical application and long term results in 55 patients. Burns 41, 132–144 (2014).

15. Reinboth, B., Hanssen, E., Cleary, E. G. & Gibson, M. A. Molecular interactions of biglycan and decorin with elastic fiber components: biglycan forms a ternary complex with tropoelastin and microfibril-associated glycoprotein 1. J. Biol. Chem. 277, 3950–3957 (2002).

16. Trowbridge, J. M., Rudisill, J. A., Ron, D. & Gallo, R. L. Dermatan sulfate binds and potentiates activity of keratinocyte growth factor (FGF-7). J. Biol. Chem. 277, 42815–42820 (2002).

17. Zimmermann, D. R., Dours-Zimmermann, M. T., Schubert, M. & Bruckner-Tuderman, L. Versican is expressed in the proliferating zone in the epidermis and in association with the elastic network of the dermis. J. Cell Biol. 124, 817–825 (1994).

18. Gilkes, D. M., Semenza, G. L. & Wirtz, D. Hypoxia and the extracellular matrix: drivers of tumour metastasis. Nat. Rev. Cancer 14,430–439 (2014).

19. Nissim, A. *et al.* Antibody fragments from a 'single pot' phage display library as immunochemical reagents. EMBO J 13, 692–698 (1994).

20. van Kuppevelt, T. H., Dennissen, M. A. B. A., van Venrooij, W. J., Hoet, R. M. A. & Veerkamp, H. Generation and application of type-specific anti-heparan sulfate antibodies using phage display technology: Further eveidence for heparan sulfate heterogeneity in the kidney. J. Biol. Chem. 273, 12960–12966 (1998).

21. Lensen, J. F. *et al.* Selection and characterization of a unique phage display-derived antibody against dermatan sulfate. Matrix Biol 25, 457–461 (2006).

22. Somogyi, P. & Takagi, H. A Note on the Use of Picric Acid - Paraformaldehyde Glutaraldehyde Fixative for Correlated Light and Electron-Microscopic Immunocytochemistry. Neuroscience 7, 1779–1783 (1982).

23. Slot, J. W. & Geuze, H. J. Sizing of protein A-colloidal gold probes for immunoelectron microscopy. J Cell Biol 90, 533–536 (1981).

24. van de Lest, C. H. A., Versteeg, E. M. M., Veerkamp, J. H. & van Kuppevelt, T. H. Quantification and characterization of glycosaminoglycans at the nanaogram level by a combined azure a-silver staining in agarose gels. Analytical Biochemistry 221, 356–361 (1994).

25. Sun, W. *et al.* Improving the cell distribution in collagen-coated poly-caprolactone knittings. Tissue Eng Part C Methods 18, 731–739 (2012).

26. de Jonge, P. K., Simaioforidis, V., Geutjes, P. J., Oosterwijk, E. & Feitz, W. F. Recent advances in ureteral tissue engineering. Curr Urol Rep 16, 465 (2015).

27. National Research Council, In Guide for the Care and Use of Laboratory Animals 8th edn (ed. The National Academies Press), Ch.1-5, 1–155 (Washington, D.C., 2011).

28. Geutjes, P. *et al.* Tissue engineered tubular construct for urinary diversion in a preclinical porcine model. J Urol 188, 653–660 (2012).

29. Yannas, I. V. & Burke, J. F. Design of an artificial skin. I. Basic design principles. J Biomed Mater Res 14, 65–81 (1980).

Chapter 4

Preparation of a growth factor gradient in porous collagen scaffolds and its effect on cell proliferation

*Herman T.B. van Moerkerk[1], **Peter J.E. Uijtdewilligen[1]**, Pauline Smits[1], Elly M. Versteeg[1], W.F. Daamen[1] and T.H. van Kuppevelt[1]*

This chapter has been adapted from *Journal of Controlled Release 2006;**116(2)**; e87-88*

Summary

A growth factor gradient was prepared in type I collagen scaffolds using a novel method. First, a gradient of glycosaminoglycans (GAGs), *i.e.* heparin, was established in porous collagen scaffolds by means of chemically crosslinking with a gradient of 0–10% *(w/v)* heparin. As a second step, heparin-binding fibroblast growth factor 2 (FGF2) was bound to these collagen-GAG scaffolds. The FGF2 gradient corresponded to the applied heparin gradient. Cell culture experiments showed that the gradient scaffold was capable of enhancing cell growth in a concentration-dependent manner.

Introduction

Gradients of effector molecules, *e.g.* growth factors and morphogens, are essential for embryonic development and stem cell control [1–3]. Therefore, mimicking gradients is of interest in the field of regenerative medicine, as they may enhance growth factor delivery and subsequent tissue regeneration [4]. The creation of a gradient of signalling molecules on collagen-based biomaterials, however, is technically challenging [2,5,6].

During embryonic development, intercellular communication is mediated by extracellular diffusion or cell-to-cell transfer of effector molecules potentially resulting in a signalling gradient. Communication via cell-to-cell transfer or transcytosis is based on the movement of effector molecules across cells or along cellular extensions. Extracellular diffusions can be described by three models, *e.g.* a free diffusion model, a hindered diffusion model and a facilitated diffusion model [7,8]. The simplest model for gradient formation is a cellular source releasing an effector molecule, which is transported via an extracellular diffusion model. Cells close to the source will be exposed to a higher concentration of the effector molecule in comparison to cells further away from the source leading to distinctive cellular responses [9]. This model is called the threshold model [10–12]. Gradients can become more difficult to interpret in the presence of multiple effector molecules or cellular sources. In both cases, the outcome of the gradient is dependent on the diffusion properties of the released molecules as well as the interaction with cellular receptors extracellularly [13,14] and targeted gene expression intercellularly [9].

An example of a gradients created by extracellular diffusion can be seen during glandular organogenesis where they play a role during epithelial branching patterning and limb formation. In the first case, gradients are created by a difference in binding affinity of

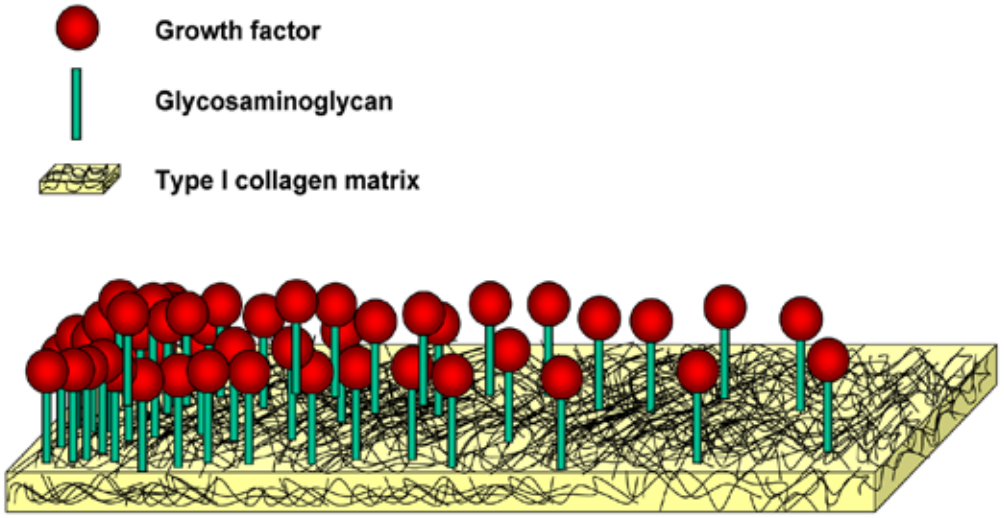

Figure 1 - Schematic overview of a collagen scaffold with a gradient of heparin and growth factor.

fibroblast growth factor 7 (FGF7) and FGF8 to heparan sulfate [14], while in the second two sources of effector molecules are present, *i.e.* the apical ectodermal ridge and the zone of polarizing activity forming a complex interplay of effector molecules like bone morphogenetic protein (BMP), sonic hedgehog (SHH) and members of the FGF family [15].

Research towards the formation and interpretation of gradients has mainly focused on embryonic development. During adult homeostasis, however, gradients are still of eminent importance. Tissue repair in the lungs is aided by a gradient of chemokines guiding circulating leukocytes to an afflicted site as this site releases chemokines restricted in diffusion by cell-bound heparan sulfate leading to a gradient [16]. In cutaneous wound repair, examples include gradients of chemokines which affect neutrophils and macrophages [17] and the VEGF-A gradient important for neovascularization that is induced by hypoxia [18,19].

Incorporation of a gradient of effector molecules in tissue-engineered constructs for wound repair may further improve their function. To create a tissue-engineered construct containing a gradient of effector molecules, we chose type I collagen as a scaffolding material and heparin to bind the effector molecules. Heparin is a glycosaminoglycan similar to heparan sulfate [20]. It has been shown that heparan sulfate is involved in the hindered diffusion model of effector molecules [7,11,14].

In this study, we made an effort to establish a growth factor gradient through a glycosaminoglycan gradient in type I collagen scaffolds to influence cellular behavior for tissue engineering purposes (Figure 1).

Experimental methods

All solutions were made using MilliQ water.

Preparation of scaffolds

Type I collagen was isolated from bovine achilles tendon [21]. Porous scaffolds [22,23] were prepared from homogeneous 0.8% (w/v) collagen dispersions in 0.25 M acetic acid in 75 cm2 culture flasks by freezing using a mixture of dry ice and ethanol and lyophilisation in a Zirbus lyophiliser (Bad Grund, Germany) [22].

Crosslinking scaffolds with a gradient of heparin

Sucrose was used to stabilize a gradient of heparin in solution. The scaffolds of 8 to 10 cm in length and 1 cm in width were attached to a gauze and placed in a 15 mL tube (Greiner Bio-one). Using the mixer part of the Biologic LP system (Bio-Rad), a gradient was created by gradually mixing a solution containing 33 mM 1-ethyl-3(-3-dimethyl aminopropyl) carbodiimide (EDC, Fluka) and 6 mM N-hydroxysuccinimide (NHS, Fluka), 25% sucrose (Sigma) and 10% heparin (Diosynth) (solution A) and a second solution containing 33 mM EDC and 6 mM NHS (solution B). This created a gradient from 100% solution A at the bottom to 100% solution B at the top of the tube. The scaffold was incubated for 16 h in the gradient, washed twice in 0.1 M Na_2HPO_4 (pH 9.1) for 1 h, washed with 1 M NaCl and 2 M NaCl for 2 h and 1 day and subsequently washed with distilled water [21]. The gradient scaffold was frozen at -80°C and lyophilized.

To visualize the stability of the gradient, fountainpen ink was added to the sucrose gradient (Figure 2).

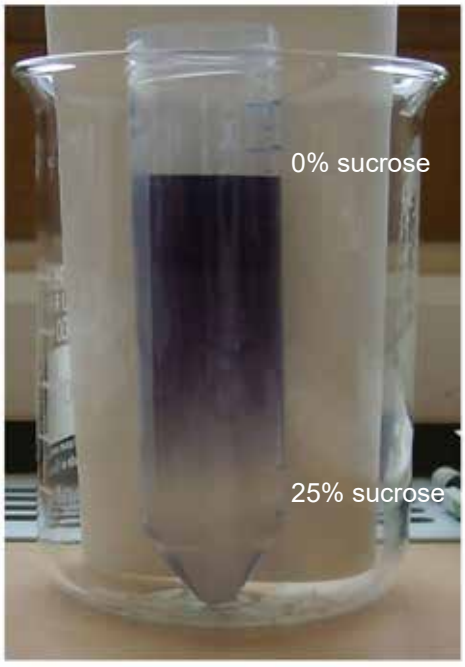

Figure 2 – A 50 ml tube containing a gradient of sucrose and ink to show the sucrose gradient.

Growth factor binding

Collagen scaffolds were disinfected using 70% ethanol by four 1 h incubations and one overnight incubation. Scaffolds were washed with sterile phosphate-buffered saline (PBS, pH 7.4) three times shortly, four times for 1 h and once overnight. Scaffolds were subsequently incubated in a solution containing 7 µg FGF2 per ml sterile PBS for 1 h at 20°C. Unbound FGF2 was removed by washing three times with PBS for 5 min.

Analysis of the scaffold

Primary amine content (TNBS assay) - Primary amine content was evaluated spectrophotometrically after reaction with 2,4,6-trinitrobenzene sulphonic acid (Sigma) using a glycine calibration curve [24]. Non-crosslinked scaffolds were used as a control. A Synergy2 BioTek microplate reader was used for meassurements.

Heparin content - The content of incorporated heparin was determined by hexosamine analysis using p-dimethylamino-benzaldehyde [25] with a heparin calibration curve [21]. Non-crosslinked scaffolds were used as a control. A Synergy2 BioTek microplate reader was used for meassurements.

Analysis of the growth factor gradient

FGF2 staining - Growth factor binding on scaffolds containing a gradient of heparin was analysed using immunostaining. A collagen scaffold containing a gradient of heparin incubated with growth factor solution was incubated overnight with blocking buffer (PBS containing 0.1% (v/v) Tween (PBST) and 3% (w/v) BSA). Scaffolds were incubated with rabbit anti–bovine FGF2 antibody (Sigma) in blocking buffer (1:1000) for 90 min. Scaffolds were washed in PBS and incubated with alkaline phosphatase conjugated goat anti-rabbit IgG (Sigma) in blocking buffer (1:1000) for 90 min. After washing in PBS, scaffolds were washed in diethanolamine solution (0.1 M diethanolamine, 0.05 M $MgCl_2$, pH 9.6). Staining of the scaffolds was performed with NBT/BCIP (nitroblue tetrazolium 5-bromo-4-chloro-3-indolyl phosphate reagent) diluted in diethanolamine (45 µl NBT, 35 µl BCIP in 10 ml diethanolamine solution) and the reaction was stopped by replacing the staining solution with MilliQ.

Cell culture

Normal rat kidney cells (NRK; ATCC CRL-6509) were seeded on collagen scaffolds 8 to 10 cm in length and 1 cm in width with a gradient of heparin with FGF2 (0.5.106 NRK cells per ml DMEM containing 20% (v/v) fetal calf serum and 4 mM glutamine) and were analysed at day 2, 4 and 7 of culturing. Scaffolds were washed twice with PBS, fixed in 4% formaldehyde in phosphate buffer (pH 7.2), and embedded in paraffin. Sections were stained using haematoxylin-eosin [26].

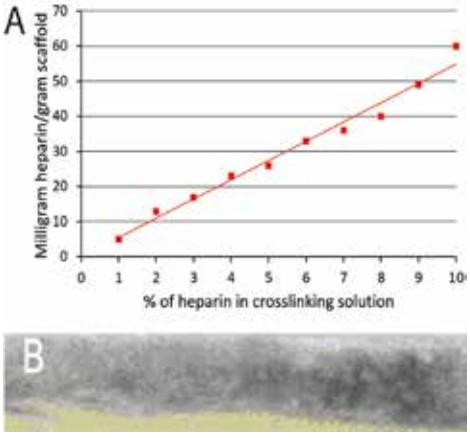

Figure 3 – Heparin content of the created gradient (A) showed an increase of bound heparin correlating to the amount of heparin present in the sucrose gradient. The created gradient was analyzed using immunostaining for FGF2, which indicated an ascending gradient of FGF2 along the scaffold (B).

Results

Primary amine content

Crosslinking of the scaffold was analysed using a TNBS assay. Compared to non-crosslinked scaffolds the number of primary amine groups were reduced with 38%±7 (mean±SD), indicating 38% crosslinking.

Heparin content

A hexosamine assay was used to determine the amount of heparin bound to the scaffold after crosslinking. Measuring the heparin content of ten samples taken along the scaffold showed that heparin was bound to the scaffolds ranging from 0 to 5.5% (Figure 3A), indicating the presence of a gradient.

FGF2 staining

To analyse the binding of growth factor to the heparin gradient on the collagen scaffold, immunostaining using an antibody against FGF2 was performed. A gradient was visible corresponding to the heparin gradient (Figure 3B). With a higher concentration of heparin, more FGF2 staining was observed.

Cell culture

Normal rat kidney (NRK) cells were used to test the bioactivity of the gradient scaffold loaded with FGF2. After 2, 4 and 7 days of culturing, haematoxylin-eosin was used to localize the NRK cells in the gradient scaffolds. Increased cell numbers were found at the side containing 5.5% in comparison to the side containing no heparin. The increase in proliferation after 7 days of culturing is shown in Figure 4. These results suggest that the gradient of FGF2 resulted in differences in proliferation along the scaffold.

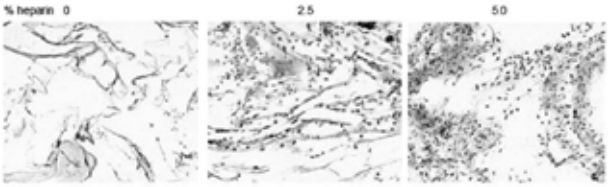

Figure 4 - Micrographs taken at different locations in a collagen scaffold with a heparin–FGF2 gradient, after 7 days of culturing. Note that with increasing FGF2 concentrations a clear increase in the number of cells was found. Sections were haematoxylin-eosin stained. Pictures were taken at an original magnification of 100X.

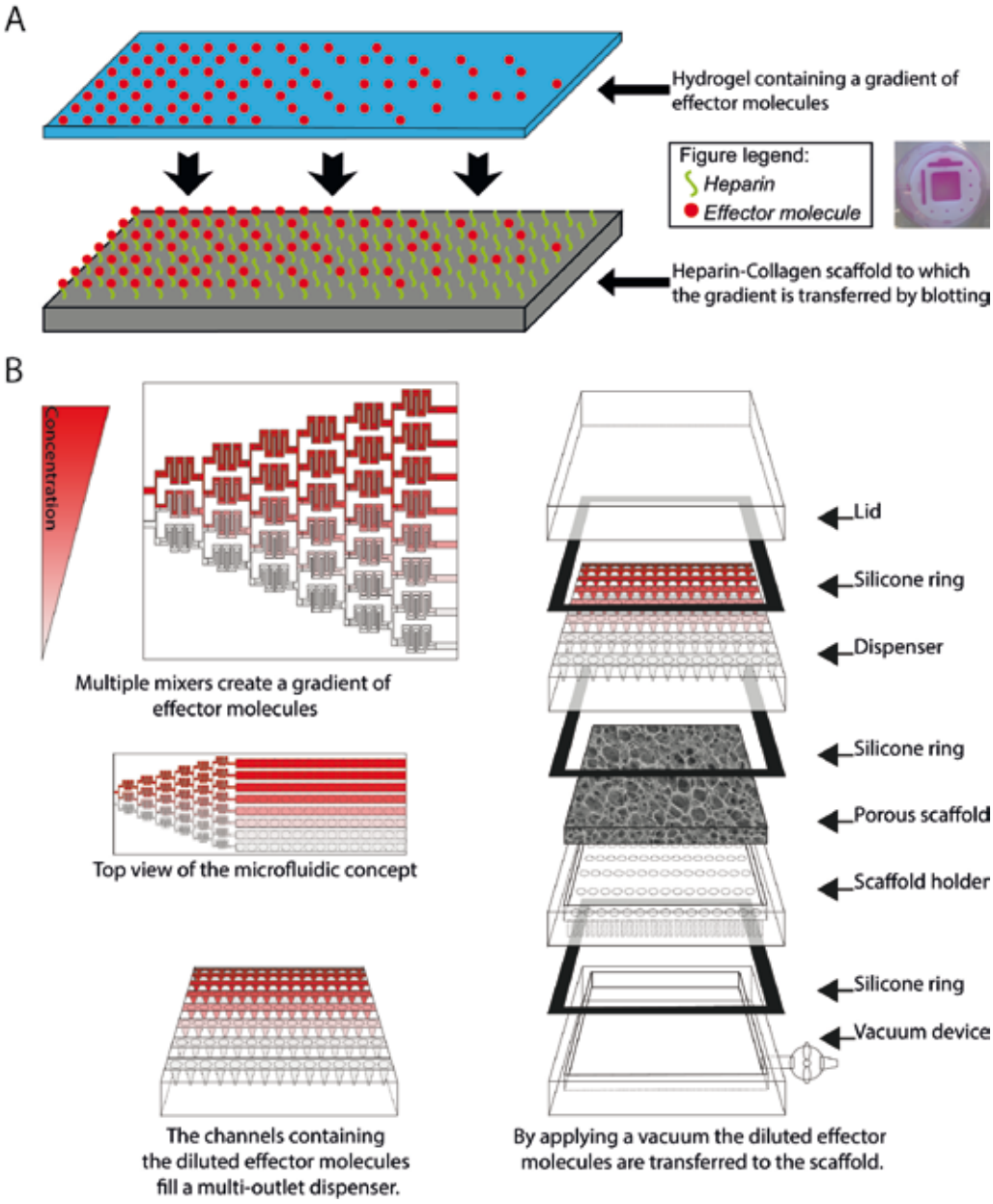

Figure 5 – Two alternative approaches towards a gradient of effector molecules. (A) Using a diffusion device a gradient of effector molecules is created in a hydrogel [34]. The gradient is subsequently transferred to the heparin-collagen scaffold by blotting. (B) Using a microfluidic device a gradient of effector molecules is created by dilution in mixers. Channels with the various concentrations are led to a dispenser with multiple-outlets. The dispenser is placed in a device similar to a dot-blot microfiltration system. The gradient is transferred to the collagen-heparin scaffold using a vacuum.

Discussion

The main aim of this research was to create a gradient of effector molecules on a collagen scaffold. Here, a gradient was created by crosslinking a collagen scaffold in the presence of a gradient of heparin sustained by sucrose. Binding of FGF2 to the scaffold with a heparin gradient resulted in a gradient of the applied growth factor, which in turn resulted in a concentration-dependent proliferation of normal rat kidney cells *in vitro*. The created gradient scaffold may be a major step forward in regenerative medicine for various tissues in both *in vitro* and *in vivo* treatments.

Heparin, closely related to the heparan sulfate glycosaminoglycan, is widely used in tissue engineered constructs to bind effector molecules [27,28]. One of the effector molecules that binds to heparin is FGF2 [29]. We therefore expected FGF2 to bind to the heparin crosslinked to the collagen scaffold, which was shown by immunostainings. The specific interaction with heparin is a confirmation of earlier studies [27].

FGF2 is part of the fibroblast growth factor family, which is involved in various cellular processes [30]. FGF2 is known to influence cellular communication in a concentration dependent manner, as *e.g.* shown by the increased proliferation of human osteosarcoma MG-63 cells in fibrin matrices with immobilized FGF2 [31] and the concentration dependent generation of neurons and glia form multipotent cortical stem cells [32]. A concentration-dependent effect of FGF2 was also found on the normal rat kidney cells used here. It has been speculated that one of the principles behind the concentration-dependent reactions of cells to fibroblast growth factors is that fibroblast growth factor receptors on the cell react to different concentrations of fibroblast growth factors [33].

The scaffold of approximately 8-10 cm in length is relatively large when compared to biological gradients found in embryonic development and adult homeostasis [7,10]. Although the large gradient was effective on cells, down-scaling of the gradient is needed. New techniques may be based on a direct gradient of effector molecules, made onto heparin-containing scaffolds without a GAG gradient (Figure 5).

The first technique we like to postulate is based on a gradient device [34] (Figure 5A), which is able to create gradients of 1 cm based on diffusion from an application point. More complex gradients can be made with this technique, since two different effector molecules can be applied in the application slots (Figure 5A). Initial pilot experiments showed that it is feasible to create an FGF2 gradient in a hydrogel (results not shown). Further research is needed to determine whether it is possible to transfer the FGF2 gradient from the hydrogel to collagen-heparin scaffolds or films.

A second potential technique is based on microfluidics [35–37]. Microfluidic based devices are used in cell culture, *e.g.* to study cellular migration by defined gradients [38,39]. One could create a gradient using microfluidics by designing a device containing several mixers, followed by a dispenser to transfer the various concentrations of effector molecule to a collagen-heparin scaffold/film by applying a vacuum (Figure 5B). The complexity of the gradient can be adapted by the number of mixers used.

Conclusion

Type I collagen scaffolds were prepared with a gradient of glycosaminoglycans and FGF2, resulting in differences in cell number along the gradient scaffold after cell culture. This opens the possibility to create gradients on tissue engineered constructs.

References

[1] T. Tabata, Y. Takei, Morphogens, their identification and regulation, Development. 131 (2004) 703–712.

[2] D.E. Discher, D.J. Mooney, P.W. Zandstra, Growth factors, matrices, and forces combine and control stem cells, Science (80-.). 324 (2009) 1673–1677.

[3] J.B. Gurdon, P.Y. Bourillot, Morphogen gradient interpretation, Nature. 413 (2001) 797–803.

[4] W.P. Daley, S.B. Peters, M. Larsen, Extracellular matrix dynamics in development and regenerative medicine., J. Cell Sci. 121 (2008) 255–264.

[5] M.P. Lutolf, J.A. Hubbell, Synthetic biomaterials as instructive extracellular microenvironments for morphogenesis in tissue engineering, Nat Biotechnol. 23 (2005) 47–55.

[6] K. Lee, E.A. Silva, D.J. Mooney, Growth factor delivery-based tissue engineering: general approaches and a review of recent developments, J R Soc Interface. 8 (2011) 153–170.

[7] P. Müller, K.W. Rogers, S.R. Yu, M. Brand, A.F. Schier, Morphogen transport., Development. 140 (2013) 1621–38.

[8] D. Yan, X. Lin, Shaping morphogen gradients by proteoglycans., Cold Spring Harb. Perspect. Biol. 1 (2009).

[9] J. Dubrulle, B.M. Jordan, L. Akhmetova, J. a Farrell, S.-H. Kim, L. Solnica-Krezel, A.F. Schier, Response to Nodal morphogen gradient is determined by the kinetics of target gene induction, Elife. 4 (2015) 1–27.

[10] H.L. Ashe, J. Briscoe, The interpretation of morphogen gradients., Development. 133 (2006) 385–394.

[11] K.W. Rogers, A.F. Schier, Morphogen Gradients: From Generation to Interpretation, Annu. Rev. Cell Dev. Biol. 27 (2011) 377–407.

[12] N. Barkai, B.Z. Shilo, Robust generation and decoding of morphogen gradients., Cold Spring Harb. Perspect. Biol. 1 (2009) 1–15.

[13] P. Muller, K.W. Rogers, B.M. Jordan, J.S. Lee, D. Robson, S. Ramanathan, A.F. Schier, Differential Diffusivity of Nodal and Lefty Underlies a Reaction-Diffusion Patterning System, Science (80-.). 336 (2012) 721–724.

[14] D.M. Ornitz, J. Xu, J.S. Colvin, D.G. McEwen, C. a MacArthur, F. Coulier, G. Gao, M. Goldfarb, Receptor specificity of the fibroblast growth factor family., J. Biol. Chem. 271 (1996) 15292–15297.

[15] J.D. Bénazet, R. Zeller, Vertebrate limb development: moving from classical morphogen gradients to an integrated 4-dimensional patterning system., Cold Spring Harb. Perspect. Biol. 1 (2009).

[16] S. Massena, G. Christoffersson, E. Hjertström, E. Zcharia, I. Vlodavsky, N. Ausmees, C. Rolny, J.-P. Li, M. Phillipson, A chemotactic gradient sequestered on endothelial heparan sulfate induces directional intraluminal crawling of neutrophils., Blood. 116 (2010) 1924–31.

[17] R. Gillitzer, M. Goebeler, Chemokines in cutaneous wound healing., J. Leukoc. Biol. 69 (2001) 513–521.

[18] S. Barrientos, O. Stojadinovic, M.S. Golinko, H. Brem, M. Tomic-Canic, Growth factors and cytokines in wound healing, Wound Repair Regen. 16 (2008) 585–601.

[19] L. Cao, D.J. Mooney, Spatiotemporal control over growth factor signaling for therapeutic neovascularization., Adv. Drug Deliv. Rev. 59 (2007) 1340–50.

[20] J.D. Esko and Lindahl, U., Molecular diversity of heparan sulfate, Jounal Clin. Investig. 108 (2001) 169–173.

[21] J.S. Pieper, a. Oosterhof, P.J. Dijkstra, J.H. Veerkamp, T.H. Van Kuppevelt, Preparation and characterization of porous crosslinked collagenous matrices containing bioavailable chondroitin sulphate, Biomaterials. 20 (1999) 847–858.

[22] W.F. Daamen, H.T.B. Van Moerkerk, T. Hafmans, L. Buttafoco, a. a. Poot, J.H. Veerkamp, T.H. Van Kuppevelt, Preparation and evaluation of molecularly-defined collagen-elastin-glycosaminoglycan scaffolds for tissue engineering, Biomaterials. 24 (2003) 4001–4009.

[23] J.S. Pieper Hafmans, T., van Wachem, P.B., van Luyn, M.J.A., Brouwer, L.A., Veerkamp, J.H., and van Kuppevelt, T.H., Loading of collagen-heparan sulfate matrices with bFGF promotes angiogenesis and tissue generation in rats, J. Biomed. Mater. Res. 62 (2002) 185–194.

[24] L.H.H. Olde Damink, P.J. Dijkstra, M.J.A. Van Luyn, P.B. Van Wachem, P. Nieuwenhuis, J. Feijen, Cross-linking of dermal sheep collagen using a water-soluble carbodiimide, Biomaterials. 17 (1996) 765–773.

[25] I. V Yannas, J.F. Burke, P.L. Gordon, C. Huang, R.H. Rubenstein, Design of an artificial skin. II. Control of chemical composition., J. Biomed. Mater. Res. 14 (1980) 107–132.

[26] J.D. Bancroft Stoeltzing, O., Theory and practice of histological techniques, Churchill Livingston, Edinburgh, UK, 1990.

[27] S.T.M. Nillesen, P.J. Geutjes, R. Wismans, J. Schalkwijk, W.F. Daamen, T.H. van Kuppevelt, Increased angiogenesis and blood vessel maturation in acellular collagen-heparin scaffolds containing both FGF2 and VEGF, Biomaterials. 28 (2007) 1123–1131.

[28] Y. Liang, K.L. Kiick, Heparin-functionalized polymeric biomaterials in tissue engineering and drug delivery applications, Acta Biomater. 10 (2014) 1588–1600.

[29] M.A. Nugent, R. V Iozzo, Fibroblast growth factor-2., Int. J. Biochem. Cell Biol. 32 (2000) 115–120.

[30] Y.-R. Yun, J.E. Won, E. Jeon, S. Lee, W. Kang, H. Jo, J.-H. Jang, U.S. Shin, H.-W. Kim, Fibroblast growth factors: biology, function, and application for tissue regeneration., J. Tissue Eng. 2010 (2010) 218142.

[31] E.D. Miller, G.W. Fisher, L.E. Weiss, L.M. Walker, P.G. Campbell, Dose-dependent cell growth in response to concentration modulated patterns of FGF-2 printed on fibrin, Biomaterials. 27 (2006) 2213–2221.

[32] X. Qian, A.A. Davis, S.K. Goderie, S. Temple, FGF2 concentration regulates the generation of neurons and glia from multipotent cortical stem cells, Neuron. 18 (1997) 81–93.

[33] N.B. Weksler, G.P. Lunstrum, E.S. Reid, W.A. Horton, Differential effects of fibroblast growth factor (FGF) 9 and FGF2 on proliferation, differentiation and terminal differentiation of chondrocytic cells *in vitro*, Biochem J. 342 Pt 3 (1999) 677–682.

[34] A. Ganser, G. Roth, J.C. van Galen, J. Hilderink, J.J.G. Wammes, I. Müller, F.N. van Leeuwen, K.-H. Wiesmüller, R. Brock, Diffusion-driven device for a high-resolution dose-response profiling of combination chemotherapy., Anal. Chem. 81 (2009) 5233–40.

[35] V. van Duinen, S.J. Trietsch, J. Joore, P. Vulto, T. Hankemeier, Microfluidic 3D cell culture: From tools to tissue models, Curr. Opin. Biotechnol. 35 (2015) 118–126.

[36] W. Saadi, S.W. Rhee, F. Lin, B. Vahidi, B.G. Chung, N.L. Jeon, Generation of stable concentration gradients in 2D and 3D environments using a microfluidic ladder chamber, Biomed. Microdevices. 9 (2007) 627–635.

[37] N.L. Jeon, S.K.W. Dertinger, D.T. Chiu, I.S. Choi, A.D. Stroock, G.M. Whitesides, Generation of solution and surface gradients using microfluidic systems, Langmuir. 16 (2000) 8311–8316.

[38] L. Wang, Y. Li, G. Huang, X. Zhang, B. Pingguan-Murphy, B. Gao, T.J. Lu, F. Xu, Hydrogel-based methods for engineering cellular microenvironment with spatiotemporal gradients., Crit. Rev. Biotechnol. 0 (2015) 1–13.

[39] S.-Y. Cheng, S. Heilman, M. Wasserman, S. Archer, M.L. Shuler, M. Wu, A hydrogel-based microfluidic device for the studies of directed cell migration., Lab Chip. 7 (2007) 763–769.

Chapter 5

Dynamic expression of genes involved in proteoglycan/ glycosaminoglycan metabolism during skin development

P.J.E. Uijtdewilligen[1]*, E.M. Versteeg*[1]*, E.M.A. van de Westerlo*[1]*, J. van der Vlag*[2]*, W.F. Daamen*[1]*, and T.H. van Kuppevelt*[1]

[1] Department of Biochemistry, Radboud university medical centre, Nijmegen Centre for Molecular Life Sciences, Nijmegen, The Netherlands

[2] Nephrology Research Laboratory and Department of Nephrology, Radboud university medical centre, Nijmegen Centre for Molecular Life Sciences, Nijmegen, The Netherlands

This chapter has been submitted.

Abstract

Glycosaminoglycans are important for cell signaling and therefore for proper embryonic development and adult homeostasis. Expression of genes involved in proteoglycan/glycosaminoglycan (GAG) metabolism, and of genes coding for growth factors known to bind GAGs, were analyzed during skin development by microarray analysis and real-time quantitative PCR. GAG related genes were organized in six categories based on their role in GAG homeostasis, *viz.* 1) production of precursor molecules, 2) production of core proteins, 3) synthesis of the linkage region, and 4) polymerization, 5) modification and 6) degradation of the GAG chain.

In all categories highly dynamic up and down regulations were observed during skin development, including differential expression of GAG modifying isoenzymes, core proteins and growth factors. In two mice models, one over-expressing heparanase and one lacking C5 epimerase, differential expression of only few genes was observed.

Data show that during skin development a highly dynamic and complex expression of GAG-associated genes occurs. This likely reflects quantitative and qualitative changes in GAGs/proteoglycans -including structural fine tuning-, which may be correlated to growth factor handling.

Introduction

During various cell signaling processes, glycosaminoglycans (GAGs), such as heparan sulfate (HS), chondroitin sulfate (CS) and dermatan sulfate (DS), play a role in binding, guiding and modulating signaling molecules, e.g. growth factors and morphogens (1–3). In skin this role can be illustrated by the importance of GAGs in adult wound healing (3–7) and in the extracellular matrix architecture formed during dermal development (8). A further example to illustrate the importance of GAGs comes from mice overexpressing heparanase -an enzyme involved in the degradation of HS-, showing accelerated hair growth (9), indicating its involvement in hair follicle morphogenesis and homeostasis. Other observations show that HS is involved in hair follicle cycling, sebaceous gland morphogenesis and homeostasis (10). Finally, HS and heparanase influence wound healing in adult mice by enhancing keratinocyte migration and stimulating blood vessel maturation (7).

Inhibition of the expression of genes coding for enzymes involved in GAG modification reactions clearly indicate the importance of GAGs during organogenesis, especially with respect to growth factor handling. For example mice deficient in Ndst1 (N-deacetylase sulfotransferase isoenzyme 1) die neonatally due to several defects in which defective sonic hedgehog (Shh) signaling is implicated (11); mice deficient in Hs2st (heparan sulfate 2-O sulfotransferase) or Glce (glucuronic acid epimerase) display renal agenesis (12,13), whereas mice deficient in Hs6st1 (heparan sulfate 6-O sulfotransferase isozyme 1) show aberrant signaling of VEGF (vascular endothelial growth factor) and impaired lung development (14). A skin phenotype of the above mouse models, however, has not been reported.

In general, it is thought that specific modifications of the GAG chain are involved in the binding and modulation of signaling molecules resulting in cell-type and/or tissue specific reactions (3,15,16). GAG mimetics like the RGTAs (regenerating agents) have been used to treat skin disorders and improve skin healing (17). To obtain insight in GAG metabolism during skin development we studied the expression of GAG related genes covering six functional classes ranging from the synthesis of precursor molecules to the synthesis and degradation of GAGs. In addition, we probed the expression of a number of (GAG binding) signaling molecules.

Materials and methods

An overview of the experimental setup on the gene expression during murine skin development is given in Figure 1.

Animals for the study on skin development

NIH guidelines for the care and use of laboratory animals (NIH publication 85–23 Rev. 1985) were followed. The study was approved by the Ethics Committee of the Radboud university medical center (DEC 2005-111, project: 81027). C57BL6/j mice were obtained from Elevage Janvier (Le Genest Saint Isle, France). Mice aged 90 days (90 days post birth [P90]) were used for timed matings and dorsal skin was collected at 14 days (E14) and 16 days post conception (E16). At E14 hair follicle development is initiated and at E16 appendage formation is almost completed in combination with a stratified epidermis and organized dermis (18,19). For the RNA samples of E14, dorsal skin of seven embryos from one female were pooled and used for RNA isolation. Skin was isolated at E14 by snap freezing the whole embryo in liquid nitrogen followed by scraping the skin layer in a cryomicrotome with a scalpel to minimize contamination with other embryonic tissues (skin is very thin at this time point). Samples were stored at -80 °C. RNA samples for E16 were taken from two females, collecting dorsal skin form 7 embryos each. In addition, skin from 1 day old pups (P1) and adult mice (P90) was collected. At P1 skin is more organized and has been exposed to air (18,19). For the two dorsal skin samples for P1, three pups from two females were taken per sample. Two adult three months old mice were used for the two dorsal skin samples at P90. Samples for RNA isolation for E16, P1 and P90 were collected by removing dorsal skin and snap freezing it in liquid nitrogen and storage at -80 °C.

Tissue of genetically modified mice

Skin samples of glucuronic acid epimerase (Glce) knockout mice (E18.5 for expression analysis; E17.5 and E18.5 for histological analysis) and of heparanase overexpression (Hpse) mice (P70) were provided by Prof. Dr. Jin-Ping Li (Department of Medical Biochemistry and Microbiology, University of Uppsala, Sweden) and Prof. Dr. Israel Vlodavsky (Vascular and Cancer Biology Research Center Rappaport Faculty of Medicine and Research Institute Technion-Israel Institute of Technology, Israel), respectively (9,20). For RNA isolation two wildtype and two mutant mice were used of both mouse models.

RNA isolation, real time quantitative PCR and microarray analysis

Frozen samples were grinded in a micro-dismembrator (Sartorius, Bunnik, The Netherlands) and RNA was isolated using the TRIZOL-method (Invitrogen, Paisley, UK) in combination with RNeasy Mini kit with DNAse step (Qiagen, Hilden, Germany). RNA quality was assessed using the Bioanalyzer system (Agilent Technologies, Amstelveen, The Netherlands). The RNA integrity numbers (RIN, 27) were 8.8±0.25 (technical replicate N=2), 8.0±0.35, 8.5±0.55 and 7.3±0.2 for E14, E16, P1 and P90 (biological replicates N=2), respectively. The same procedure was used for the RNA isolation for

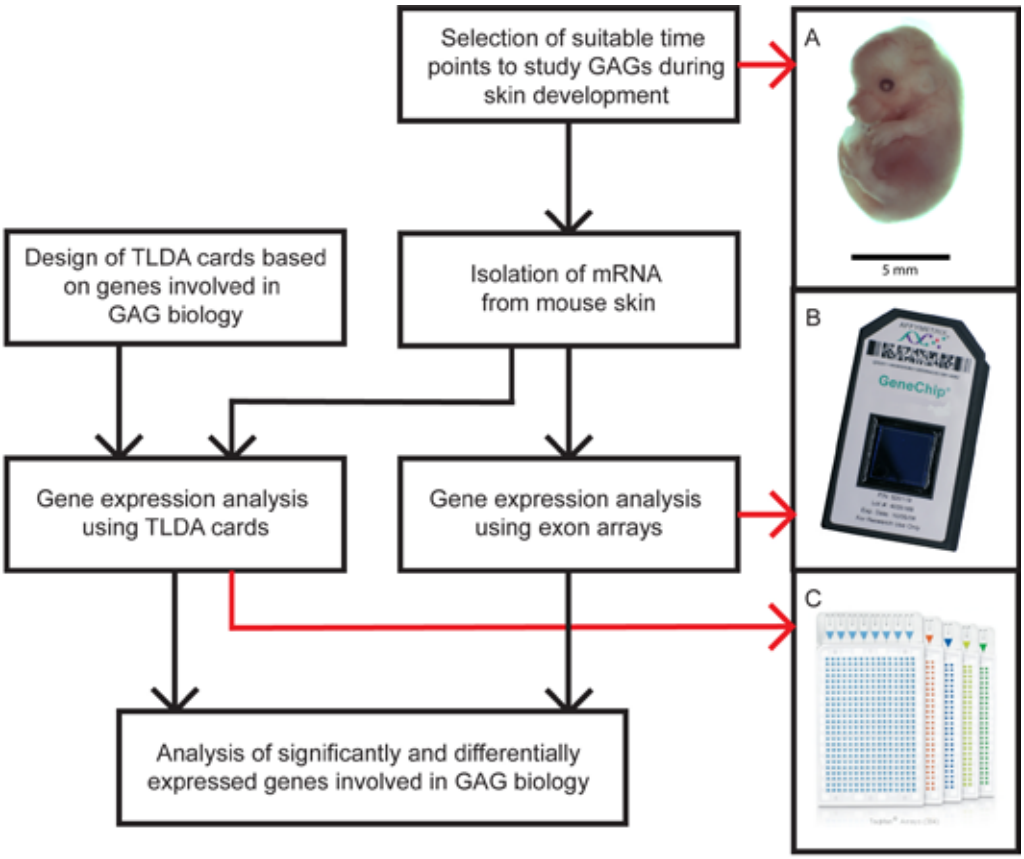

Figure 1 – Experimental setup used for the analysis of gene expression involved in GAG biology during skin development in mice. Based on literature data, specific time points in skin development were selected. (A) A mouse embryo at 14 days post conception. RNA was isolated, verified and subsequently analysed with GeneChip exon arrays (B) and TLDA gene expression cards (C).

the Glce knockout mouse and Hpse overexpression mouse. The RIN was 6.5±0.51 for *Glce*-/- samples and 8.0±0.48 for *Glce*+/+ and 6.3±0.3 and 7.7±0.6 for HPA-TG and HPA-WT, respectively (all biological replicate N=2).

Gene Chip Mouse exon 1.0 ST Arrays (Affymetrix, High Mycombe, UK) were used to analyse gene expression for E14, E16, P1 and P90 using 1 µg of RNA per chip. Expression data were preprocessed to check sensitivity and specificity of the results based on Kadota *et al.* (2009) as shown in Uijtdewilligen *et al.* (2016) (18,22). Gene level expression data were calculated for the CORE transcripts (probe sets supported by RefSeq mRNAs) using Affymetrix Expression Console software with quantile normalization (all arrays are considered to have an equal intensity distribution), GC content background correction (probes with high GC-content hybridize better, corrected for with built-in probes with different known GC-contents) and summarization with the

RMA algorithm (23). Data were imported into GeneSpring GX 7.3 (Agilent Technologies), duplicates were averaged and the expression of each transcript was normalized to the median per array.

Real Time-Quantitative PCR (qPCR) was performed using custom designed Taqman Low Density arrays (TLDA) (Applied Biosystems, Nieuwerkerk aan de IJssel, The Netherlands) containing probes against genes involved in GAG metabolism and GAG binding proteins (Supplementary data table 1). Glce and Hpse samples were analyzed using qPCR using custom designed TLDA with an adapted design containing additional GAG related genes (Supplementary data table 2).

For the TLDA cards, 100 ng cDNA in Taqman Universal PCR Master Mix (Applied Biosystems) was loaded on the TLDA card per slot and run on a 7900HT Fast Real-Time PCR System (Applied Biosystems). Expression was analyzed based on the threshold cycle (Ct) which was obtained using the SDS 2.3 software and RQ Manager 1.2 of Applied Biosystems using the combined expression data of the tested TLDA cards. In Microsoft Excel the reference genes for ΔCt calculation were checked for stability of expression by analyzing the results of the reference genes across all used TLDA cards and selecting the reference genes with the smallest deviation across the cards tested. Subsequently ΔCT values were calculated using a reference gene with the smallest difference between the average Ct found for the gene of interest and for the reference gene. The obtained ΔCt values were further processed using the $2^{-\Delta\Delta Ct}$ method using P90 as a calibration point in case of the developmental study, and the wildtype background (C57BL6 mice) data in case of the two mouse models (24).

Statistical methods

Statistical significance of the exon array data was analyzed using ANOVA and Benjamini-Hoghberg multiple testing correction (25). Statistical significance of the TLDA card data was tested with an unpaired T-test (2-tailed) using Microsoft Excel. Data with a statistical threshold of $p<0.10$ and a fold threshold of >2.0 were considered statistically significant.

Table 1: Comparison of the number of differentially expressed genes during skin development in mice (p<0.10, fold>2.0) based on real-time qPCR and on exon array analysis.

Total genes	System	E14vsP90		E16vsP90		P1vsP90	
		2.0 Fold Down	*2.0 Fold Up*	*2.0 Fold Down*	*2.0 Fold Up*	*2.0 Fold Down*	*2.0 Fold Up*
Production of percursors							
43	TLDA	1	4	3	2	1	2
43	EXON	2	6	2	0	1	0
	Overlap	0	2	2	0	1	0
Core proteins							
14	TLDA	2	3	1	1	2	2
14	EXON	3	2	1	1	0	2
	Overlap	2	2	0	1	0	2
Preparation of linkage region							
8	TLDA	0	1	0	1	0	1
8	EXON	0	2	0	0	0	0
	Overlap	0	0	0	0	0	0
Glycosaminoglycan chain polymerisation							
13	TLDA	1	4	1	2	0	2
13	EXON	1	2	0	0	0	0
	Overlap	0	0	0	0	0	0
Glycosaminoglycan chain modification							
32	TLDA	1	9	0	5	0	8
32	EXON	1	3	0	3	0	1
	Overlap	1	2	0	1	0	0
Glycosaminoglycan chain degradation							
19	TLDA	2	2	3	1	0	1
19	EXON	3	1	1	1	2	0
	Overlap	2	1	1	1	0	0
Growth factors							
37	TLDA	0	13	3	8	1	11
37	EXON	2	14	3	10	1	4
	Overlap	0	10	2	8	0	4

** P values for the exon array measurements were calculated using Benjamini–Hochberg multi-testing correction. P values for the TLDA assay were calculated using an unpaired T-test.*

Overlap refers to genes differentially expressed in both TLDA card and exon array.

Results

Genes involved in glycosaminoglycan (GAG) synthesis, modification and degradation were studied during skin development at 14 and 16 days post conception (E14 and E16, respectively) and at one day post birth (P1), and compared to mature skin of a 3 month old mouse (P90). In addition, two mouse models, *viz.* a Glce knockout mouse (E18.5) and a HPSE overexpression mouse model (P70) were analysed. Taqman low density array (TLDA) cards were designed to contain genes involved in GAG metabolism (Supplementary data table 1 and 2). The expression data obtained using TLDA cards and exon arrays were screened for genes with 2-fold differential expression at a statistical threshold of $p<0.10$ (Tables 1, 2, 3 and 4, Supplementary data tables 4, 5 and 6).

In Tables 1-3 and Supplementary data table 3, an overview is given of the differentially expressed genes applying TLDA cards and exon arrays. In all categories of genes involved in GAG metabolism, *i.e.* production of precursor molecules, core proteins, synthesis of linkage region, and polymerization, modification and degradation of the GAG chain, differences in expression were found (Tables 1-3). This indicates a highly dynamic expression pattern during skin development. Interestingly, some isoenzymes were up, whereas other isoenzymes were down regulated, further stressing metabolic complexity. This is for instance the case with GFPT1 and 2, both rate limiting enzymes involved in the production of hexosamines, and the isoenzymes HS 3-O sulfotransferase 6 and 3b1.

With respect to the core proteins, differential expression was found for both HS and CS/DS proteoglycans. Differential expression was found for two of the four syndecans, viz. Sdc1 and Sdc4, three of the six glypicans, viz. Gpc2, Gpc3 and Gpc6, and for Hspg2 (Table 2 and 3). The syndecans were down regulated, while the glypicans were upregulated, indicating an embryonic role for glypicans as described in literature (4,26). Hspg2, a secreted HS presenting proteoglycan coding for perlecan (3), was found to be upregulated (Table 2 and 3). Based on the exon array the CS/DS core protein of versican (Vcan) was upregulated at all time points (Supplementary data table 5).

The upregulated expression of genes involved in the synthesis of the linkage region may signal increased GAG synthesis during development since after the formation of the linkage region the GAG chain is formed. For HS polymerization differential expression was found for *e.g. Extl1* and *Extl2*. *Extl1* showed down regulation at E14 while *Extl2* was upregulated, both enzymes are involved in the initiation and elongation of the HS chain (27).

During and after synthesis of the glycosaminoglycan chain, disaccharide units within the chain are specifically modified. These modifications determine which effector molecules can bind to the chain, and thus play a role in cell signaling (1,2). Upregulated expression was found for three of the four N-deacetylase/N-sulfotransferases (*Ndst*; TLDA cards, Table 2), especially isoenzyme Ndst3. Upregulation was also found for two out of seven genes coding for 3-O-sulfotransferases (*Hs3st1* and *Hs3st3b1*), involved in 3-O sulfation of GlcNS and GlnNAc residues, whereas one was down regulated (*Hs3st6*).

The GlcNS and GlcNAc residues can also be 6-O sulfated by 6-O-sulfotransferases (Hs6st) (27) and selectively desulfated extracellularly by two sulfatases (*Sulf1* and *Sulf2*) aided by two cofactors (*Sumf1* and *Sumf2*) (3,27,28). Hs6st2 was upregulated at all time points (Table 3). *Sulf1* was upregulated during embryonic development, whereas *Sumf2* was upregulated at E14 (Table 2 and 3). These results indicate that specific expression of GAG modifying enzymes may play a role in specific cellular signaling during skin development.

Within the class of genes encoding for GAG chain degradation enzymes, two genes were differentially expressed. Heparanase expression was down regulated at E14 and P1 (Table 2 and 3), whereas N-sulfoglucosamine sulfohydrolase (*Sgsh*) was downregulated during embryonic development at E16 (Table 2) and at E14 (Table 3).

In addition to genes involved in GAG metabolism, the TLDA card contained 37 genes encoding growth factors, which were also present in the microarray (Table 2 and 3). Differential expression was found by both TLDA card and microarray analysis for 10, 9 and 4 growth factors at E14, E16 and P1 respectively. Examples are insulin-like growth factor 2 (*Igf2*), wingless-related integration site 6 (*Wnt6*) and *Wnt7b*. *Igf2* was dramatically upregulated at all time points, as expected based on previous research (18). *Wnt6* was also upregulated at all time points, while *Wnt7b* was upregulated only during embryonic development.

Next to their expression during development, gene expression of GAG associated genes was studied in a *Glce* (glucuronyl epimerase) knockout mouse model and a heparanase overexpression mouse model using TLDA cards. In the *Glce* knockout mice six genes were differentially expressed (Table 4). Three of them are involved in CS and DS proteoglycans, and were downregulated, *i.e.* aggrecan (*Acan*), asporin (*Aspn*) and chondroitin sulfate N-acetylgalactosaminyltransferase 2 (*Csgalnact2*). Up/down regulation was not found for HS related genes, except for Glce, which was downregulated as expected. For the heparanase overexpression mouse model, in which a human heparanase was overexpressed (9), the results showed only one gene to be differentially expressed, i.e aggrecan (*Acan*) which was 2.5 fold upregulated. The complete results of both the *Glce* knockout mouse and Hpse overexpression mouse are given in Supplementary data table 6.

Table 2: Differentially expressed GAG related genes during skin development in mice in comparison to mature skin (p<0.10) based on real-time qPCR.

Gene symbol	Full gene name and probe set	E14 vs. P90 P-value	E14 vs. P90 Relative change	E16 vs. P90 P-value	E16 vs. P90 Relative change	P1 vs. P90 P-value	P1 vs. P90 Relative change
Production of precursors							
Galk1 ‡	Galactokinase 1 Mm00444182_m1	***0.029***	***5.897***	***0.057***	***3.867***	***0.074***	***3.043***
Galt ‡	Gal-1-P-Uridylyltransferase Mm00489459_g1	*0.042*	*0.573*	***0.027***	***0.497***	0.832	0.964
Gfpt1 ‡	Glu-Fru-6-P-Transaminase 1 Mm00600127_m1	***0.002***	***2.378***	0.160	1.273	0.282	1.481
Gfpt2 ‡	Glu-Fru-6-P-Transaminase 2 Mm00496565_m1	0.269	0.772	***0.079***	***0.494***	0.356	0.780
Hk2 ‡	Hexokinase 2 Mm00443385_m1	*0.027*	*0.652*	0.253	1.390	*0.586*	*0.904*
Pgm3 ‡	Phosphoglucomutase 2 Mm00459270_m1	*0.058*	*1.876*	0.296	1.249	*0.098*	*1.470*
Pgm5 ‡	Phosphoglucomutase 5 Mm00723432_m1	***0.002***	***4.053***	***0.033***	***2.792***	***0.019***	***2.515***
Slc13a5 ‡	Solute Carrier Family 13 Member A5 Mm00523288_m1	Not detected		Not detected		Not detected	
Slc26a9 ‡	Solute Carrier Family 26 Member A9 Mm00628490_m1	Not detected		0.036	0.264	0.023	0.318
Slc35a3 ‡	Solute Carrier Family 35 Member a3 Mm00523288_m1	***0.008***	***0.444***	*0.060*	*0.567*	0.455	0.811
Core proteins							
Cd44	CD44 Molecule Mm01277164_m1	*0.018*	*0.536*	0.171	0.637	0.223	1.385
Gpc2 ‡	Glypican 2 Mm00549650_m1	***0.005***	***11.686***	0.638	1.294	0.369	1.249
Gpc3 †	Glypican 3 Mm00516722_m1	***0.000***	***6.765***	***0.019***	***3.734***	***0.013***	***8.044***
Gpc6 ‡	Glypican 6 Mm00516235_m1	***0.027***	***2.880***	0.275	1.376	0.130	1.926
Hspg2 ‡	Perlecan Mm01181179_g1	*0.030*	*1.504*	*0.064*	*1.959*	***0.007***	***3.325***
Sdc1 ‡	Syndecan 1 Mm00448918_m1	***0.012***	***0.293***	0.107	0.313	***0.069***	***0.403***
Sdc4 †	Syndecan 4 Mm00488527_m1	***0.002***	***0.201***	***0.039***	***0.240***	***0.065***	***0.471***
Preparation of linkage region							
B3gat1	β-1,3-Glucuronyltransferase 1 Mm00661499_m1	Not detected		Not detected		Not detected	
B3gat2	β-1,3-Glucuronyltransferase 2 Mm00549042_m1	Not detected		Not detected		Not detected	
B4galt2 ‡	β-1,4-Galactosyltransferase 2 Mm00479556_m1	***0.023***	***4.562***	***0.059***	***2.679***	***0.038***	***3.384***

Gene symbol	Full gene name and probe set	E14 vs. P90 P-value	E14 vs. P90 Relative change	E16 vs. P90 P-value	E16 vs. P90 Relative change	P1 vs. P90 P-value	P1 vs. P90 Relative change
Glycosaminoglycan chain polymerisation							
Chpf ‡	Chondroitin Polymerizing Factor Mm01262239_g1	***0.000***	***2.991***	*0.059*	*1.865*	***0.050***	***2.401***
Chsy1 ‡	CS Synthase 1 Mm01319178_m1	***0.013***	***3.900***	***0.024***	***2.282***	***0.072***	***2.229***
Chsy3 ‡	CS Synthase 3 Mm01545329_m1	***0.026***	***4.006***	***0.075***	***2.184***	0.101	2.013
Csgalnact1 ‡	CS-GalNAc-transferase 1 Mm00555164_m1	***0.099***	***0.496***	***0.098***	***0.475***	0.634	1.128
Extl1 ‡	Exostoses (multiple)-like 1 Mm00621977_s1	Not detected		Not detected		Not detected	
Extl2 ‡	Exostoses (multiple)-like 2 Mm00469621_m1	***0.007***	***2.043***	0.660	1.220	0.106	1.765
Has2 ‡	Hyaluronan Synthase 2 Mm00515089_m1	0.188	1.933	0.235	1.705	0.410	1.577
Glycosaminoglycan chain modification							
Chst11 ‡	Chondroitin 4-O-Sulfotransferase 1 Mm00517563_m1	***0.002***	***3.000***	*0.087*	*1.195*	*0.087*	*1.957*
Chst14 ‡	Dermatan 4 Sulfotransferase 1 Mm00511291_s1	***0.026***	***2.459***	0.156	1.513	0.203	1.707
Chst2 ‡	Carbohydrate Sulfotransferase 2 Mm00490018_g1	***0.014***	***3.664***	***0.010***	***3.145***	***0.006***	***2.773***
Chst3 ‡	Chondroitin 6-O-Sulfotransferase 1 Mm00489736_m1	***0.041***	***3.241***	0.152	1.941	***0.028***	***3.550***
Chst8 ‡	GalNAc-4-O-Sulfotransferase 1 Mm00558321_m1	***0.089***	***2.587***	0.221	0.591	0.139	2.280
Hs3st1 ‡	HS 3-O-sulfotransferase Mm01964038_m1	*0.051*	*1.796*	*0.039*	*1.937*	***0.027***	***2.809***
Hs3st3b1‡	HS 3-O-sulfotransferase 3b1 Mm00479621_m1	***0.004***	***3.204***	***0.028***	***2.511***	***0.002***	***2.629***
Hs3st6 ‡	HS 3-O-sulfotransferase 6 Mm01299930_m1	***0.006***	***0.208***	*0.089*	*0.664*	*0.041*	*1.765*
Hs6st2	HS 6-O-sulfotransferase 2 Mm00479296_m1	Not detected		Not detected		Not detected	
Ndst1 ‡	N-deacet./N-sulfotrans. 1 Mm00447005_m1	0.118	1.487	0.140	1.449	***0.054***	***2.202***
Ndst2 ‡	N-deacet./N-sulfotrans. 2 Mm00447818_m1	*0.008*	*1.347*	***0.001***	***2.017***	***0.002***	***2.021***
Ndst3 ‡	N-deacet./N-sulfotrans. 3 Mm00453178_m1	***0.004***	***4.708***	***0.041***	***7.910***	***0.004***	***12.034***
Sulf1 ‡	Sulfatase 1 Mm00552283_m1	***0.004***	***4.644***	***0.079***	***2.674***	***0.089***	***2.077***
Sumf2 ‡	Sulfatase modifying factor 2 Mm01197721_m1	***0.008***	***2.657***	0.104	2.023	*0.038*	*1.857*
Glycosaminoglycan chain degradation							
ArsJ ‡	Arylsulfatase J Mm00557970_m1	***0.013***	***7.805***	***0.010***	***12.075***	***0.014***	***7.146***
ArsK ‡	Arylsulfatase K Mm00513099_m1	0.306	0.801	***0.059***	***0.466***	0.143	0.678
Galns ‡	Galactosamine (N-Acetyl)-6-Sulfatase Mm00489575_m1	***0.000***	***2.648***	*0.066*	*1.674*	*0.091*	*1.584*

Gene symbol	Full gene name and probe set	E14 vs. P90		E16 vs. P90		P1 vs. P90	
		P-value	Relative change	P-value	Relative change	P-value	Relative change
Hpse ‡	Heparanase Mm00461768_m1	***0.044***	***0.304***	0.342	1.450	0.169	0.578
Hyal1 ‡	Hyaluronoglucosamini-dase 1 Mm00476206_m1	***0.001***	***0.198***	***0.008***	***0.288***	*0.006*	*0.607*
Sgsh ‡	N-Sulfoglucosamine Sulfohydrolase Mm00450747_m1	*0.055*	*0.647*	***0.002***	***0.435***	0.644	0.897
Growth factors							
Areg	Amphiregulin Mm00437583_m1	Not detected		Not detected		0.656	0.834
Bmp3 ‡	Bone morphogenetic growth factor 3 Mm00557790_m1	***0.007***	***4.270***	***0.004***	***7.240***	***0.002***	***11.628***
Bmp5 ‡	Bone morphogenetic growth factor 5 Mm00432091_m1	***0.022***	***12.051***	0.303	1.788	0.587	1.300
Ctgf ‡	Connective tissue growth factor Mm01192931_g1	0.668	1.079	***0.011***	***0.232***	*0.076*	*0.580*
Fgf10 ‡	Fibroblast growth factor 10 Mm00433275_m1	*0.063*	*1.649*	*0.050*	*1.801*	***0.093***	***2.262***
Fgf13 ‡	Fibroblast growth factor 13 Mm00438910_m1	***0.002***	***3.205***	*0.059*	*1.750*	0.181	1.544
Fgf2 ‡	Fibroblast growth factor 2 Mm01285715_m1	0.277	0.651	0.166	0.539	0.382	1.446
Fgf20	Fibroblast growth factor 20 Mm00748347_m1	Not detected		Not detected		Not detected	
Fgf22 ‡	Fibroblast growth factor 22 Mm00445749_m1	Not detected		0.386	0.632	*0.060*	*0.614*
Fgf7 ‡	Fibroblast growth factor 7 Mm00433291_m1	*0.045*	*0.606*	***0.002***	***0.394***	*0.087*	*0.630*
Fgf8	Fibroblast growth factor 8 Mm00438921_m1	Not detected		Not detected		Not detected	
Figf ‡	C-fos induced growth factor Mm01131929_m1	*0.081*	*1.397*	*0.030*	*1.787*	0.545	0.834
Gdf10 ‡	Growth differentaition factor 10 Mm03024279_s1	***0.015***	***3.181***	0.454	1.143	0.166	1.519
Hbegf ‡	Heparin-binding epidermal growth factor Mm00439305_g1	Not detected		***0.015***	***0.347***	***0.016***	***0.423***
Hdgf †	Hepatoma-derived growth factor Mm00725733_s1	0.257	1.221	0.737	0.911	0.975	1.008
Igf1 ‡	Insulin-like growth factor 1 Mm00439560_m1	0.320	1.207	0.217	0.705	0.364	0.790
Igf2 †	Insulin-like growth factor 2 Mm00439565_g1	***0.000***	***592.335***	***0.002***	***338.094***	***0.001***	***416.096***
Nog ‡	Noggin Mm01297833_s1	***0.054***	***2.945***	***0.019***	***2.935***	***0.021***	***3.067***
Pdgfa ‡	Platelet-derived growth factor a Mm01205760_m1	***0.021***	***3.005***	Not detected		***0.016***	***3.669***
Pdgfb ‡	Platelet-derived growth factor b Mm01298578_m1	0.321	1.098	*0.033*	*1.468*	***0.010***	***2.096***
Pdgfc ‡	Platelet-derived growth factor c Mm00480205_m1	Not detected		***0.016***	***2.362***	Not detected	
Pdgfd ‡	Platelet-derived growth factor d Mm00546829_m1	Not detected		0.288	0.709	0.139	1.644
Shh	Sonic hedgehog Mm00436527_m1	Not detected		Not detected		Not detected	

Gene symbol	Full gene name and probe set	E14 vs. P90		E16 vs. P90		P1 vs. P90	
		P-value	Relative change	P-value	Relative change	P-value	Relative change
Tgfb1 ‡	Transforming growth factor beta 1 Mm01178820_m1	*0.027*	*0.540*	0.488	0.817	0.157	1.372
Tgfb2 ‡	Transforming growth factor beta 2 Mm01321739_m1	***0.039***	***2.697***	0.757	1.081	0.127	1.809
Tgfb3 ‡	Transforming growth factor beta 3 Mm01307950_m1	***0.033***	***2.420***	*0.094*	*1.854*	***0.034***	***2.517***
Vegfa ‡	Vascular endothelial growth factor a Mm01281447_m1	0.394	1.108	0.112	1.613	0.461	1.358
Vegfb	Vascular endothelial growth factor b Mm00442102_m1	Not detected		Not detected		Not detected	
Vegfc ‡	Vascular endothelial growth factor c Mm00437313_m1	*0.024*	*1.839*	0.303	1.250	*0.015*	*1.996*
Wnt10b ‡	Wingless-related integration site 10b Mm00442104_m1	0.180	5.829	0.122	9.688	0.105	11.748
Wnt16 ‡	Wingless-related integration site 16 Mm00446420_m1	***0.066***	***2.094***	***0.016***	***4.809***	***0.014***	***4.362***
Wnt2 ‡	Wingless-related integration site 2 Mm00470018_m1	***0.054***	***3.144***	*0.090*	*3.555*	*0.074*	*3.760*
Wnt2b	Wingless-related integration site 2b Mm00437330_m1	Not detected		Not detected		Not detected	
Wnt3a ‡	Wingless-related integration site 3a Mm00437337_m1	0.394	1.610	0.441	1.520	0.840	1.106
Wnt6 ‡	Wingless-related integration site 6 Mm00437353_m1	***0.015***	***11.709***	***0.018***	***10.400***	***0.016***	***10.758***
Wnt7a	Wingless-related integration site 7a Mm00437355_m1	Not detected		Not detected		Not detected	
Wnt7b ‡	Wingless-related integration site 7b Mm00437357_m1	***0.003***	***4.180***	***0.056***	***6.076***	***0.003***	***4.181***

Numbers in italic are significant (p<0.10); numbers in bold are >2 fold differentially expressed. Gene symbols indicated with a †-symbol are normalized using GAPDH as a reference gene. Gene symbols indicated with a ‡-symbol are normalized using TBP as a reference gene. Genes, for which a signal was not or only partly detected at a given timepoint or multiple timepoints and therefore a fold change and/or p-value could not be calculated based on the available data, are given as 'not detected'. Gene symbol for which all timepoints were classified as 'not detected' do not show a symbol for the used reference gene due to lack of data for a calculation.

Discussion

GAGs play a regulating role during embryonic development of various organs (1–3). Therefore, we examined the expression of genes involved in GAG metabolism during skin development using custom designed Taqman Low Density Arrays (TLDA card) and exon arrays. To structure the data we studied gene expression in six functional classes, *viz.* the production of precursor molecules, the synthesis of core proteins and the linkage region, and the synthesis, modification and degradation of the GAG chain proper. In addition we studied a number of growth factors, since GAGs are involved in their regulation including growth factor diffusion and signaling (29).

With respect to core proteins, the heparan sulfate proteoglycans syndecan and glypican showed notable differential expression (Table 2 and 3). Glypicans play an important role in development and cell signaling (26,30–33), and we found upregulation of 3 out of 6 glypican core proteins. *Gpc3* was upregulated during embryonic development and one day post birth, suggesting that this glypican has a role during skin development. A possible function of *Gpc3* in skin has been suggested for the *Gpc3*-null mouse, which showed pigmentation defects (34). Humans deficient in *Gpc3* suffer from the Simpson-Golabi-Behmel syndrome (SBGS). Based on the symptoms of SGBS and the phenotype found for the *Gpc3*-null mice, it has been suggested that *Gpc3* is involved in the regulation of hedgehog signaling (31), a signaling pathway involved in skin appendage formation (35,36). Surprisingly, the *Gpc3*-null mice did not show a defect in appendage formation (34), indicating a functional but not essential role. Further research is needed to elucidate the role of *Gpc3* and the two other differentially expressed glypicans, i.e. *Gpc2* and *Gpc6*.

Syndecans are described to take part in adult wound healing (4,6,37). We found downregulation of the core proteins of two syndecans during embryonic development, which could indicate that these proteoglycans do not play a major role during skin development. In literature, however, it has been shown that *Sdc1* is involved in hair follicle development based on immunohistochemical data (38,39).

In the class of GAG chain polymerization, we found differential expression of genes encoding for the initiation of HS or CS/DS synthesis. HS chain polymerization is initiated by the addition of GlcNAc by *Extl2* (40) or *Extl3* (41), while CS/DS chain polymerization is initiated by the addition of GalNAc by *Csgalnact1* (42). *Extl2* was upregulated during early skin development (Table 2), while *Csgalnact1* was downregulated (Supplementary data Table 5), which suggests that during early skin development HS production is stimulated in comparison to CS/DS production.

Enzyme mediated chemical modifications of the GAG chains result in the creation of specific binding sites for effector molecules (43). Enzymes forming the class of N-deacetylase/sulfotransferases (Ndst's) are initiating elements in this respect. Especially *Ndst3* was upregulated, being one of four enzymes responsible for the removal of the acetyl group from the N-acetylated glycosamine and for the addition of a sulfate group. The additional expression of *Ndst3* in combination with *Ndst1* and *Ndst2* points to the fine-tuning of HS chains for specific recognition of ligands. *Ndst3* has a higher deacetylation activity in comparison to the N-sulfotransferase activity, while *Ndst1*

and *Ndst2* have a slightly higher N-sulfotransferase activity (44). In addition, the data on the expression of heparan sulfate 3-O sulfotransferases (Hs3sts) (45) and heparan sulfate 6-O-sulfotransferases (Hs6sts) (46) suggest dynamic and specific modification of HS chains.

Three genes encoding for enzymes involved in HS and CS/DS degradation were differentially expressed, one of them being *Hpse* (heparanase). *Hpse* is down regulated at E14 and at P1, but not at E16 at which time point hair follicle development is taking place. *Hpse* has been reported to be involved in this process (47,48).

Glycosaminoglycans are involved in growth factor regulation during developmental processes (1–3). We therefore studied 37 growth factors implied in skin development. A number of genes encoding growth factors were differentially expressed during development and the data are in line with earlier results for e.g. *Igf2* (18), *Wnt6* and *Wnt7b* (49). Although speculative, the dynamics in GAG structure may be correlated to the dynamics of growth factors.

Next to skin development we also studied gene expression in skin of a *Glce* (glucuronyl epimerase) knockout mouse and a Hpse (heparanase) overexpression mouse (9,12). In the *Glce* knockout mice relatively few genes were differentially expressed, suggesting that skin is relatively unaffected by the lack of *Glce* in line with the observation that skin in these mice is phenotypically normal (20). The skin phenotype of the Hpse overexpression mouse shows accelerated hair growth (9). Gene expression analysis of this model showed only one differentially expressed gene (aggrecan).These results may touch upon the regulation of translation of mRNAs coding for GAG related enzymes. Enzymes involved in the synthesis and modification of GAGs as well genes coding for (some) growth factors share a common alternative translation mechanism via IRES sites (50,51). In general mRNAs are translated by the ribosomal scanning mechanism which scans for short leader sequences of 50 to 70 nucleotides (51,52). The leader sequences of the HS modifying enzymes and growth factors are characterized by long but structured sequences, which are not recognized by the ribosomal scanning mechanism (51,52). Within these sequences internal ribosomal entry sites (IRES) allow alternative translation e.g. under stress conditions (52). This indicates that in addition to mRNA levels an additional control mechanism on the translational level may be present.

Taken the data together, it is concluded that a highly dynamic expression of genes involved in GAG metabolism and in GAG-binding growth factors is associated with skin development. This indicates the importance of fine tuning of GAG structures during developmental processes. Further studies should focus on the biochemical analysis of the GAGs chains themselves.

Table 3: Differentially expressed GAG related genes during skin development in mice in comparison to mature skin (p<0.10) based on gene Chip Mouse Exon 1.0 ST Arrays

Gene symbol	Full gene name and probe set	E14 vs. P90 Stepup P-value	E14 vs. P90 Fold change	E16 vs. P90 Stepup P-value	E16 vs. P90 Fold change	P1 vs. P90 Stepup P-value	P1 vs. P90 Fold change
Production of precursors							
Galk1	Galactokinase 1 6792485	***0.030***	***4.242***	0.126	2.483	0.231	2.194
Galt	Gal-1-P-Uridylyltransferase 6912944	0.664	0.814	0.231	1.864	0.665	1.340
Gfpt1	Glu-Fru-6-P-Transaminase 1 6947679	***0.020***	***2.110***	0.077	1.682	0.801	1.081
Gfpt2	Glu-Fru-6-P-Transaminase 2 6780767	0.176	0.610	***0.087***	***0.426***	0.229	0.547
Hk2	Hexokinase 2 6954982	***0.003***	***0.451***	*0.040*	*1.375*	*0.039*	*0.655*
Pgm3	Phosphoglucomutase 2 6997513	***0.083***	***2.193***	0.676	1.178	*0.654*	*1.286*
Pgm5	Phosphoglucomutase 5 6872290	***0.058***	***2.338***	***0.104***	***2.209***	***0.291***	***1.696***
Slc13a5	Solute Carrier Family 13 Member A5 6789531	***0.003***	***2.588***	*0.059*	*1.322*	0.576	1.075
Slc26a9	Solute Carrier Family 26 Member A9 6753079	**0.012**	**0.227**	***0.090***	***0.471***	***0.091***	***0.392***
Slc35a3	Solute Carrier Family 35 Member A3 6908510	0.105	0.767	*0.596*	*0.925*	0.572	0.890
Core proteins							
Cd44	CD44 Molecule 6889258	***0.009***	***0.370***	0.144	0.728	0.873	0.955
Gpc2	Glypican 2	Not measured		Not measured		Not measured	
Gpc3	Glypican 3 7016826	***0.003***	***4.339***	***0.013***	***3.305***	***0.015***	***4.721***
Gpc6	Glypican 6 6821985	***0.019***	***2.767***	0.109	1.747	0.193	1.640
Hspg2	Perlecan 6917933	0.309	1.183	*0.075*	*1.554*	***0.042***	***2.230***
Sdc1	Syndecan 1 6793226	***0.031***	***0.380***	***0.067***	***0.413***	0.103	0.424
Sdc4	Syndecan 4 6892905	***0.017***	***0.341***	*0.094*	*0.536*	0.215	0.621
Preparation of linkage region							
B3gat1	β-1,3-Glucuronyltransferase 1 6987632	***0.008***	***3.467***	0.256	1.302	0.828	0.929
B3gat2	β-1,3-Glucuronyltransferase 2 6748174	***0.009***	***3.241***	0.286	1.269	0.690	1.129
B4galt2	β-1,4-Galactosyltransferase 2 6924869	*0.039*	*1.726*	*0.053*	*1.856*	0.176	1.477

Gene symbol	Full gene name and probe set	E14 vs. P90 Stepup P-value	E14 vs. P90 Fold change	E16 vs. P90 Stepup P-value	E16 vs. P90 Fold change	P1 vs. P90 Stepup P-value	P1 vs. P90 Fold change
Glycosaminoglycan chain polymerisation							
Chpf	Chondroitin Polymerizing Factor 6759816	*0.071*	*1.679*	0.182	1.459	0.309	1.403
Chsy1	CS Synthase 1	Not measured		Not measured		Not measured	
Chsy3	CS Synthase 3 6861281	0.429	1.153	*0.056*	*1.769*	0.849	1.058
Cs-galnact1	CS-GalNAc-transferase 1 6983073	0.137	0.512	0.202	0.541	0.974	0.975
Extl1	Exostoses (multiple)-like 1 6926017	***0.025***	***0.407***	0.149	0.625	0.144	0.505
Extl2	Exostoses (multiple)-like 2 6900659	*0.085*	*1.702*	0.819	1.066	0.518	1.272
Has2	Hyaluronan Synthase 2 6854042	***0.095***	***2.107***	0.157	1.969	0.537	1.403
Glycosaminoglycan chain modification							
Chst11	Chondroitin 4-O-Sulfotransferase 1 6769366	*0.049*	*1.922*	0.465	1.208	*0.239*	*1.531*
Chst14	Dermatan 4 Sulfotransferase 1 6880476	0.151	1.491	0.506	1.191	0.773	1.122
Chst2	Carbohydrate Sulfotransferase 2 6997990	***0.035***	***2.302***	***0.072***	***2.160***	0.207	1.682
Chst3	Chondroitin 6-O-Sulfotransferase 1 6774295	0.885	1.034	0.108	1.545	0.162	1.530
Chst8	GalNAc-4-O-Sulfotransferase 1 6966453	0.945	1.007	0.569	1.054	0.420	1.108
Hs3st1	HS 3-O-sulfotransferase 1 6937654	*0.074*	*1.658*	0.105	1.688	0.119	1.824
Hs3st3b1	HS 3-O-sulfotransferase 3b1 6788991	0.683	1.178	0.253	1.634	0.511	1.432
Hs3st6	HS 3-O-sulfotransferase 6 6849317	***0.019***	***0.406***	0.291	0.771	0.721	1.130
Hs6st2	HS 6O-sulfotransferase 2 7016808	***0.004***	***6.417***	***0.012***	***5.609***	***0.041***	***3.080***
Ndst1	N-Deacetylase and N-Sulfotransferase 1 6865926	*0.090*	*1.363*	*0.056*	*1.649*	*0.067*	*1.763*
Ndst2	N-Deacetylase and N-Sulfotransferase 2 6823122	0.822	1.044	*0.059*	*1.697*	*0.083*	*1.733*
Ndst3	N-Deacetylase and N-Sulfotransferase 3 6908958	0.173	2.472	0.111	3.856	0.122	4.860
Sulf1	Sulfatase 1 6747641	***0.010***	***4.522***	***0.051***	***2.546***	0.232	1.627
Sumf2	Sulfatase modifying factor 2	Not measured		Not measured		Not measured	
Glycosaminoglycan chain degradation							
ArsJ	Arylsulfatase J 6901136	***0.003***	***2.498***	***0.006***	***3.164***	*0.031*	*1.702*
ArsK	Arylsulfatase K 6814451	0.368	0.784	0.102	0.543	0.514	0.779
Galns	Galactosamine (N-Acetyl)-6-Sulfatase 6985943	*0.087*	*1.671*	0.322	1.311	0.786	1.115
Hpse	Heparanase	***0.021***	***0.267***	0.540	1.244	***0.095***	***0.360***

Gene symbol	Full gene name and probe set	E14 vs. P90 Stepup P-value	E14 vs. P90 Fold change	E16 vs. P90 Stepup P-value	E16 vs. P90 Fold change	P1 vs. P90 Stepup P-value	P1 vs. P90 Fold change
Hpse	Heparanase 6940363	***0.021***	***0.267***	0.540	1.244	***0.095***	***0.360***
Hyal1	Hyaluronoglucosamini-dase 1 6992224	***0.003***	***0.154***	***0.011***	***0.222***	***0.041***	***0.402***
Sgsh	N-Sulfoglucosamine Sulfohydrolase 6792702	***0.017***	***0.458***	*0.052*	*0.537*	0.201	0.699
Growth factors							
Areg	Amphiregulin 6932394	***0.016***	***0.157***	***0.043***	***0.200***	0.333	0.550
Bmp3	Bone morphogenetic growth factor 3 6932718	0.280	1.392	***0.067***	***2.381***	0.100	2.365
Bmp5	Bone Morphogenetic growth factor 5 6990569	***0.001***	***7.247***	0.141	1.191	0.688	1.057
Ctgf	Connective tissue growth factor 6766623	0.148	0.729	***0.025***	***0.366***	***0.068***	***0.485***
Fgf10	Fibroblast growth factor 10 6810592	0.138	1.521	***0.057***	***2.250***	***0.094***	***2.142***
Fgf13	Fibroblast growth factor 13 7017134	***0.012***	***2.998***	*0.075*	*1.824*	0.296	1.391
Fgf2	Fibroblast growth factor 2 6896850	0.201	0.664	0.279	0.696	0.952	0.967
Fgf20	Fibroblast growth factor 20 6981854	0.659	1.228	0.125	2.483	0.777	1.220
Fgf22	Fibroblast growth factor 22 6769141	***0.005***	***0.329***	0.972	0.994	*0.097*	*0.646*
Fgf7	Fibroblast growth factor 7 6880900	0.531	0.740	***0.078***	***0.286***	0.212	0.418
Fgf8	Fibroblast growth factor 8 6873363	0.492	0.883	0.655	1.085	0.682	0.895
Figf	C-fos induced growth factor 7015007	*0.051*	*1.734*	*0.062*	*1.909*	0.548	0.832
Gdf10	Growth differentiation factor 10 6818153	***0.028***	***2.334***	0.757	1.086	0.894	1.060
Hbegf	Heparin-binding epidermal growth factor 6864680	*0.037*	*0.551*	*0.063*	*0.547*	*0.087*	*0.530*
Hdgf	Hepatoma-derived growth factor 6899028	0.104	1.246	0.575	1.070	0.409	1.147
Igf1	Insulin-like growth factor 1 6769597	0.235	0.631	0.173	0.537	0.398	0.641
Igf2	Insulin-like growth factor 2 6972317	***0.001***	***59.615***	***0.002***	***55.864***	***0.002***	***52.364***
Nog	Noggin 6790670	0.275	2.605	0.517	1.773	0.677	1.712
Pdgfa	Platelet-derived growth factor a 6942654	***0.028***	***2.013***	***0.035***	***2.347***	***0.057***	***2.338***
Pdgfb	Platelet-derived growth factor b 6837144	*0.037*	*0.704*	0.199	1.197	0.157	1.298
Pdgfc	Platelet-derived growth factor c 6898686	***0.019***	***2.152***	***0.035***	***2.207***	0.902	1.042
Pdgfd	Platelet-derived growth factor d 6986677	0.925	0.952	0.191	0.504	0.790	1.205
Shh	Sonic hedgehog 6936889	0.448	0.595	0.308	2.117	0.152	4.571

Gene symbol	Full gene name and probe set	E14 vs. P90		E16 vs. P90		P1 vs. P90	
		Stepup P-value	Fold change	Stepup P-value	Fold change	Stepup P-value	Fold change
Tgfb1	Transforming growht factor beta 1 6959236	0.106	0.552	0.241	0.653	0.975	0.981
Tgfb2	Transforming growht factor beta 2 6764953	***0.057***	***2.441***	0.448	1.335	0.264	1.802
Tgfb3	Transforming growth factor beta 3 6802449	***0.026***	***2.386***	0.238	1.408	0.100	2.077
Vegfa	Vascular endothelial growth factor a 6855659	0.779	0.875	0.721	1.174	0.940	1.061
Vegfb	Vascular endothelial growth factor b 6871273	*0.008*	*1.461*	*0.031*	*1.318*	*0.060*	*1.277*
Vegfc	Vascular endothelial growth factor c 6976200	***0.088***	***2.120***	0.477	1.316	0.316	1.700
Wnt10b	Wingless-related integration site 10b 6838399	0.629	1.280	0.120	2.812	0.240	2.325
Wnt16	Wingless-related integration site 16 6944581	0.358	1.180	***0.026***	***2.402***	*0.093*	*1.710*
Wnt2	Wingless-related integration site 2 6951974	***0.057***	***3.047***	***0.082***	***3.260***	0.122	3.219
Wnt2b	Wingless-related integration site 2b 6907887	***0.009***	***2.189***	***0.024***	***2.030***	*0.077*	*1.590*
Wnt3a	Wingless-related integration site 3a 6788662	0.457	1.199	0.103	1.728	0.684	1.159
Wnt6	Wingless-related integration site 6 6750567	***0.011***	***3.166***	***0.032***	***2.668***	***0.064***	***2.352***
Wnt7a	Wingless-related integration site 7a 6955539	***0.060***	***2.117***	0.131	1.865	0.395	1.456
Wnt7b	Wingless-related integration site 7b 6837582	***0.072***	***2.297***	***0.050***	***3.623***	0.237	1.912

Numbers in Italic are significant (p<0.10); numbers in bold are >2 fold differentially expressed. Genes indicated as 'not measured' represent genes for which probes were not available on the used exon array version.

Table 4: Differentially expressed genes in C5 epimerase (Glce) knockout mouse (p<0.10) based on real-time qPCR.

Gene symbol	Full gene name and probe set	P-value	Relative change
Production of precursors			
Gnpnat1	Glucosamine-Phosphate N-Acetyltransferase 1 Mm00834602_mH	***0.033***	***0.468***
Slc2a4	Solute Carrier Family 2 Member 4 Mm01245507_g1	***0.086***	***2.526***
Core proteins			
Acan	Aggrecan Mm00545807_m1	***0.005***	***0.242***
Aspn	Asporin Mm00445945_m1	***0.010***	***0.382***
Glycosaminoglycan chain polymerisation			
Csgalnact 2	CS N-Acetylgalactosaminyltransferase 2 Mm00513340_m1	***0.049***	***0.431***
Glycosaminoglycan chain modification			
Glce	Glucuronic Acid Epimerase Mm00473667_m1	***0.013***	***0.079***

Numbers in Italic are significant (p<0.10); numbers in bold are >2 fold differentially expressed.

All genes were normalized using 18S RNA as a reference gene.

Acknowledgements

This study was financially supported by the Dutch Program for Tissue Engineering (DPTE6735). We like to thank the Microarray Facility Nijmegen of the Radboud university medical center (The Netherlands) for carrying out the array experiments and assistance with the data analysis. The Central Animal Laboratory of the Radboud university medical center is acknowledged for assistance with the animal experiments. We like to thank Affymetrix, part of ThermoFisher scientific, for using the image of a Affymetrix genechip in figure 1B (permission requested). We like to thank Life technologies, part of ThermoFisher scientific, for using the image of the TLDA carts in figure 1C (permission requested).

References

1 Bülow H E, Hobert O. The Molecular Diversity of Glycosaminoglycans Shapes Animal Development. Annu Rev Cell Dev Biol 2006: 22: 375–407.

2 Häcker U, Nybakken K, Perrimon N. Heparan sulphate proteoglycans: the sweet side of development. Nat Rev Mol Cell Biol 2005: 6: 530–541.

3 Sarrazin S, Lamanna W C, Esko J D. Heparan sulfate proteoglycans. Cold Spring Harb Perspect Biol 2011: 3: 1–33.

4 Gallo R, Kim C, Kokenyesi R et al. Syndecans-1 and -4 are induced during wound repair of neonatal but not fetal skin. J Invest Dermatol 1996: 107: 676–83.

5 Echtermeyer F, Streit M, Wilcox-Adelman S et al. Delayed wound repair and impaired angiogenesis in mice lacking syndecan-4. J Clin Invest 2001: 107: R9–R14.

6 Elenius V, Götte M, Reizes O et al. Inhibition by the soluble syndecan-1 ectodomains delays wound repair in mice overexpressing syndecan-1. J Biol Chem 2004: 279: 41928–41935.

7 Zcharia E, Zilka R, Yaar A et al. Heparanase accelerates wound angiogenesis and wound healing in mouse and rat models. FASEB J 2005: 19: 211–21.

8 Maccarana M, Kalamajski S, Kongsgaard M et al. Dermatan sulfate epimerase 1-deficient mice have reduced content and changed distribution of iduronic acids in dermatan sulfate and an altered collagen structure in skin. Mol Cell Biol 2009: 29: 5517–5528.

9 Zcharia E, Metzger S, Chajek-Shaul T et al. Transgenic expression of mammalian heparanase uncovers physiological functions of heparan sulfate in tissue morphogenesis, vascularization, and feeding behavior. FASEB J 2004: 18: 252–263.

10 Coulson-Thomas V J, Gesteira T F, Esko J et al. Heparan sulfate regulates hair follicle and sebaceous gland morphogenesis and homeostasis. J Biol Chem 2014: 289: 25211–25226.

11 Grobe K, Inatani M, Pallerla S R et al. Cerebral hypoplasia and craniofacial defects in mice lacking heparan sulfate Ndst1 gene function. Development 2005: 132: 3777–3786.

12 Li J P, Gong F, Hagner-McWhirter A et al. Targeted disruption of a murine glucuronyl C5-epimerase gene results in heparan sulfate lacking L-iduronic acid and in neonatal lethality. J Biol Chem 2003: 278: 28363–28366.

13 Jia J, Maccarana M, Zhang X et al. Lack of L-iduronic acid in heparan sulfate affects interaction with growth factors and cell signaling. J Biol Chem 2009: 284: 15942–15950.

14 Habuchi H, Nagai N, Sugaya N et al. Mice deficient in heparan sulfate 6-O-sulfotransferase-1 exhibit defective heparan sulfate biosynthesis, abnormal placentation, and late embryonic lethality. J Biol Chem 2007: 282: 15578–15588.

15 Esko J D, Selleck S B. Order out of chaos: assembly of ligand binding sites in heparan sulfate. Annu Rev Biochem 2002: 71: 435–471.

16 Ledin J, Staatz W, Li J P et al. Heparan sulfate structure in mice with genetically modified heparan sulfate production. J Biol Chem 2004: 279: 42732–42741.

17 Tong M, Tuk B, Hekking I M et al. Stimulated neovascularization, inflammation resolution and collagen maturation in healing rat cutaneous wounds by a heparan sulfate glycosaminoglycan mimetic, OTR4120. Wound Repair Regen 2009: 17: 840–852.

18 Uijtdewilligen P J E, Versteeg E M M, Gilissen C et al. Towards embryonic-like scaffolds for skin tissue engineering: Identification of effector molecules and construction of scaffolds. J Tissue Eng Regen Med 2016: 10: E34–E44.

19 Rossant J, Tam P P L. Mouse Development: Patterning, Morphogenesis, and Organogenesis. First edit. London, UK: Academic Press, 2002.

20 Li J P, Gong F, Darwish K El et al. Characterization of the D-Glucuronyl C5-epimerase Involved in the Biosynthesis of Heparin and Heparan Sulfate. J Biol Chem 2001: 276: 20069–20077.

21 Schroeder A, Mueller O, Stocker S et al. The RIN: an RNA integrity number for assigning integrity values to RNA measurements. BMC Mol Biol 2006: 7: 3.

22 Kadota K, Shimizu K. Evaluating methods for ranking differentially expressed genes applied to microArray quality control data. BMC Bioinformatics 2011: 12: 227.

23 Lammers G, Gilissen C, Nillesen S T M et al. High density gene expression microarrays and gene ontology analysis for identifying processes in implanted tissue engineering constructs. Biomaterials 2010: 31: 8299–8312.

24 Livak K J, Schmittgen T D. Analysis of Relative Gene Expression Data Using Real-Time Quantitative PCR and the 2−ΔΔCT Method. Methods 2001: 25: 402–408.

25 Benjamini Y, Hochberg Y. Controlling the false discovery rate: a practical and powerful approach to multiple testing. J R Stat Soc 1995: 57: 289–300.

26 Song H H, Filmus J. The role of glypicans in mammalian development. Biochim Biophys Acta - Gen Subj 2002: 1573: 241–246.

27 Esko J D, Lindahl U. Molecular diversity of heparan sulfate. J Clin Investig 2001: 108: 169–173.

28 Buono M, Visigalli I, Bergamasco R et al. Sulfatase modifying factor 1-mediated fibroblast growth factor signaling primes hematopoietic multilineage development. J Exp Med 2010: 207: 1647–60.

29 Yan D, Lin X. Shaping morphogen gradients by proteoglycans. Cold Spring Harb Perspect Biol 2009: 1: 1–17.

30 Campos-Xavier A B, Martinet D, Bateman J et al. Mutations in the Heparan-Sulfate Proteoglycan Glypican 6 (GPC6) Impair Endochondral Ossification and Cause Recessive Omodysplasia. Am J Hum Genet 2009: 84: 760–770.

31 Capurro M I, Xu P, Shi W et al. Glypican-3 Inhibits Hedgehog Signaling during Development by Competing with Patched for Hedgehog Binding. Dev Cell 2008: 14: 700–711.

32 Pellegrini M, Pilia G, Pantano S et al. Gpc3 expression correlates with the phenotype of the Simpson-Golabi- Behmel syndrome. Dev Dyn 1998: 213: 431–439.

33 Cat B De, David G. Developmental roles of the glypicans. Semin Cell Dev Biol 2001: 12: 117–125.

34 Chiao E, Fisher P, Crisponi L et al. Overgrowth of a mouse model of the Simpson-Golabi-Behmel syndrome is independent of IGF signaling. Dev Biol 2002: 243: 185–206.

35 Chuong C M, Patel N, Lin J et al. Sonic hedgehog signaling pathway in vertebrate epithelial appendage morphogenesis: perspectives in development and evolution. Cell Mol Life Sci 2000: 57: 1672–81.

36 Zhou J X, Jia L W, Liu W M et al. Role of sonic hedgehog in maintaining a pool of proliferating stem cells in the human fetal epidermis. Hum Reprod 2006: 21: 1698–1704.

37 Stepp M A, Gibson H E, Gala P H et al. Defects in keratinocyte activation during wound healing in the syndecan-1-deficient mouse. J Cell Sci 2002: 115: 4517–4531.

38 Richardson G D, Fantauzzo K A, Bazzi H et al. Dynamic expression of Syndecan-1 during hair follicle morphogenesis. Gene Expr Patterns 2009: 9: 454–460.

39 Song H K, Lee S H, Goetinck P F. FGF-2 signaling is sufficient to induce dermal condensations during feather development. Dev Dyn 2004: 231: 741–749.

40 Nadanaka S, Zhou S, Kagiyama S et al. EXTL2, a member of the EXT family of tumor suppressors, controls glycosaminoglycan biosynthesis in a xylose kinase-dependent manner. J Biol Chem 2013: 288: 9321–9333.

41 Kim B T, Kitagawa H, Tamura J et al. Human tumor suppressor EXT gene family members EXTL1 and EXTL3 encode alpha 1,4- N-acetylglucosaminyltransferases that likely are involved in heparan sulfate/ heparin biosynthesis. Proc Natl Acad Sci U S A 2001: 98: 7176–7181.

42 Sato T, Gotoh M, Kiyohara K et al. Differential roles of two N-acetylgalactosaminyltransferases, CSGalNAcT-1, and a novel enzyme, CSGalNAcT-2. Initiation and elongation in synthesis of chondroitin sulfate. J Biol Chem 2003: 278: 3063–3071.

43 Varki A, Cummings R D, Esko J et al. Essentials of Glycobiology. 1999.

44 Aikawa J I, Grobe K, Tsujimoto M et al. Multiple isozymes of heparan sulfate/ heparin GlcNAc N-deacetylase/GlcN N-sulfotransferase. Structure and activity of the fourth member, NDST4. J Biol Chem 2001: 276: 5876–5882.

45 Kuppevelt T H Van, Dennisseni M A B A, Venrooij W J Van et al. Generation and application of type-specific anti-heparan sulfate antibodies using phage display technology: Further evidence for heparan sulfate heterogeneity in the kidney. J Biol Chem 1998: 273: 12960–12966.

46 Habuchi H, Kimata K. Mice deficient in heparan sulfate 6-o-sulfotransferase-1. Prog Mol Biol Transl Sci 2010: 93: 79–111.

47 Malgouries S, Donovan M, Thibaut S et al. Heparanase 1: A key participant of inner root sheath differentiation program and hair follicle homeostasis. Exp Dermatol 2008: 17: 1017–1023.

48 Patel V N, Knox S M, Likar K M et al. Heparanase cleavage of perlecan heparan sulfate modulates FGF10 activity during ex vivo submandibular gland branching morphogenesis. Development 2007: 134: 4177–4186.

49 Widelitz R B. Wnt signaling in skin organogenesis. Organogenesis 2008: 4: 123–33.

50 Créancier L, Morello D, Mercier P et al. Fibroblast growth factor 2 internal ribosome entry site (IRES) activity ex vivo and in transgenic mice reveals a stringent tissue-specific regulation. J Cell Biol 2000: 150: 275–281.

51 Grobe K, Esko J D. Regulated translation of heparan sulfate N-acetylglucosamine N-deacetylase/N-sulfotransferase isozymes by structured 5`-untranslated regions and internal ribosome entry sites. J Biol Chem 2002: 277: 30699–30706.

52 Hellen C U T, Sarnow P. Internal ribosome entry sites in eukaryotic mRNA molecules. Genes Dev 2001: 15: 1593–1612.

Supplementary data

This chapter is supported by 6 supplementary tables. Supplementary data table 1 and 2 are presented on the following pages. The other supplementary tables can be requested by sending an email to Peter Uijtdewilligen, peterudw@outlook.com.

Supplementary data table 1: Design TLDA cart version 1

This design was used for the developmental study

Production of precursors

Taqman Assay ID	Gene symbol	Function
Mm00511302_m1	*Adpgk*	Phosphorylation of glucose into glucose-6-P
Mm00617772_g1	*Gale*	Conversion of UDP-GlcNAc to UDP-GalNAc
Mm00444182_m1	*Galk1*	Phosphorylation of Galactose into Galactose-1-P
Mm00613268_m1	*Galk2*	Phosphorylation of N-Acetylgalactosamine (GalNAc) into GalNAc-1P)
Mm00489459_g1	*Galt*	UDP-activation of Glucose-1-P and Galactose-1-P
Mm00439129_m1	*Gck*	Phosphorylation of glucose into glucose-6-P
Mm00600127_m1	*Gfpt1*	Conversion of fructose-6-P into glucosamine-6-P (Glc-6-P)
Mm00496565_m1	*Gfpt2*	Conversion of fructose-6-P into Glc-6-P
Mm00834602_mH	*Gnpnat1*	Conversion of Glc-6-P into N-Acetylglucosamine-6-P (GlcNAc-6-P)
Mm02026122_g1	*Gpi1*	Isomerisation of glucose-6-P into fructose-6-P
Mm00439344_m1	*Hk1*	Phosphorylation of glucose into glucose-6-P
Mm00443385_m1	*Hk2*	Phosphorylation of glucose into glucose-6-P
Mm00480214_m1	*Miox*	Conversion of Myo-inositol into UDP-GlcA
Mm00479878_m1	*Nagk*	Phosphorylation of GlcNAc to GlcNAC-6-P
Mm00442283_m1	*Papss1*	Synthesis of PAPS complex
Mm00442295_m1	*Papss2*	Synthesis of PAPS complex
Mm00804141_m1	*Pgm1*	Conversion of glucose-6-P into glucose-1-P
Mm00728285_s1	*Pgm2*	Conversion of glucose-6-P into glucose-1-P
Mm00459270_m1	*Pgm3*	Conversion of GlcNAc-6-P into GlcNAc-1-P
Mm00723432_m1	*Pgm5*	Conversion of glucose-6-P into glucose-1-P
Mm00490339_m1	*Slc13a1*	Transport of sulphate from the extracellular space to cytoplasm
Mm00556495_m1	*Slc13a4*	Transport of sulphate from the extracellular space to cytoplasm
Mm01334459_m1	*Slc13a5*	Transport of sulphate from the extracellular space to cytoplasm
Mm00626632_m1	*Slc26a11*	Transport of sulphate from the extracellular space to cytoplasm
Mm00432896_m1	*Slc26a2*	Transport of sulphate from the extracellular space to cytoplasm
Mm00506742_m1	*Slc26a6*	Transport of sulphate from the extracellular space to cytoplasm
Mm00524162_m1	*Slc26a7*	Transport of sulphate from the extracellular space to cytoplasm
Mm00524836_m1	*Slc26a8*	Transport of sulphate from the extracellular space to cytoplasm
Mm00628490_m1	*Slc26a9*	Transport of sulphate from the extracellular space to cytoplasm
Mm00446504_m1	*Slc35a2*	Transport from cytoplasm to Golgi system of UDP-GalNAc and UDP-Galactose
Mm00523288_m1	*Slc35a3*	Transport from cytoplasm to Golgi system of UDP-GlcNAc
Mm00782997_s1	*Slc35a4*	Transport from cytoplasm to Golgi system of UDP-GalNAc and UDP-Galactose
Mm00450258_m1	*Slc35b1*	Transport from cytoplasm to Golgi system of UDP-GalNAc and UDP-Galactose
Mm01269910_m1	*Slc35b2*	Transport of PAPS comples from cytoplasm to Golgi system
Mm00506275_m1	*Slc35b3*	Transport of PAPS comples from cytoplasm to Golgi system
Mm00480588_m1	*Slc35b4*	Transport from cytoplasm to Golgi system of UDP-GlcNAc and UDP-Xylose
Mm00624959_m1	*Slc35d1*	Transport from cytoplasm to Golgi system of UDP-GalNAc and UDP-GlcA
Mm01304830_m1	*Slc35d2*	Transport from cytoplasm to Golgi system of UDP-GlcNAc
Mm01717003_m1	*Slc35d3*	Paralog of Slc35d1
Mm00505476_m1	*Uap1*	UDP-activation of GlcNAc-1-P and GalNAc-1-P
Mm00447643_m1	*Ugdh*	Conversion of UDP-glucose into UDP-glucuronic acid (UDP-GlcA)
Mm00454826_m1	*Ugp2*	UDP-activation of Glucose-1-P
Mm00550735_m1	*Uxs1*	Conversion of UDP-GlcA into UDP-xylose

Core proteins

Taqman Assay ID	Gene symbol	Function
Mm01545840_m1	*Agrn*	Proteoglycan carring HS present in ECM
Mm01277164_m1	*Cd44*	Proteoglycan carring HS and hyaluronic acid on cell surface
Mm00487131_m1	*Col18a1*	Proteoglycan carring HS present in basement membrane
Mm00497305_m1	*Gpc1*	Proteoglycan carring HS present on cell surface via GPI-anchor
Mm00549650_m1	*Gpc2*	Proteoglycan carring HS present on cell surface via GPI-anchor
Mm00516722_m1	*Gpc3*	Proteoglycan carring HS present on cell surface via GPI-anchor
Mm00515035_m1	*Gpc4*	Proteoglycan carring HS present on cell surface via GPI-anchor
Mm00615599_m1	*Gpc5*	Proteoglycan carring HS present on cell surface via GPI-anchor
Mm00516235_m1	*Gpc6*	Proteoglycan carring HS present on cell surface via GPI-anchor
Mm01181179_g1	*Hspg2*	Proteoglycan carring HS present in ECM
Mm00448918_m1	*Sdc1*	Proteoglycan carring HS present on cell surface
Mm00484718_m1	*Sdc2*	Proteoglycan carring HS present on cell surface
Mm01179831_m1	*Sdc3*	Proteoglycan carring HS present on cell surface
Mm00488527_m1	*Sdc4*	Proteoglycan carring HS present on cell surface

Preparation of linkage region

Taqman Assay ID	Gene symbol	Function
Mm00504458_s1	*B3galt6*	Transferring UDP-galactose to galactose-xylose on proteoglycan
Mm00661499_m1	*B3gat1*	Transferring UDP-GlcA to galactose-galactose-xylose on proteoglycan
Mm00549042_m1	*B3gat2*	Transferring UDP-GlcA to galactose-galactose-xylose on proteoglycan
Mm00470389_m1	*B3gat3*	Transferring UDP-GlcA to galactose-galactose-xylose on proteoglycan
Mm00479556_m1	*B4galt2*	Transfering UDP-galactose to GlcNAc, Glc, and Xyl.
Mm00461357_m1	*B4galt7*	Transferring UDP-galactose to xylose on proteoglycan
Mm00558690_m1	*Xylt1*	Transferring UDP-xylose to proteoglycan
Mm00461181_m1	*Xylt2*	Transferring UDP-xylose to proteoglycan

Glycosaminoglycan chain polymerisation

Taqman Assay ID	Gene symbol	Function
Mm01262239_g1	*Chpf*	Transferring UDP-GlcA to GalNAc at end of sugar chain (CS)
Mm01319178_m1	*Chsy1*	Transferring UDP-GlcA to GalNAc at end of sugar chain (CS)
Mm01545329_m1	*Chsy3*	Transferring UDP-GlcA to GalNAc at end of sugar chain (CS)
Mm00555164_m1	*Csgalnact1*	Transferring UDP-GalNAc to GlcA at end of sugar chain (CS)
Mm00513340_m1	*Csgalnact2*	Transferring UDP-GalNAc to GlcA at end of sugar chain (CS)
Mm00468769_m1	*Ext1*	Transferring UDP-GlcNAc to GlcA at end of sugar chain (HS)
Mm00468775_m1	*Ext2*	Transferring UDP-GlcNAc to GlcA at end of sugar chain (HS)
Mm00621977_s1	*Extl1*	Transferring UDP-GlcA to GlcNAc at end of sugar chain (HS)
Mm00469621_m1	*Extl2*	Transferring UDP-GlcA to GlcNAc at end of sugar chain (HS)
Mm00516994_m1	*Extl3*	Transferring UDP-GlcA to GlcNAc at end of sugar chain (HS)
Mm00468496_m1	*Has1*	Polymerisation of hyaluronic acid
Mm00515089_m1	*Has2*	Polymerisation of hyaluronic acid
Mm00515091_m1	*Has3*	Polymerisation of hyaluronic acid

Glycosaminoglycan chain modification

Taqman Assay ID	Gene symbol	Function
Mm00517563_m1	*Chst11*	Sulfation at the 4-O postion of GalNAc untis (CS)
Mm00546416_s1	*Chst12*	Sulfation at the 4-O postion of GalNAc untis (CS)
Mm01186255_s1	*Chst13*	Sulfation at the 4-O postion of GalNAc untis (CS)
Mm00511291_s1	*Chst14*	Sulfation at the 4-O postion of GalNAc untis (CS)
Mm00513227_m1	*Chst15*	Sulfation at the 6-O postion of GalNAc untis (CS)
Mm00490018_g1	*Chst2*	Sulfation at the 6-O postion of GalNAc untis (CS)
Mm00489736_m1	*Chst3*	Sulfation at the 6-O postion of GalNAc untis (CS)
Mm00488783_s1	*Chst4*	Sulfation at the 6-O postion of GalNAc untis (CS)
Mm00517342_m1	*Chst5*	Sulfation at the 6-O postion of GalNAc untis (CS)
Mm00491466_m1	*Chst7*	Sulfation at the 6-O postion of GalNAc untis (CS)
Mm00558321_m1	*Chst8*	Sulfation at the 4-O postion of GalNAc untis (CS)
Mm01722279_m1	*Chst9*	Sulfation at the 4-O postion of GalNAc untis (CS)
Mm00552923_m1	*Dse*	Epimerisation of GlcA unit into iduronic acid unit (IdoA) (CS)
Mm00473667_m1	*Glce*	Epimerisation of GlcA unit into iduronic acid unit (IdoA) (HS)
Mm00478684_m1	*Hs2st1*	Sulfation at the 2-O position of GlcA and IdoA units (HS)
Mm01964038_s1	*Hs3st1*	Sulfation at the 3-O position of GlcNAc and GlcNS units sulfated at the 6-O position (HS)
Mm00616933_m1	*Hs3st2*	Sulfation at the 3-O position of GlcNAc and GlcNS units sulfated at the 6-O position (HS)
Mm00780907_s1	*Hs3st3a1*	Sulfation at the 3-O position of GlcNAc and GlcNS units sulfated at the 6-O position (HS)
Mm00479621_m1	*Hs3st3b1*	Sulfation at the 3-O position of GlcNAc and GlcNS units sulfated at the 6-O position (HS)
Mm01299930_m1	*Hs3st6*	Sulfation at the 3-O position of GlcNAc and GlcNS units sulfated at the 6-O position (HS)
Mm01229698_s1	*Hs6st1*	Sulfation at the 6-O position of GlcNAc and N-sulfated-glucuronic acid units (GlcNS) (HS)
Mm00479296_m1	*Hs6st2*	Sulfation at the 6-O position of GlcNAc and GlcNS units (HS)
Mm00479297_m1	*Hs6st3*	Sulfation at the 6-O position of GlcNAc and GlcNS units (HS)
Mm00447005_m1	*Ndst1*	N-de-acetylation and N-sulfation of GlcNAc unit (HS)
Mm00447818_m1	*Ndst2*	N-de-acetylation and N-sulfation of GlcNAc unit (HS)
Mm00453178_m1	*Ndst3*	N-de-acetylation and N-sulfation of GlcNAc unit (HS)
Mm00480767_m1	*Ndst4*	N-de-acetylation and N-sulfation of GlcNAc unit (HS)
Mm00552283_m1	*Sulf1*	Desulfation of the 6-O positon of 6-O sulfated GlcNAc and GlcNS units (HS)
Mm00511193_m1	*Sulf2*	Desulfation of the 6-O positon of 6-O sulfated GlcNAc and GlcNS units (HS)
Mm00461213_m1	*Sumf1*	Cofactor for Sulf1 and Sulf 2 (HS)
Mm01197721_m1	*Sumf2*	Cofactor for Sulf1 and Sulf 2 (HS)
Mm00616790_m1	*Ust*	Sulfation at the 2-O position of GlcA and IdoA units (CS)

Glycosaminoglycan chain degradation

Taqman Assay ID	Gene symbol	Function
Mm00802167_m1	*Arsb*	Desulfation of the 4-O position of 4-O sulfated GalNAc units (CS)
Mm00557970_m1	*Arsj*	Desulfation of the 4-O position of 4-O sulfated GalNAc units (CS)
Mm00513099_m1	*Arsk*	Desulfation of proteoglycans, paralog of IDS
Mm00489575_m1	*Galns*	Desulfation of the 6-O positon of 6-O sulfated GalNAc units (CS)
Mm00659592_m1	*Gns*	Desulfation of the 6-O positon of 6-O sulfated GlcNAc and GlcNS units (HS)
Mm00446954_g1	*Gusb*	Hydrolysation of GlcA from sugar chain (HS and Hyaluronic acid and CS)
Mm00599877_m1	*Hexa*	Hydrolysation of GalNAc units (CS) and GlcNAc untis (hyaluronic acid) from sugar chain
Mm00599880_m1	*Hexb*	Hydrolysation of GalNAc units (CS) and GlcNAc untis (hyaluronic acid) from sugar chain
Mm00519485_m1	*Hgsnat*	Acetylation of desulfated GlcNS units (HS)
Mm00461768_m1	*Hpse*	Degradation of HS chains extracellularly
Mm00476206_m1	*Hyal1*	Degradation of hyaluronic acid chain
Mm00477731_m1	*Hyal2*	Degradation of hyaluronic acid chain
Mm00662097_m1	*Hyal3*	Degradation of hyaluronic acid chain
Mm00494868_m1	*Ids*	Desulfation of 2-O sulfated IdoA and GlcA units (HS and CS)
Mm00515143_m1	*Idua*	Hydrolysation of IdoA unit from sugar chain (HS and CS)
Mm00452409_m1	*Mgea5*	Degradation of hyaluronic acid chain
Mm00476274_m1	*Naga*	Hydrolysis N-GalNAc moieties from glycoconjugates.
Mm00479175_m1	*Naglu*	Hydrolysation of GlcNAc from sugar chain (HS)
Mm00450747_m1	*Sgsh*	Desulfation of GlcNS units (HS)

Growth factors

Taqman Assay ID	Gene symbol	Function
Mm00437583_m1	*Areg*	Amphiregulin **
Mm00557790_m1	*Bmp3*	Bone morphogenetic growth factor 3 **
Mm00432091_m1	*Bmp5*	Bone morphogenetic growth factor 5 **
Mm01192931_g1	*Ctgf*	Connective tissue growth factor, embryonic growth factor in skin development **
Mm00433275_m1	*Fgf10*	Fibroblast growth factor 10 **
Mm00438910_m1	*Fgf13*	Fibroblast growth factor 13 **
Mm01285715_m1	*Fgf2*	Fibroblast growth factor 2 **
Mm00748347_m1	*Fgf20*	Fibroblast growth factor 20 **
Mm00445749_m1	*Fgf22*	Fibroblast growth factor 22 **
Mm00433291_m1	*Fgf7*	Fibroblast growth factor 7 **
Mm00438921_m1	*Fgf8*	Fibroblast growth factor 8 **
Mm01131929_m1	*Figf*	C-fos induced growth factor **
Mm03024279_s1	*Gdf10*	Growth differentiation factor 10 **
Mm00439305_g1	*Hbegf*	Heparin-binding epidermal growth factor **
Mm00725733_s1	*Hdgf*	Hepatoma-derived growth factor **
Mm00439560_m1	*Igf1*	Insulin-like growth factor 1 **
Mm00439565_g1	*Igf2*	Insulin-like growth factor 2 **
Mm01297833_s1	*Nog*	Noggin **
Mm01205760_m1	*Pdgfa*	Platelet-derived growth factor a **
Mm01298578_m1	*Pdgfb*	Platelet-derived growth factor b **
Mm00480205_m1	*Pdgfc*	Platelet-derived growth factor c **
Mm00546829_m1	*Pdgfd*	Platelet-derived growth factor d **
Mm00436527_m1	*Shh*	Sonic hedgehog **
Mm01178820_m1	*Tgfb1*	Transforming growth factor beta 1 **
Mm01321739_m1	*Tgfb2*	Transforming growth factor beta 2 **
Mm01307950_m1	*Tgfb3*	Transforming growth factor beta 3 **
Mm01281447_m1	*Vegfa*	Vascular endothelial growth factor a **
Mm00442102_m1	*Vegfb*	Vascular endothelial growth factor b **
Mm00437313_m1	*Vegfc*	Vascular endothelial growth factor c **
Mm00442104_m1	*Wnt10b*	Wingless-related integration site 10b **
Mm00446420_m1	*Wnt16*	Wingless-related integration site 16 **
Mm00470018_m1	*Wnt2*	Wingless-related integration site 2 **
Mm00437330_m1	*Wnt2b*	Wingless-related integration site 2b **
Mm00437337_m1	*Wnt3a*	Wingless-related integration site 3a **
Mm00437353_m1	*Wnt6*	Wingless-related integration site 6 **
Mm00437355_m1	*Wnt7a*	Wingless-related integration site 7a **
Mm00437357_m1	*Wnt7b*	Wingless-related integration site 7b **

Putatively involved

Taqman Assay ID	Gene symbol	Function
Hs99999901_s1	*18S*	Reference gene
Mm00802173_g1	*Arsa*	Desulfation of cerebroside
Mm00546931_m1	*Arsg*	Paralog of Arsa
Mm00480272_s1	*B3galnt1*	Transferring UDP-GalNAc or UDP-GlcNAc to N-GlcNAc, Galactose or N-GalNAc
Mm01189804_m1	*B4galnt3*	Transferring UDP-GalNAc or UDP-GlcNAc to N-GlcNAc, Galactose or N-GalNAc
Mm00625968_g1	*B4galnt4*	Transferring UDP-GalNAc or UDP-GlcNAc to N-GlcNAc, Galactose or N-GalNAc
Mm00473986_m1	*C1galt1*	Transferring UDP-Gal to N-GalNAc.
Mm00480676_m1	*C1galt1c1*	C1GALT1-specific chaperone 1
Mm00517855_m1	*Chst1*	Involved in sulfation of keratin sulfate
Mm03302249_g1	*Gapdh*	Reference gene
Mm00516323_m1	*Gla*	Hydrolysis of galactose units
Mm00515342_m1	*Glb1*	Hydrolysis of galactose units
Mm00464245_m1	*Glb1l2*	Hydrolysis of galactose units
Mm01254913_g1	*Gnpda1*	Conversion of GlcNAc-6-P into fructose-6-P
Mm00503573_m1	*Gnpda2*	Conversion of GlcNAc-6-P into fructose-6-P
Mm00434647_m1	*Khk*	Phosphorylating fructose to fructose-1-P
Mm00502002_m1	*Kl*	Putative glucuronidase
Mm00473122_m1	*Klb*	Putative glucuronidase
Mm00491720_m1	*Renbp*	Concersion of N-GlcNAc to N-acetylmannosamine
Mm00555344_m1	*Slc17a5*	Transport of GlcA from lysosoom to cytoplasm
Mm00445313_m1	*Slc26a3*	Transferring chloride ions across the cell membrane in exchange for bicarbonate ions
Mm00442308_m1	*Slc26a4*	Transferring chloride ions across the cell membrane
Mm00446145_m1	*Slc26a5*	Protein functions as a molecular motor in motile outer hair cells of the cochlea
Mm00442341_m1	*Slc35a1*	Putative CMP-Sialic Acid Transporter
Mm01277045_m1	*Tbp*	Reference gene
Mm00495930_m1	*Ugt8a*	Transfere galactose to ceramide

* Glc, glucosamine; GlcNAc, N-acetylated glucosamine; Gal, galactosamine; GalNAc, N-acetylated galactosamine; GlcA, glucuronic acid; IdoA, iduronic acid.

**Uijtdewilligen *et al* , 2016.

Supplementary data table 2: Design TLDA cart version 2

This design was used for analysis of skin from Glce knock out and HSPEtg mice

Production of precursors

Taqman Assay ID	Gene symbol	Function
Mm00511302_m1	*Adpgk*	Phosphorylation of glucose into glucose-6-P
Mm00617772_g1	*Gale*	Conversion of UDP-GlcNAc to UDP-GalNAc
Mm00444182_m1	*Galk1*	Phosphorylation of Galactose into Galactose-1-P
Mm00613268_m1	*Galk2*	Phosphorylation of N-Acetylgalactosamine (GalNAc) into GalNAc-1P)
Mm00489459_g1	*Galt*	UDP-activation of Glucose-1-P and Galactose-1-P
Mm00439129_m1	*Gck*	Phosphorylation of glucose into glucose-6-P
Mm00600127_m1	*Gfpt1*	Conversion of fructose-6-P into glucosamine-6-P (Glc-6-P)
Mm00496565_m1	*Gfpt2*	Conversion of fructose-6-P into Glc-6-P
Mm00834602_mH	*Gnpnat1*	Conversion of Glc-6-P into N-Acetylglucosamine-6-P (GlcNAc-6-P)
Mm02026122_g1	*Gpi1*	Isomerisation of glucose-6-P into fructose-6-P
Mm00439344_m1	*Hk1*	Phosphorylation of glucose into glucose-6-P
Mm00443385_m1	*Hk2*	Phosphorylation of glucose into glucose-6-P
Mm00480214_m1	*Miox*	Conversion of Myo-inositol into UDP-GlcA
Mm00479878_m1	*Nagk*	Phosphorylation of GlcNAc to GlcNAC-6-P
Mm00442283_m1	*Papss1*	Synthesis of PAPS complex
Mm00442295_m1	*Papss2*	Synthesis of PAPS complex
Mm00804141_m1	*Pgm1*	Conversion of glucose-6-P into glucose-1-P
Mm00728285_s1	*Pgm2*	Conversion of glucose-6-P into glucose-1-P
Mm00459270_m1	*Pgm3*	Conversion of GlcNAc-6-P into GlcNAc-1-P
Mm00723432_m1	*Pgm5*	Conversion of glucose-6-P into glucose-1-P
Mm00490339_m1	*Slc13a1*	Transport of sulphate from the extracellular space to cytoplasm
Mm00556495_m1	*Slc13a4*	Transport of sulphate from the extracellular space to cytoplasm
Mm01334459_m1	*Slc13a5*	Transport of sulphate from the extracellular space to cytoplasm
Mm00626632_m1	*Slc26a11*	Transport of sulphate from the extracellular space to cytoplasm
Mm00432896_m1	*Slc26a2*	Transport of sulphate from the extracellular space to cytoplasm
Mm00506742_m1	*Slc26a6*	Transport of sulphate from the extracellular space to cytoplasm
Mm00524162_m1	*Slc26a7*	Transport of sulphate from the extracellular space to cytoplasm
Mm00524836_m1	*Slc26a8*	Transport of sulphate from the extracellular space to cytoplasm
Mm00628490_m1	*Slc26a9*	Transport of sulphate from the extracellular space to cytoplasm
Mm01192270_m1	*Slc2a1 (new)*	Sugar transport across plasma membrane
Mm00453716_m1	*Slc2a10 (new)*	Sugar transport across plasma membrane
Mm00619244_m1	*Slc2a12 (new)*	Sugar transport across plasma membrane
Mm00446230_g1	*Slc2a2 (new)*	Sugar transport across plasma membrane
Mm00441483_m1	*Slc2a3 (new)*	Sugar transport across plasma membrane
Mm01245507_g1	*Slc2a4 (new)*	Sugar transport across plasma membrane
Mm00600311_m1	*Slc2a5 (new)*	Sugar transport across plasma membrane
Mm00554217_m1	*Slc2a6 (new)*	Sugar transport across plasma membrane
Mm00444634_m1	*Slc2a8 (new)*	Sugar transport across plasma membrane
Mm01211147_m1	*Slc2a9 (new)*	Sugar transport across plasma membrane
Mm00446504_m1	*Slc35a2*	Transport from cytoplasm to Golgi system of UDP-GalNAc and UDP-Galactose
Mm00523288_m1	*Slc35a3*	Transport from cytoplasm to Golgi system of UDP-GlcNAc
Mm00782997_s1	*Slc35a4*	Transport from cytoplasm to Golgi system of UDP-GalNAc and UDP-Galactose
Mm00450258_m1	*Slc35b1*	Transport from cytoplasm to Golgi system of UDP-GalNAc and UDP-Galactose
Mm01269910_m1	*Slc35b2*	Transport of PAPS comples from cytoplasm to Golgi system
Mm00506268_m1	*Slc35b3*	Transport of PAPS comples from cytoplasm to Golgi system
Mm00480588_m1	*Slc35b4*	Transport from cytoplasm to Golgi system of UDP-GlcNAc and UDP-Xylose
Mm00624959_m1	*Slc35d1*	Transport from cytoplasm to Golgi system of UDP-GalNAc and UDP-GlcA
Mm01304830_m1	*Slc35d2*	Transport from cytoplasm to Golgi system of UDP-GlcNAc
Mm01717003_m1	*Slc35d3*	Paralog of Slc35d1
Mm00769477_m1	*Uap1*	UDP-activation of GlcNAc-1-P and GalNAc-1-P
Mm00447643_m1	*Ugdh*	Conversion of UDP-glucose into UDP-glucuronic acid (UDP-GlcA)
Mm00454826_m1	*Ugp2*	UDP-activation of Glucose-1-P
Mm00550735_m1	*Uxs1*	Conversion of UDP-GlcA into UDP-xylose

Core proteins

Taqman Assay ID	Gene symbol	Function
Mm00545807_m1	*Acan (new)*	Proteoglycan carring CS or DS
Mm01264855_m1	*Agrn*	Proteoglycan carring HS present in ECM
Mm00445945_m1	*Aspn (new)*	Proteoglycan carring CS or DS
Mm00476090_m1	*Bcan (new)*	Proteoglycan carring CS or DS
Mm00455918_m1	*Bgn (new)*	Proteoglycan carring CS or DS
Mm01277164_m1	*Cd44*	Proteoglycan carring HS and hyaluronic acid on cell surface
Mm00487131_m1	*Col18a1*	Proteoglycan carring HS present in basement membrane
Mm00483872_m1	*Col9a2 (new)*	Proteoglycan carring CS or DS
Mm00507256_m1	*Cspg4 (new)*	Proteoglycan carring CS or DS
Mm00516549_m1	*Cspg5 (new)*	Proteoglycan carring CS or DS
Mm03003496_s1	*Dcn (new)*	Proteoglycan carring CS or DS
Mm00514611_m1	*Epyc (new)*	Proteoglycan carring CS or DS
Mm00497305_m1	*Gpc1*	Proteoglycan carring HS present on cell surface via GPI-anchor
Mm00549650_m1	*Gpc2*	Proteoglycan carring HS present on cell surface via GPI-anchor
Mm00516722_m1	*Gpc3*	Proteoglycan carring HS present on cell surface via GPI-anchor
Mm00515035_m1	*Gpc4*	Proteoglycan carring HS present on cell surface via GPI-anchor
Mm00615599_m1	*Gpc5*	Proteoglycan carring HS present on cell surface via GPI-anchor
Mm00516235_m1	*Gpc6*	Proteoglycan carring HS present on cell surface via GPI-anchor
Mm00469183_m1	*Hmmr (new)*	Hyaluronan-Mediated Motility Receptor
Mm01181165_m1	*Hspg2*	Proteoglycan carring HS present in ECM
Mm00484007_m1	*Ncan (new)*	Proteoglycan carring CS or DS
Mm00448918_m1	*Sdc1*	Proteoglycan carring HS present on cell surface
Mm00484718_m1	*Sdc2*	Proteoglycan carring HS present on cell surface
Mm01179831_m1	*Sdc3*	Proteoglycan carring HS present on cell surface
Mm00488527_m1	*Sdc4*	Proteoglycan carring HS present on cell surface
Mm00484015_m1	*Smc3 (new)*	Proteoglycan carring CS or DS
Mm01169070_m1	*Srgn (new)*	Proteoglycan carring CS or DS
Mm01283063_m1	*Vcan (new)*	Proteoglycan carring CS or DS

Preparation of linkage region

Taqman Assay ID	Gene symbol	Function
Mm00504458_s1	*B3galt6*	Transferring UDP-galactose to galactose-xylose on proteoglycan
Mm00661499_m1	*B3gat1*	Transferring UDP-GlcA to galactose-galactose-xylose on proteoglycan
Mm00549042_m1	*B3gat2*	Transferring UDP-GlcA to galactose-galactose-xylose on proteoglycan
Mm00470389_m1	*B3gat3*	Transferring UDP-GlcA to galactose-galactose-xylose on proteoglycan
Mm00479556_m1	*B4galt2*	Transfering UDP-galactose to GlcNAc, Glc, and Xyl.
Mm00461357_m1	*B4galt7*	Transferring UDP-galactose to xylose on proteoglycan
Mm00558690_m1	*Xylt1*	Transferring UDP-xylose to proteoglycan
Mm00461181_m1	*Xylt2*	Transferring UDP-xylose to proteoglycan

Glycosaminoglycan chain polymerisation

Taqman Assay ID	Gene symbol	Function
Mm01262239_g1	*Chpf*	Transferring UDP-GlcA to GalNAc at end of sugar chain (CS)
Mm01319178_m1	*Chsy1*	Transferring UDP-GlcA to GalNAc at end of sugar chain (CS)
Mm01545329_m1	*Chsy3*	Transferring UDP-GlcA to GalNAc at end of sugar chain (CS)
Mm00555164_m1	*Csgalnact1*	Transferring UDP-GalNAc to GlcA at end of sugar chain (CS)
Mm00513340_m1	*Csgalnact2*	Transferring UDP-GalNAc to GlcA at end of sugar chain (CS)
Mm00468769_m1	*Ext1*	Transferring UDP-GlcNAc to GlcA at end of sugar chain (HS)
Mm00468775_m1	*Ext2*	Transferring UDP-GlcNAc to GlcA at end of sugar chain (HS)
Mm00621977_s1	*Extl1*	Transferring UDP-GlcA to GlcNAc at end of sugar chain (HS)
Mm00469621_m1	*Extl2*	Transferring UDP-GlcA to GlcNAc at end of sugar chain (HS)
Mm00516994_m1	*Extl3*	Transferring UDP-GlcA to GlcNAc at end of sugar chain (HS)
Mm00468496_m1	*Has1*	Polymerisation of hyaluronic acid
Mm00515089_m1	*Has2*	Polymerisation of hyaluronic acid
Mm00515091_m1	*Has3*	Polymerisation of hyaluronic acid

Glycosaminoglycan chain modification

Taqman Assay ID	Gene symbol	Function
Mm00517563_m1	*Chst11*	Sulfation at the 4-O postion of GalNAc untis (CS)
Mm00546416_s1	*Chst12*	Sulfation at the 4-O postion of GalNAc untis (CS)
Mm01186255_s1	*Chst13*	Sulfation at the 4-O postion of GalNAc untis (CS)
Mm00511291_s1	*Chst14*	Sulfation at the 4-O postion of GalNAc untis (CS)
Mm00513227_m1	*Chst15*	Sulfation at the 6-O postion of GalNAc untis (CS)
Mm00490018_g1	*Chst2*	Sulfation at the 6-O postion of GalNAc untis (CS)
Mm00489736_m1	*Chst3*	Sulfation at the 6-O postion of GalNAc untis (CS)
Mm00517342_m1	*Chst5*	Sulfation at the 6-O postion of GalNAc untis (CS)
Mm00491466_m1	*Chst7*	Sulfation at the 6-O postion of GalNAc untis (CS)
Mm00558321_m1	*Chst8*	Sulfation at the 4-O postion of GalNAc untis (CS)
Mm01722279_m1	*Chst9*	Sulfation at the 4-O postion of GalNAc untis (CS)
Mm00552923_m1	*Dse*	Epimerisation of GlcA unit into iduronic acid unit (IdoA) (CS)
Mm00473667_m1	*Glce*	Epimerisation of GlcA unit into iduronic acid unit (IdoA) (HS)
Mm00478684_m1	*Hs2st1*	Sulfation at the 2-O position of GlcA and IdoA units (HS)
Mm01964038_s1	*Hs3st1*	Sulfation at the 3-O position of GlcNAc and GlcNS units sulfated at the 6-O position (HS)
Mm00616933_m1	*Hs3st2*	Sulfation at the 3-O position of GlcNAc and GlcNS units sulfated at the 6-O position (HS)
Mm00780907_s1	*Hs3st3a1*	Sulfation at the 3-O position of GlcNAc and GlcNS units sulfated at the 6-O position (HS)
Mm00479621_m1	*Hs3st3b1*	Sulfation at the 3-O position of GlcNAc and GlcNS units sulfated at the 6-O position (HS)
Mm01192940_m1	*Hs3st5 (new)*	Sulfation at the 3-O position of GlcNAc and GlcNS units sulfated at the 6-O position (HS)
Mm01299930_m1	*Hs3st6*	Sulfation at the 3-O position of GlcNAc and GlcNS units sulfated at the 6-O position (HS)
Mm01229698_s1	*Hs6st1*	Sulfation at the 6-O position of GlcNAc and N-sulfated-glucuronic acid units (GlcNS) (HS)
Mm00479296_m1	*Hs6st2*	Sulfation at the 6-O position of GlcNAc and GlcNS units (HS)
Mm00479297_m1	*Hs6st3*	Sulfation at the 6-O position of GlcNAc and GlcNS units (HS)
Mm00447005_m1	*Ndst1*	N-de-acetylation and N-sulfation of GlcNAc unit (HS)
Mm00447818_m1	*Ndst2*	N-de-acetylation and N-sulfation of GlcNAc unit (HS)
Mm00453178_m1	*Ndst3*	N-de-acetylation and N-sulfation of GlcNAc unit (HS)
Mm00480767_m1	*Ndst4*	N-de-acetylation and N-sulfation of GlcNAc unit (HS)
Mm00552283_m1	*Sulf1*	Desulfation of the 6-O positon of 6-O sulfated GlcNAc and GlcNS units (HS)
Mm01248026_m1	*Sulf2*	Desulfation of the 6-O positon of 6-O sulfated GlcNAc and GlcNS units (HS)
Mm00461213_m1	*Sumf1*	Cofactor for Sulf1 and Sulf 2 (HS)
Mm01197721_m1	*Sumf2*	Cofactor for Sulf1 and Sulf 2 (HS)
Mm00616790_m1	*Ust*	Sulfation at the 2-O position of GlcA and IdoA units (CS)

Glycosaminoglycan chain degradation

Taqman Assay ID	Gene symbol	Function
Mm00503655_s1	*Arsb*	Desulfation of the 4-O position of 4-O sulfated GalNAc units (CS)
Mm00557970_m1	*Arsj*	Desulfation of the 4-O position of 4-O sulfated GalNAc units (CS)
Mm00513099_m1	*Arsk*	Desulfation of proteoglycans, paralog of IDS
Mm00489576_m1	*Galns*	Desulfation of the 6-O positon of 6-O sulfated GalNAc units (CS)
Mm00659592_m1	*Gns*	Desulfation of the 6-O positon of 6-O sulfated GlcNAc and GlcNS units (HS)
Mm01197698_m1	*Gusb*	Hydrolysation of GlcA from sugar chain (HS and Hyaluronic acid and CS)
Mm00599877_m1	*Hexa*	Hydrolysation of GalNAc units (CS) and GlcNAc untis (hyaluronic acid) from sugar chain
Mm00599880_m1	*Hexb*	Hydrolysation of GalNAc units (CS) and GlcNAc untis (hyaluronic acid) from sugar chain
Mm00519485_m1	*Hgsnat*	Acetylation of desulfated GlcNS units (HS)
Mm00461768_m1	*Hpse*	Degradation of HS chains extracellularly
Mm00477731_m1	*Hyal2*	Degradation of hyaluronic acid chain
Mm00662097_m1	*Hyal3*	Degradation of hyaluronic acid chain
Mm00494868_m1	*Ids*	Desulfation of 2-O sulfated IdoA and GlcA units (HS and CS)
Mm00515143_m1	*Idua*	Hydrolysation of IdoA unit from sugar chain (HS and CS)
Mm00452409_m1	*Mgea5*	Degradation of hyaluronic acid chain
Mm00476274_m1	*Naga*	Hydrolysis N-GalNAc moieties from glycoconjugates.
Mm00479175_m1	*Naglu*	Hydrolysation of GlcNAc from sugar chain (HS)
Mm00480053_m1	*Nat6;Hyal1*	Degradation of hyaluronic acid chain
Mm00450747_m1	*Sgsh*	Desulfation of GlcNS units (HS)

Growth factors

Taqman Assay ID	Gene symbol	Function
Mm01192933_g1	*Ctgf*	Connective tissue growth factor, embryonic growth factor in skin development **
Mm00433275_m1	*Fgf10*	Fibroblast growth factor 10 **
Mm01285715_m1	*Fgf2*	Fibroblast growth factor 2 **
Mm00438917_m1	*Fgf4 (new)*	Growth factor (Uijtdewilligen et al, 2013)**
Mm00433291_m1	*Fgf7*	Fibroblast growth factor 7 **
Mm00438921_m1	*Fgf8*	Fibroblast growth factor 8 **
Mm01131929_m1	*Figf*	C-fos induced growth factor **
Mm00439305_g1	*Hbegf*	Heparin-binding epidermal growth factor **
Mm01205760_m1	*Pdgfa*	Platelet-derived growth factor a **
Mm01298578_m1	*Pdgfb*	Platelet-derived growth factor b **
Mm03053266_s1	*Pdgfc*	Platelet-derived growth factor c **
Mm00546829_m1	*Pdgfd*	Platelet-derived growth factor d **
Mm00436527_m1	*Shh*	Sonic hedgehog **
Mm01178819_m1	*Tgfb1*	Transforming growth factor beta 1 **
Mm01321739_m1	*Tgfb2*	Transforming growth factor beta 2 **
Mm01307950_m1	*Tgfb3*	Transforming growth factor beta 3 **
Mm01281449_m1	*Vegfa*	Vascular endothelial growth factor a **
Mm00442102_m1	*Vegfb*	Vascular endothelial growth factor b **
Mm01202432_m1	*Vegfc*	Vascular endothelial growth factor c **

Putatively involved

Taqman Assay ID	Gene symbol	Function
Hs99999901_s1	*18S*	Reference gene
Mm00607939_s1	*Actb (new)*	Reference gene
Mm00802173_g1	*Arsa*	Desulfation of cerebroside
Mm00546931_m1	*Arsg*	Paralog of Arsa
Mm00473986_m1	*C1galt1*	Transferring UDP-Gal to N-GalNAc.
Mm00480676_m1	*C1galt1c1*	C1GALT1-specific chaperone 1
Mm00517855_m1	*Chst1*	Involved in sulfation of keratin sulfate
Mm03302249_g1	*Gapdh*	Reference gene
Mm00516323_m1	*Gla*	Hydrolysis of galactose units
Mm00515342_m1	*Glb1*	Hydrolysis of galactose units
Mm00464245_m1	*Glb1l2*	Hydrolysis of galactose units
Mm01254913_g1	*Gnpda1;Gm8615*	Conversion of GlcNAc-6-P into fructose-6-P
Mm00503573_m1	*Gnpda2*	Conversion of GlcNAc-6-P into fructose-6-P
Mm01324427_m1	*Hprt1 (new)*	Reference gene
Mm00502002_m1	*Kl*	Putative glucuronidase
Mm00473122_m1	*Klb*	Putative glucuronidase
Mm00555344_m1	*Slc17a5*	Transport of GlcA from lysosoom to cytoplasm
Mm00442341_m1	*Slc35a1*	Putative CMP-Sialic Acid Transporter
Mm01277042_m1	*Tbp*	Reference gene
Mm00495930_m1	*Ugt8a*	Transfere galactose to ceramide

Gene symbols marked with new are added in the second version of the TLDA cart.

* Glc, glucosamine; GlcNAc, N-acetylated glucosamine; Gal, galactosamine; GalNAc, N-acetylated galactosamine; GlcA, glucuronic acid; IdoA, iduronic acid.

**Uijtdewilligen et al, 2016.

Chapter 6

Overexpression of heparanase and loss of heparan sulphate are involved in emphysematous lesions

*Nicole C. Smits[1,2], **Peter J.E. Uijtdewilligen[1]**, Antoine A. Robbesom[1],*

Mieke M. J. F. Koenders[1], Elly M. M. Versteeg[1], Johan van der Vlag[3],

Jo H. Berden[3], Israel Vlodavsky[4], Eyal Zcharia[4], Jin-ping Li[5],

Johan Bulten[6], P. N. Richard Dekhuijzen[7] and Toin H. van Kuppevelt[1]

[1] Department of Biochemistry, Radboud university medical centre, Nijmegen Centre for Molecular Life Sciences, Nijmegen, The Netherlands

[2] Department of Medicine, Heart and Vascular Research Center, Geisel School of Medicine at Dartmouth, Hanover, NH, USA

[3] Nephrology Research Laboratory and Department of Nephrology, Radboud university medical centre, Nijmegen Centre for Molecular Life Sciences, Nijmegen, The Netherlands

[4] Cancer and Vascular Biology Research Centre, The Bruce Rappaport Faculty of Medicine, Haifa, Israel

[5] Department of Medical Biochemistry and Microbiology, Biomedical Centre, Uppsala University, Uppsala, Sweden, Departments of

[6] Pathology, Radboud university medical centre, Nijmegen, The Netherlands

[7] Pulmonary Diseases, Radboud university medical centre, Nijmegen, The Netherlands

Abstract

At the time of clinical diagnosis, the process of parenchymal destruction, characteristic for emphysema, is already in an advanced state and this hampers the identification of early molecular alterations. In this study we took the somewhat unconventional approach to evaluate lung specimens from individuals on basis of early signs of microscopic emphysema. The overall aim of the study was to determine which extracellular matrix (ECM) components are affected in the initial stage of human emphysema, and if similar alterations can induce emphysematous lesions in mice.

Four groups of specimens were analysed by immunohistochemistry to study alterations of ECM components. Three groups were made based on the destructive index (DI), the most sensitive morphological parameter for emphysema, and on the mean linear intercept (MLI). Groups included 1) normal tissue (DI<30%, MLI normal, n = 6), 2) slightly affected tissue (DI 30%-80%, MLI normal, n = 8), and 3) moderately affected tissue (DI>80%, MLI increased, n = 7). For comparison, specimens from patients with severe airflow limitations/emphysema were included as 4th group.

In human, an increase in DI correlated with a specific decrease in heparan sulfate (HS) proteoglycans (both side chain and core protein), and an increase in heparanase expression. Other matrix components such as elastin, collagens and laminin were not correlated. The lungs of genetically modified mice that overexpress heparanase (HPSEtg) were evaluated as a possible animal model for emphysema. The prime molecular changes found in human lungs were mirrored in the lungs of HPSEtg mice, whereas these mice developed age-related emphysematous lesions.

Loss of heparan sulfate and increase of heparanase in parenchymal lung tissue are associated with the development of emphysema in humans and induce emphysematous lesions in mice.

Introduction

Pulmonary emphysema is defined as “a condition of the lung characterised by abnormal permanent enlargement of airspaces distal to the terminal bronchioles, accompanied by the destruction of their walls, and without obvious fibrosis” [1–3]. Emphysema is a disabling progressive disease that takes many years to develop, cigarette smoking being a main risk factor [4, 5]. It is generally thought that proteases and free radicals released by inflammatory cells and induced by chronic cigarette smoke exposure overwhelm the anti-proteolytic and anti-oxidant defences [4, 6, 7], and mediate destruction of lung tissue [8–11] and impede repair [12, 13].

A major challenge in research on early pathogenic events of emphysema is the time span between initiation and clinical manifestation. At the time of clinical diagnosis the process of parenchymal destruction is already in an advanced stage, precluding identification of early molecular events. Morphological analysis of lung parenchyma allows for early identification of emphysematous lesions. This especially holds for the destructive index (DI), which is a measure for early parenchymal destruction and has a high sensitivity towards mild forms of emphysema [14]. The DI is a more sensitive parameter in comparison to the main linear intercept (MLI), which is a parameter for airspace enlargement and is generally used for morphometric analysis of emphysema [15].

In addition to proteases and oxidative stress (free radicals) that cause destruction of lung tissue, an impeded repair may also play a role in the pathogenesis of emphysema [16, 17]. Maintenance of structural lung tissue after injury as well as tissue repair requires production of numerous extracellular matrix (ECM) components in proper quantities and sequence. In lung alveoli, the ECM forms a strong expansile framework that supports the alveolar epithelial-capillary interface. ECM molecules, in particular proteoglycans, may affect inflammatory processes as observed in tissue repair by interaction with and regulation of the activity of inflammatory mediators [18, 19]. In emphysema, lung tissue is not able to restore the integrity of alveolar tissue after chronic, smoke-induced damage. In this respect, impaired repair may imply an abnormal ECM, resulting in altered structure and function of tissue.

Since loss of elasticity is an important hallmark of emphysema most attention towards the underlying pathogenesis has focused on elastin as the main target of destruction. However, little is known about destruction of individual ECM components at the early onset of emphysema. Research interest is changing from the abundant fibrillar components to the more regulatory molecules in the ECM like glycosaminoglycans, including heparan sulfate (HS) [20–22], chondroitin sulfate and dermatan sulfate [16, 23].

Proteoglycans are proteins with one or more covalently attached glycosaminoglycans. The best studied glycosaminoglycan is HS, known to bind and modulate various cytokines and growth factors, such as fibroblast growth factor 2 (FGF2) and vascular endothelial growth factor (VEGF) [19], which play a role during inflammatory processes. For the binding of signalling molecules the sulphation pattern of the glycosaminoglycan is important [23]. It has been shown for instance that during idiopathic pulmonary fibrosis

the 6-O sulphation of HS is altered, which may lead to aberrant regulation of the fibrotic responses to transforming growth factor beta 1 [24].

Various knock out mouse models for genes involved in HS-proteoglycan biosynthesis have shown that altered expression can lead to altered inflammatory reactions [23]. For instance, syndecan 1, a membrane bound HS proteoglycan, is involved in the regulation of neutrophils in injured lungs [25]. HS plays a role in the phenotype of type I and type II alveolar cell in the lung [26]. The basal membrane beneath type I alveolar cells is more sulfated in comparison to the basal membrane beneath type II cells and it has been shown that sulphation of glycosaminoglycans plays a role in the transdifferentiation of type II to type I alveolar cells [26]. In general, it is assumed that HS has an anti-inflammatory effect [18] and is involved in the regulation of stem cells [26]. The involvement of chondroitin- and dermatan sulfate in pulmonary emphysema has been shown in a RNA interference study for chondroitin sulfotransferase 3 (Chst3), an enzyme involved in 6-O sulphation. Inhibiting expression of Chst3 resulted in a decrease in the macrophage accumulation during the inflammatory response [27].

In this study, we focussed on ECM components, especially heparan sulfate proteoglycans, in lung tissue from subjects with early signs of tissue destruction as revealed by morphometric analysis. Molecular alterations found were mimicked in lung tissue from genetically modified mice overexpressing human heparanase, an enzyme that degrades heparan sulfate [28], and the lungs were analysed for emphysematous lesions.

Materials & Methods

Materials

Chemicals and antibodies

All chemicals were purchased from Merck (Darmstadt, Germany), unless stated otherwise. Alexa 594-conjugated goat anti-rabbit IgG, Alexa 488-conjugated goat anti-mouse IgM (μ chain), and Alexa 594-conjugated goat anti-mouse IgG2b were from Molecular Probes (Eugene, OR). FITC-conjugated donkey anti-goat IgG, mouse anti bovine α-elastin (clone BA-4), and rabbit anti-EHS mouse laminin were from Sigma Immuno Chemicals (St. Louis, MO). Rabbit anti bovine-type I collagen was from Chemicon International, Inc. (Temecula, CA). Goat anti human-type IV collagen was from Southern Biotechnology Associates (Birmingham, AL). Mouse anti-human heparanase 1 (clone HP3/17) was from Insight Biopharmaceuticals Ltd. (Rehovat, Israel). Mouse anti-human CD4 and CD8 were from Dakopatts (Glostrup, Denmark). Peroxidase labelled goat anti-mouse IgG was from Thermo Scientific (Rockford, USA). Mowiol (4-88) was obtained from Calbiochem (La Jolla, CA). Aminoethyl carbazole (red) substrate kit was from Zymed Laboratories Inc. (San Fransisco, CA). Mouse monoconal antibody 6B6, directed against human decorin, a dermatan sulfate proteoglycan, was from Seikagaku (Tokyo, Japan). Goat polyclonal antibody Bl31 [29] was directed against the core protein of human agrin (a HS proteoglycan). Mouse monoclonal antibody JM72 [30] was directed against domain AGR10 of the core protein of human agrin. Mouse monoclonal anti-rat HS antibody JM403 was directed against a HS domain containing glucuronic acid-rich sequences with N-unsubstituted glucosamine units [31, 32]. All incubations were performed at ambient temperature (22 °C) unless stated otherwise.

Human lung specimens

Lung tissue was obtained from 21 patients with various degrees of microscopic emphysema and from 3 patients with evident airflow limitation. Informed consent was obtained from each patient, and the study was approved by the local ethics committee. Characteristics of the study group are given in Table 1. Specimens from patients with microscopic emphysema were subdivided into groups based on the DI, the most sensitive morphological parameter for emphysema, and the MLI (see below for morphometry). Patients were grouped as follows: 1) normal tissue (DI<30%, MLI normal), 2) slightly affected tissue (DI 30%-80%, MLI normal), and 3) moderately affected tissue (DI>80%, MLI increased). Lung tissue was obtained during lobectomy for lung cancer at the University Lung Centre Nijmegen or the Rijnstate Hospital Arnhem, the Netherlands. Samples derived from the upper and the lower lobes, and from the left and right lung were examined. Specimens (1 cm3) were taken from resected lung lobes, not showing any sign of the underlying disease for which the patient underwent surgery. For comparison, lung tissue from patients with severe emphysema, (patients who underwent lung volume reduction surgery, $n = 3$) were included.

Lung function tests were performed before surgery. Static and dynamic lung function tests were performed with a wet spirometer and with a closed circuit helium dilution method (Pulmonet III, Sensormedics, Bilthoven, The Netherlands). Diffusion capacity

for carbon monoxide per liter/lung (alveolar) volume (DL,CO/VA) was measured with the single breath-holding carbon monoxide method (Sensormedics 2450), and was corrected for actual hemoglobin. Measurements were performed at least 12 h after smoking. Predicted spirometric values were derived from the ERS standards.

Morphological characterisation of lung specimens

Parenchymal destruction

The degree of emphysema was evaluated by the DI, using a microscopic point count technique [14, 15]. Microscopic fields were selected, devoid of large bronchi(oli), vessels, collapsed tissue, or extensive fibrosis. From each lung specimen, an average of 5 different sections was used, and representative non-overlapping fields were selected. Alveolar, and duct spaces lying underneath the counting points were evaluated for the presence of destruction. Destruction was defined on one or more of the following criteria: [1] at least two alveolar wall defects, [2] at least two intraluminal parenchymal rags in alveolar ducts, [3] clearly abnormal morphology, or [4] classic emphysematous changes [14]. The percentage of all the points falling into the several categories of destroyed airspaces was computed to reveal the DI. In general, 750 counting points were analysed per specimen.

Airspace enlargement

Enlargement of the airspaces was determined by the MLI measurement technique originally described by Dunill [33], which reflects the average size of alveoli. To determine the MLI, the same images as described above were used. A transparent sheet with 10 horizontal and 11 vertical lines was laid over the images, and intercepts of alveolar walls with these lines were counted. Values were corrected for tissue shrinkage by measuring the dimensions before and after histological processing. The correction factor was 0.832, in accordance with data from Weibel [34].

Immunohistochemistry

Cryosections (4-5 µm) were rehydrated for 10 min in PBS, blocked in PBS containing 2% (wt/vol) bovine serum albumin (BSA) for 20 min, and incubated with the primary antibody for 60 min. Following each incubation, cryosections were washed in PBS (3 x 5 min). Antibody JM72 was used at 1:250 dilution, anti-heparanase 1 antibody was used at 1:200 dilution, anti-type I collagen, antibody BI31, antibody JM403, and all secondary antibodies were used at 1:100 dilution. All other primary antibodies were used at 1:50 dilution. Cryosections were fixed in 96% ethanol, air dried, and embedded in Mowiol (10% (wt/vol) in 0.1 M Tris-HCl, pH 8.5/25% (vol/vol) glycerol/2.5% (wt/vol) NaN3).

Next to fluorescent detection, heparanase expression was also detected using an aminoethyl carbazole (red) substrate kit. Briefly, sections were rehydrated for 10 min in Tris-buffered saline (TBS), blocked in TBS containing 1% (wt/vol) BSA for 30 min, and incubated with the anti-heparanase 1 antibody for 60 min. Sections were washed in TBS, and incubated with 1000-fold diluted peroxidase labelled goat anti-mouse for 60 min. Sections were washed in PBS for 5 min, rinsed in 50 mM NaAc buffer (pH 5.0), and peroxidase activity was detected using aminoethyl carbazole (red) substrate.

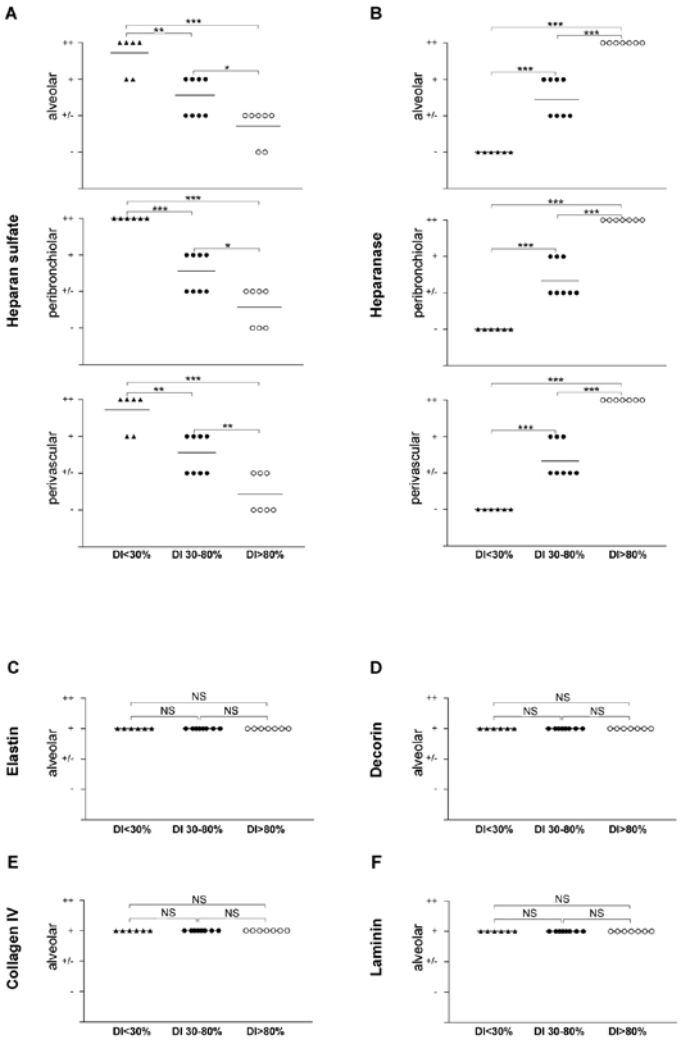

Figure 1. Scatter plots showing the relation between staining for extracellular matrix (ECM) components and the destructive index (DI). Sections of human lung specimens with normal (DI<30%, MLI normal), slightly affected (DI 30-80%, MLI normal), or moderately affected (DI>80%, MLI increased) parenchyma were incubated with antibodies against heparan sulfate (HS; A), heparanase (B), elastin (C), decorin (D), type IV collagen (E), and laminin (F). Immunoreactivity was scored using semi-quantitative criteria (-, no reactivity; +/-, weak reactivity; +, strong reactivity; +/+, very strong reactivity). Note that staining intensity for HS decreased with increasing DI, whereas staining for heparanase increased with increasing DI. There were no differences in staining for other ECM components such as elastin, decorin, type IV collagen, and laminin between the three groups.

NS, not significant; DI, destructive index; MLI, mean linear intercept; ECM, extracellular matrix

Sections were rinsed in water, counterstained with hematoxylin, washed with running tap water for 10 min, further washed with demineralised water for 5 min, and embedded in Kaiser's gelatin. As controls, primary or conjugated antibodies were omitted. Lung sections were randomly coded, and immunoreactivity was scored independently using semi-quantitative criteria (-, no reactivity; +/-, weak reactivity; +, strong reactivity; ++ very strong reactivity) by two observers. Scoring between the observers was consistent as deduced from regression analysis (r^2 = 0.82–0.92).

Immunohistochemical detection of inflammatory cells was performed on 4 µm paraformaldehyde-fixed, paraffin embedded lung tissue sections. The numerical density of inflammatory cells in lung parenchyma was determined, including alveolar wall tissue. Cells within the lumen of conducting airways and blood vessels were not included. The density of inflammatory cells (CD4 and CD8 positive cells) in lung parenchyma was determined by and expressed as a percentage of total cell numbers. Total cell numbers were defined as the total number of nuclei. Ten randomly selected, non-overlapping fields at a magnification of 400× were counted in each tissue section. Using this method, up to 5,000 cells were counted in each section.

Table 1. Characteristics of patients including morphometric analysis (DI and MLI)

	Normal* (n = 6) (DI < 30%)	Slightly affected* (n = 8) (DI 30 - 80%)	Moderately affected* (*n* = 7) (DI > 80%)	LVR patients *(n = 3)*
Age (yr)	51 ± 9	59 ± 9	67 ± 8	56 ± 5
Male/female	5 / 1	7 / 1	7 / 0	3 / 0
Smoking (Ex/C)	3 / 3	2 / 6	2 / 5	3 / 0
Pack-years	26 ± 10	40 ± 19	37 ± 15	30 ± 15
DI, %	21 ± 9	55 ± 9	85 ± 4	**
MLI, mm	0.23 ± 0.03	0.24 ± 0.03	0.30 ± 0.06	**
FEV_1, % pred	70 ± 10	73 ± 14 (6)	72 ± 16	
FEV_1/VC	62 ± 10 (n=4)	68 ± 11 (6)	60 ± 12	22 ± 9
TLC, % pred	97 ± 11 (n=4)	86 ± 14 (7)	99 ± 16	108 ± 19
K_{CO}, % pred	86 ± 25	75 ± 21	73 ± 18 (7)	41 ± 20

Ex, ex-smokers, not smoking for at least one year; C, current smokers; DI, Destructive Index; MLI, Mean Linear Intercept; FEV1, forced expiratory volume in 1 second; % pred, percentage of predicted value; VC, vital capacity; TLC, total lung capacity; RV, residual volume; KCO, diffusion capacity for CO; LVR, lung volume reduction.

**All values are presented as means ± SD. **: DI and MLI were not assessed due to the advanced parenchymal destruction of the tissue*

( ): indicates number of patients if different from numbers indicated as n-number

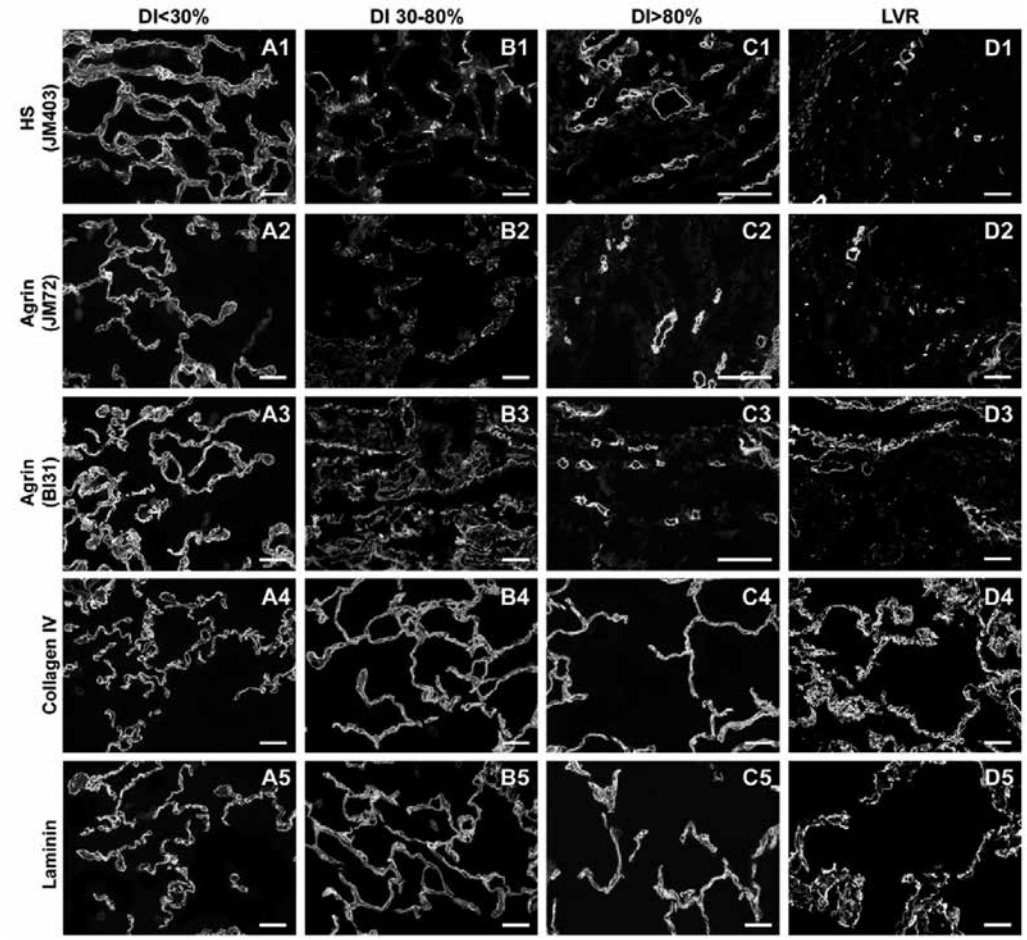

Figure 2. Expression of extracellular matrix components in lung tissue. Lung tissue from morphologically characterised human specimens with Destructive Index (DI) <30%; MLI normal (A), DI 30-80%; MLI normal (B), DI>80%; MLI increased (C), and from lung volume reduction (LVR) patients (D) was incubated with antibodies against the alveolar basement membrane components heparan sulfate (HS; antibody JM403 (A1-D1), agrin (antibody JM72 (A2-D2, and antibody BI31 (D3-D3), type IV collagen (A4-D4), and laminin (A5-D5). Note the decrease in HS, and agrin staining in lung tissue with DI 30-80%, and DI>80% as well as in LVR patients. Staining for other basement membrane associated components (type IV collagen and laminin) was not aberrant. Scale bars, 50 µm.

DI, destructive index; MLI, mean linear intercept

Statistical analysis

Statistical analysis was done with tests for non-parametric data: Kruskal-Wallis (four groups), Spearman's coefficient of rank correlation, and the Mann-Whitney U test for multiple comparisons. Data were analysed with the Statistical Package for the Social Sciences 12.01 (SPSS Inc., Chicago, IL), and GraphPad Prism®, version 4.0 (GraphPad Software Inc., San Diego, CA) computer programs. Values of $P < 0.05$ were considered significant.

Heparanase overexpressing mice

The homozygous mouse strain overexpressing human heparanase and the respective control mice (C57BL background) were described previously by Prof. I. Vlodavsky and Dr. J-p Li [28]. In brief, full-length human heparanase cDNA was subcloned into pCAGGS plasmid at EcoRI-XbaI sites under constitutive control of the chicken β-actin promoter and expressed in all tissues. The plasmid was digested with SalI-PstI and the resulting linear fragment was microinjected to fertilised eggs of C57BL/6 x Balb/c origin to produce transgenic mice overexpressing the heparanase cDNA.

Tissue processing

Each specimen (about 1 cm^3) was cut into pieces of equal size. One part was immersed in phosphate buffered saline (PBS, pH 7.2), inflated under vacuum (13kPa) for 20 min using a routine water stream-driven device (water aspirator) to restore alveolar dimensions [35], frozen in liquid nitrogen, and stored at -80°C. This part was used for immunohistochemistry (see below). The other part was similarly inflated in PBS containing 4% formalin and further processed for paraffin embedding. Sections (4-5 μm) were then cut, hematoxylin-eosin stained, and used for morphological characterisation. All sections were blinded and scored independently by two observers.

Gene expression analysis

To analyse gene expression in mice overexpressing heparanase (HPSEtg mice), lung samples of 70-day-old mice were used. Two lung samples of HPSEtg mice and two lung samples of the wildtype background (C57BL6 mice) were taken and snap frozen in liquid nitrogen and stored at -80°C. Frozen samples were grinded in a microdismembrator (Sartorius, Bunnik, the Netherlands) and RNA was isolated using the TRIZOL-method (Invitrogen, Paisley, UK) in combination with RNeasy Mini kit including a DNAse step (Qiagen, Hilden, Germany). RNA quality was checked using the Bioanalyzer system (Agilent Technologies, Amstelveen, the Netherlands). The RNA integrity numbers and the rRNA ratios were 7.6 and 1.0 respectively for the first transgenic sample; 6.5 and 0.9 for the second transgenic sample; 6.8 and 0.9 for the first wild type sample; and 7.2 and 1.0 for the second wild type sample, respectively. Based on criteria described by Schroeder et al. (2006) [36] the samples were of sufficient quality for gene expression analysis. cDNA was prepared from RNA samples using the Superscript III First-Strand Synthesis system (Invitrogen) with random hexamers. RNA-derived cDNA quality was evaluated by PCR (Fast start Taq polymerase, Roche, Almere, the Netherlands) using primers for GAPDH (Forward primer 5`-TGATGGGTGTGAACCACGAG-3` and reverse primer 5`-GGGCCATCCACAGTCTTCTG-3`).

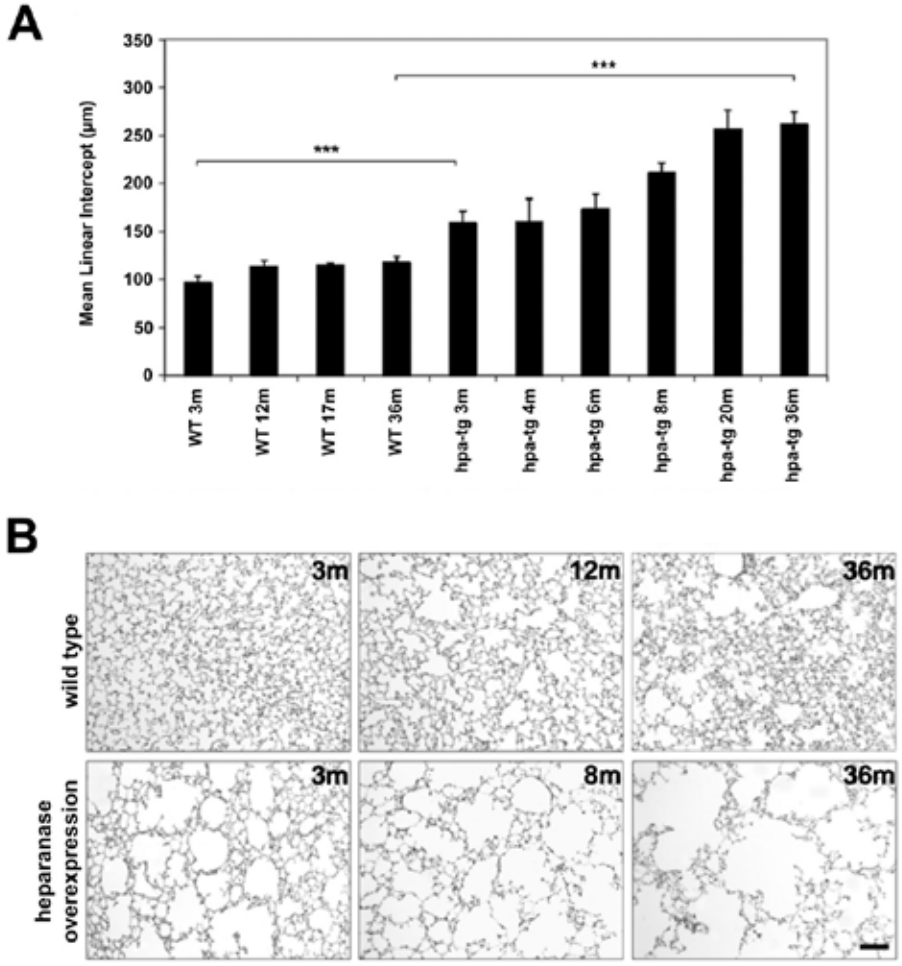

Figure 3. A-B; Overexpression of heparanase initiates emphysematous lesions in mice. A: Mean Linear Intercept (MLI) values (mean ± SD, n = 6) of lungs of wild type (WT) and heparanase overexpressing mice (HPSEtg mice) at different ages. B: Hematoxylin-eosin stained sections of lungs from wild type and HPSEtg mice at different ages. In heparanase overexpressing mice enlargement of airspaces could be observed in lungs of 3-months-old mice, and this was increased with age. m = months. C; CD8 T-lymphocytes in lung parenchyma from subjects with microscopical emphysema expressed as percentage of total cell numbers (total number of nuclei) in lung parenchyma. Horizontal bars represent mean values (Mann-Whitney U test). D, Lung tissue from subjects with normal (left panel) and moderately affected lung tissue (right panel) demonstrating immunoreactivity for inflammatory cells (CD8 and CD4). Note the increase in CD4 and CD8 cells in moderately affected lung tissue.

***, P < 0.05; ***, P < 0.0001.*

Scale bars, 50 µm. HPSEtg mice, heparanase overexpressing mice.

Gene expression was analysed using Real Time-Quantitative PCR (QPCR) using custom designed Taqman Low Density arrays (TLDA) (Applied Biosystems, Nieuwekerk aan de IJssel, the Netherlands) containing probes for genes involved in production of precursors (53 genes); core proteins (28); preparation of linkage region (8 genes); glycosaminoglycan (GAG) chain polymerisation (13); GAG chain modification (32); GAG chain degradation (19); growth factors (19); genes with a putative role in GAG metabolism (15); and reference genes (5). An overview of the genes evaluated, including probe set numbers can be found in Supplementary data Table 1.

For the TLDA carts, 100 ng cDNA in Taqman Universal PCR Master Mix (Applied Biosystems) was loaded per slot as described in the manufacturer's protocol and run on a 7900HT Fast Real-Time PCR System (Applied Biosystems). Expression was analysed based on the threshold cycle (Ct) using SDS 2.3 software and RQ Manager 1.2 (Applied Biosystems).

In Microsoft Excel the reference genes 18S RNA, ActB, Gapdh, Hprt and Tbp, for dCt calculation were checked for stability of expression. Each reference gene was used to calculate the dCt for the other reference genes. The average dCt and standard deviation across all carts was calculated. Based on this analysis three reference genes were found suitable based on an acceptable standard deviation (maximal ±0.5), *viz.* ActB, GAPDH and TBP. Based on the average Ct across all carts a reference gene was chosen for a specific gene. For genes with a Ct between 26.5 and 34.5 Tbp (average Ct of 30.5) was used; for genes with a Ct between 19.6 and 27.6 Gapdh (average Ct of 23.6) was used; and for genes with a Ct between 16.8 and 24.8 ActB (average Ct of 20.8) was used. For some genes two separate dCt values were calculated based on two reference genes. dCT values were further processed applying the $2^{-\Delta\Delta CT}$ method using the wild type background (C57BL6 mice) data as the calibrator point [37]. Statistical significance was tested with an unpaired T-test (2-tailed) using Microsoft Excel. A statistical threshold of $p<0.100$ and a fold threshold of >1.5 were used.

Results

Morphological data

Lung specimens from 21 subjects were morphologically characterised for emphysematous lesions using the DI as a marker for early parenchymal destruction and the MLI as a marker for airspace enlargement (Table 1) [38]. Please note that for normal, unaffected lungs of non-smoking individuals in the fifth-sixth decade of life, the DI is between 0-30% [14]. Based on the DI, three groups were grouped as follows: 1) normal tissue (DI<30%, MLI normal); 2) slightly affected tissue (DI 30-80%, MLI normal), and 3) moderately affected tissue (DI>80%, MLI increased). A comparison was made with lung specimens from patients with severe emphysema (LVR (lung volume reduction) patients, $n = 3$).

Reduced heparan sulfate expression is associated with early signs of parenchymal destruction

The expression of ECM components in the lung parenchyma of patients was evaluated by immunohistochemistry. In lung tissue from patients without microscopic emphysema (DI<30%, MLI normal) HS was abundantly present in alveolar walls as well as in peribronchiolar and perivascular areas (Figure 1A, Figure 2A1 and Figure 4D). However, in slightly affected tissue (DI 30-80%, MLI normal), a reduced and discontinuous staining for HS was observed in alveolar basement membranes, as well as in peribronchiolar and perivascular areas (Figure 1A, 2B1 and 4E). In moderately affected tissue (DI>80%, MLI increased), the reduction of HS in alveolar basement membranes was more pronounced (Figure 2C1 and 4F), whereas capillaries remained strongly positive (Figure 2C1). Staining for other basement membrane components such as type IV collagen and laminin and for the interstitial matrix components elastin and decorin (a dermatan sulfate proteoglycan) did not reveal differences in staining among the three groups (Figure 1, C-F and Figure 2, A4-D4 and A5-D5). Also, staining for type I collagen was not aberrant between groups (data not shown). In lung tissue derived from LVR patients the expression of HS was decreased (Figure 2, D1-D3) whereas staining for collagen IV and laminin was unaltered (Figure 2, D4-D5), as was staining for decorin (not shown).

In normal tissue (DI<30%, MLI normal) heparanase could not be detected (Figure 1B and Figure 4A). In contrast, heparanase expression was markedly increased in slightly as well as moderately affected lung tissue (Figure 1B and Figure 4, B and C). Heparanase expression was found in alveolar and peribronchiolar areas (primarily associated with epithelial cells), and in perivascular areas. Lung tissue derived from LVR patients showed an increase in heparanase expression (Figure 4Q).

Staining for the core protein of agrin, a major HS proteoglycan, revealed a continuous basement membrane staining in alveolar tissue, and in bronchiolar and vascular areas in normal tissue (Figure 2, A2 and A3). Discontinuous and reduced staining was observed in slightly affected tissue (Figure 2, B2 and B3), and was more prominent in moderately affected tissue (Figure 2, C2 and C3). Staining of capillaries was strongly

positive in tissues of all groups (Figure 2, C2 and C3). Strongly reduced staining for the core protein of agrin was also observed in lung specimens from LVR patients (Figure 2, D2 and D3).

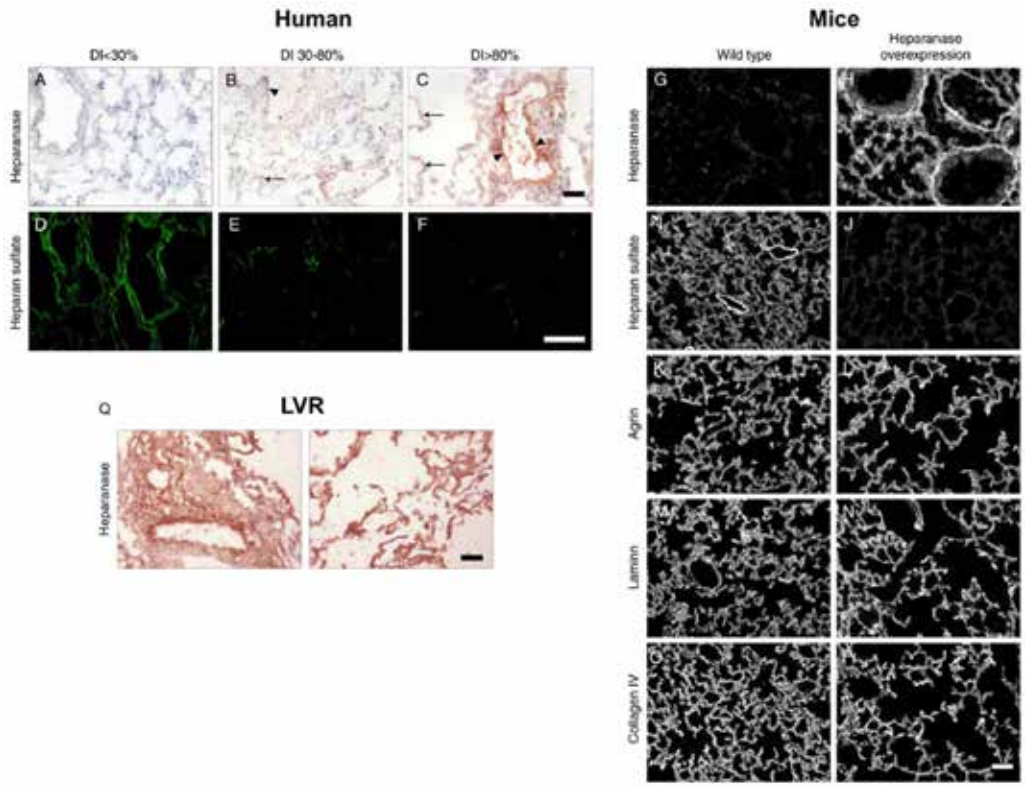

Figure 4. Overexpression of heparanase is associated with loss of heparan sulfate (HS). A-F: morphologically analysed sections of subjects with normal (DI<30%, MLI normal A, D), slightly affected (DI 30-80%, MLI normal B, E), or moderately affected (DI>80%, increased MLI C, F) lung parenchyma were incubated with antibodies against human heparanase (A-C) or HS (D-F). Heparanase expression increased with DI in alveolar basement membranes (arrows), perivascular areas (arrowheads), and peribronchiolar areas (not shown), whereas HS decreased.

Scale bars, 50 µm. G-P: Lung tissue from wild type mice (G-O, 3 months old), and HPSEtg mice (H-P, 3 months old) were stained with antibodies against heparanase (G, H), HS (I, J), agrin core protein (K, L), laminin (M, N), and type IV collagen (O, P). Note the increase in heparanase and loss of HS in transgenic mice. Staining for other matrix components was not affected. Q: Expression of heparanase in lung tissue from LVR patients.

Scale bar, 50 µm. DI, destructive index; HPSEtg mice, heparanase overexpressing mice.

Microscopic emphysema is associated with increased CD4 and CD8 infiltration

Several reports have shown that in patients with emphysema an ongoing inflammatory process is present [39, 40]. We assessed inflammation in lung tissue from subjects without clinically evident airflow limitation by the number of CD4 and CD8 T-lymphocytes. We found that subjects with moderately affected tissue (DI>80%, MLI increased) showed more CD4 and CD8 T-lymphocytes in lung parenchyma compared to subjects with slightly affected tissue (DI 30%-80%, MLI normal). Also, subjects with slightly affected tissue (DI 30%-80%, MLI normal) demonstrated more CD4 and CD8 T-lymphocytes in lung parenchyma compared to normal tissue (DI<30%, MLI normal) (Figure 3C, D).

Heparanase overexpression induces emphysematous lesions

To investigate whether airspace enlargement and emphysematous lesions could be initiated by overexpression of heparanase, an enzyme that degrades HS, we examined the lungs of transgenic mice overexpressing mammalian heparanase. Mice aged from 3 months to 3 years were studied (Figure 3). In heparanase overexpressing mice, the MLI increases significantly over time. Compared to wild type mice at 3 months of age, the MLI in heparanase overexpressing mice increased 1.6-fold (1.59 ± 0.13 versus 0.97 ± 0.07 in wild types; $P < 0.0001$, $n = 6$), and up to 2.2-fold (2.61 ± 0.13 versus 1.17 ± 0.06 in wild types; $P < 0.0001$, $n = 6$) was noted in 3-year-old mice. Figure 3B clearly shows the presence of enlarged airspaces in lung sections from heparanase overexpressing mice.

Using immunohistochemistry we evaluated heparanase expression in lungs from wild type versus HPSEtg mice. Heparanase could not be detected in wild type mice (Figure 4G), whereas in heparanase overexpressing mice it was abundantly present throughout the lungs (Figure 4H). As expected, HS expression was greatly reduced in heparanase overexpressing mice (Figure 4 I, J). Staining intensity for other basement membrane components such as the core protein of agrin (Figure 4, K and L), laminin (Figure 4, M and N), and interstitial components such as elastin (data not shown) and collagen (type IV collagen, Figure 4, O and P) did not differ between wild type and heparanase overexpressing mice.

In addition to immunohistochemistry we evaluated gene expression in heparanase overexpressing mice (Supplementary data Table 1), focussing on genes involved in the metabolism of glycosaminoglycans. Four genes were found to be differentially expressed, three of them involved in HS biosynthesis, *viz.*: HS 3-O-sulfotransferase 3a1 (Hs3st3a1), HS 6-O-sulfotransferase 1 (Hs6st1) and GlcNAc-Proteoglycan-4-Beta-GlcA-transferase (Ext1) at 2.1, 1.6 and 1.7-fold respectively (Table 2). The fourth gene found to be significantly differentially expressed was beta-glucuronidase (GusB) at 1.6-fold. GusB is involved in the degradation of HS. These results suggest that at the mRNA level a number of HS biosynthetic genes are upregulated resulting in structurally altered HS. In addition a number of other genes were differentially expressed, including Pgm1, Pgm2, Slc2a9, Slc34a4, Slc35b1, Ugp2, Aspn, Chst5, Chst8 and Pdgfa (Supplementary data Table 1).

Discussion

This study shows that loss of HS and increased expression of heparanase are associated with early signs of emphysema. Overexpression of heparanase, resulting in loss of HS, induced age-related emphysematous lesions in mice.

HS is increasingly considered as a regulatory polysaccharide, binding and modulating a number of effector molecules and ECM components. It has been coined “master regulator of interactions” [41]. HS interacts with various classes of proteins that are involved in the pathogenesis of emphysema. These include proteases and protease inhibitors [42], enzymes involved in neutralising reactive oxygen species like superoxide dismutase [43–47] and xanthine oxidase [47–49], chemokines [50], and growth factors/ cytokines [12, 51]. In addition, HS proteoglycans interact with basement membrane components, which is necessary for basement membrane barrier integrity in pulmonary tissue. Diminished presence of HS and agrin in the lungs may therefore affect basement membrane integrity. In animal models HS proteoglycans have been implicated in the pathogenesis of emphysema. Specific inhibition of proteoglycan synthesis induces emphysematous lesions in rats [52]. In elastase-induced emphysema in rats, HS is readily removed from the lung by degradation of the protein core of the HS proteoglycans [53], and as a consequence the protective, protease (elastase) inhibiting capacity of HS [54] is lost. Elastase-induced emphysema can be prevented by administration of HS [54]. The only long-lasting change (one year) observed in elastase-induced emphysema is a decrease in the ratio HS/collagen and HS/elastin [55]. HS can be depolymerised by reactive oxygen and nitrogen species [56] both present in cigarette smoke, and reactive oxygen species can induce the expression of heparanase [57]. Additionally, rats exposed to cigarette smoke show a decrease in HS content in the lung [58].

In lungs of human emphysematous patients biochemical alterations in glycosaminoglycans composition, including HS, have been observed [59, 60] but the results are contradictory. In line with previous work [61], the present study confirms a diminished HS staining in patients with clinically evident emphysema, and extent this observation to parenchymal lung tissue characterised by early signs of parenchymal tissue destruction i.e. tissue with a normal LMI value, but an increase DI index. We also found diminished agrin, a HS-proteoglycan present in basement membranes of parenchymal lung tissue, whereas staining for other basement membrane-specific components remained unaltered.

All subjects included in this study are current or ex-smokers. During smoke exposure, the lungs are continuously exposed to numerous amounts of oxidants and free radicals. This phenomenon, which is known as oxidant stress [62, 63] is also believed to be a central factor in the pathogenesis of emphysema. Previous studies have shown that reactive oxygen species (ROS) are able to degrade proteoglycan core proteins [64, 65] and glycosaminoglycans including HS and heparin [66–70]. Apart from HS degradation, ROS are able to inhibit *de novo* synthesis of proteoglycans [64–66, 69, 71]. ROS could therefore have a direct toxic effect in the alveolar wall resulting in, for example, a structurally altered HS. We observed alteration in HS biosynthetic enzymes which is in line with modified HS structures.

Table 2. Differential expression of genes involved in the metabolism of glycosaminoglycans in HPSEtg

Gene symbol	Function †	Probe set	Hpse overexpression based on reference gene TBP	
			P-value	Relative fold expression
Genes involved in HS synthesis				
Ext1	GlcNAc-Proteoglycan-4-Beta-GlcA-transferase	Mm00468769_m1	***0.028***	***1.734***
Hs6st1	6-O-sulfation of GlcNAc/NS	Mm01229698_s1	***0.037***	***1.643***
Hs3st3a1	3-O-sulfation of GlcNAc/NS/6S	Mm00780907_s1	***0.060***	***2.131***
Genes involved in HS breakdown				
Gusb	Beta-glucuronidase, glucuronic acid degradation	Mm01197698_m1	***0.086***	***1.564***

An important inflammatory process is present in central and peripheral airways of subjects with COPD [8, 72–74] and studies have demonstrated that it is mainly the CD8-positive cell subset that increases in number in these patients [72, 73]. Here, where we used tissue from subjects with early signs of tissue destruction, we found higher numbers of CD8 and CD4 T-lymphocytes in moderately affected lung tissue (DI>80%; MLI increased) when compared to slightly affected tissue (DI 30-80%; MLI normal) and normal tissue (DI<30%; MLI normal), further indicating the role of immune cells in parenchymal destruction [75].

We have implicated a role for HS in the onset and early stages of emphysema. If there is a correlation between the onset of emphysema and HS, it is possible that HS expression could be used as a diagnostic tool to detect emphysema at an earlier stage than current methods. In normal functioning tissue HS binds ligands and thereby modulates cell signalling and cell migration [23]. Aberrant amounts or structure of HS may lead to malfunction. For example, NDST1 deficient endothelial cells display poorly sulfated HS, leading to impaired neutrophil trafficking due to impaired binding of L-selectins to HS [76]. The interaction between HS and selectins could be of importance for leukocytes as well, since these cells also display selectins. It has been reported that selectins on leukocytes interact with HS presented on the blood vessel wall, which stops the migration of leukocytes and allows transmigration across the blood vessel wall and subsequently regulate the inflammatory response [18]. As shown in the NDST1 deficient endothelial cells, a small change in HS sugar chain modifications leads to impaired binding of HS to selectins. This suggestion seems to be in accordance with a study by Oudijk et al. (2003) in which the authors speculate that improper homing of leukocytes causes inflammation in the surrounding tissue [77]. The improper homing could be a result of hampered binding to HS. In addition to the role of HS in the inflammatory response, a role in the maintenance of stem cells has been suggested [26]. The basal membrane beneath type II alveolar stem cells contains a specific amount of sulphation. It is possible that

due to the increased expression of sulfotransferases the level of sulphation of the basal lamina is altered, leading to aberrant stem cell function. To investigate the role of HS in the regulation of the inflammatory responses during the onset of emphysema additional research is required. This research should be focussed on the sugar level. The gene expression data of HPSEtg mice presented in this study, together with gene expression data on heparanase mouse skin (results not shown) and results of an EXTL2-null mouse model [78], gene expression levels are suggested to be only slightly affected, while at the sugar level modifications lead to clearly distinguishable effects.

In conclusion, our results provide a clear link between heparanase, HS and pulmonary emphysema. We demonstrated that in human lung parenchyma heparanase is overexpressed at an early stage of tissue destruction. Of note, overexpression of heparanase in mice causes emphysematous lesions, which become more severe over time as they do in the human situation. Increased heparanase expression may therefore be a crucial early pathogenic event in emphysema, and may be a promising pharmacological target. Currently, a number of heparanase inhibitors such as PI-88, PG545 and Roneparstat are in clinical trials for their capacity to inhibit cancer progression, angiogenesis and metastasis [79, 80] . Heparanase may be an attractive pharmacological target because it appears that only one form of heparanase is present, in contrast to e.g. the family of matrix metalloproteinases. Therefore, understanding the role of heparanase and HS in the onset of emphysema may lead to new therapeutic approaches to control this disease.

Acknowledgments

The authors wish to express their gratitude to the staff and members of the Department of Lung Diseases, University Lung Centre Nijmegen, and Canisius-Wilhelmina Hospital, Nijmegen, The Netherlands for providing the lung specimens. This study was financially supported by the Dutch Program for Tissue Engineering (DPTE6735).

References

1. Snider GL, J. K, Thurlbeck WM, Bengali ZH. The definition of emphysema. Report of a National Heart, Lung, and Blood Institute, Division of Lung Diseases Workshop. Am Rev Respir Dis 1985; 132: 182–185.

2. Zhang J, Lin XF, Bai CX. Comparison of clinical features between non-smokers with COPD and smokers with COPD: a retrospective observational study. Int J Chron Obs. Pulmon Dis 2014; 9: 57–63.

3. Di Marco F, Tantucci C, Pellegrino G, Centanni S. Chronic obstructive pulmonary disease diagnosis: the simpler the better? Not always. Eur J Intern Med 2013; 24: 199–202.

4. Clancy J, Turner C. Smoking and COPD: the impact of nature-nurture interactions. Br J Nurs 2013; 22: 820,822-826.

5. Morse D, Rosas IO. Tobacco Smoke-Induced Lung Fibrosis and Emphysema. Annu Rev Physiol 2013; 76: 493–513.

6. Mahadeva R, Shapiro SD. Chronic obstructive pulmonary disease * 3: Experimental animal models of pulmonary emphysema. Thorax 2002; 57: 908–914.

7. Li CJ, Liu Y, Chen Y, Yu D, Williams KJ, Liu ML. Novel proteolytic microvesicles released from human macrophages after exposure to tobacco smoke. Am J Pathol 2013; 182: 1552–1562.

8. Eidelman D, Saetta MP, Ghezzo H, Wang NS, Hoidal JR, King M, Cosio MG. Cellularity of the alveolar walls in smokers and its relation to alveolar destruction. Functional implications. Am Rev Respir Dis 1990; 141: 1547–1552.

9. Overbeek SA, Braber S, Koelink PJ, Henricks PA, Mortaz E, LoTam Loi AT, Jackson PL, Garssen J, Wagenaar GT, Timens W, Koenderman L, Blalock JE, Kraneveld AD, Folkerts G. Cigarette smoke-induced collagen destruction; key to chronic neutrophilic airway inflammation? PLoS One 2013; 8: e55612.

10. Fallica J, Boyer L, Kim B, Serebreni L, Varela L, Hamdan O, Wang L, Simms T, Damarla M, Kolb TM, Mitzner W, Hassoun PM, Damico R. Macrophage Migration Inhibitory Factor (MIF) is a Novel Determinant of Cigarette Smoke-induced Lung Damage. Am J Respir Cell Mol Biol 2014; 51: 94–103.

11. Kratzer A, Salys J, Nold-Petry C, Cool C, Zamora M, Bowler R, Koczulla AR, Janciauskiene S, Edwards MG, Dinarello CA, Taraseviciene-Stewart L. Role of IL-18 in second-hand smoke-induced emphysema. Am J Respir Cell Mol Biol 2013; 48: 725–732.

12. Timens, W., Coers, W., Van Straaten, J.F.M., Postma DS. Extracellular matrix and inflammation: a role forfibroblast-mediated defective tissue repair in the pathogenesis of emphysema? Eur Respir Rev 1997; 7: 119–123.

13. Preobrazhenska O, Wright JL, Churg A. Regional heterogeneity in murine lung fibroblasts from normal mice or mice exposed once to cigarette smoke. PLoS One 2012; 7: e39761.

14. Saetta M, Shiner RJ, Angus GE, Kim WD, Wang NS, King M, Ghezzo H, Cosio MG. Destructive index: a measurement of lung parenchymal destruction in smokers. Am Rev Respir Dis 1985; 131: 764–769.

15. Koike K, Ishigami A, Sato Y, Hirai T, Yuan Y, Kobayashi E, Tobino K, Sato T, Sekiya M, Takahashi K, Fukuchi Y, Maruyama N, Seyama K. Vitamin C Prevents Cigarette Smoke-Induced Pulmonary Emphysema in Mice and Provides Pulmonary Restoration. Am J Respir Cell Mol Biol 2013; 50: 347–357.

16. Takahashi A, Majumdar A, Parameswaran H, Bartolak-Suki E, Suki B. Proteoglycans Maintain Lung Stability in an Elastase-Treated Mouse Model of Emphysema. Am J Respir Cell Mol Biol 2014; 51: 26–33.

17. Brandsma CA, Timens W, Jonker MR, Rutgers B, Noordhoek JA, Postma DS. Differential effects of fluticasone on extracellular matrix production by airway and parenchymal fibroblasts in severe COPD. Am J Physiol Lung Cell Mol Physiol 2013; 305: L582-9.

18. Li JP, Vlodavsky I. Heparin, heparan sulfate and heparanase in inflammatory reactions. Thromb Haemost 2009; 102: 823–828.

19. Presta M, Andres G, Leali D, Dell'Era P, Ronca R. Inflammatory cells and chemokines sustain FGF2-induced angiogenesis. Eur Cytokine Netw 2009; 20: 39–50.

20. Update: future directions for research on diseases of the lung. The American Thoracic Society. Am J Respir Crit Care Med 1998; 158: 320–334.

21. Tocchi A, Parks WC. Functional interactions between matrix metalloproteinases and glycosaminoglycans. FEBS J. 2013. p. 2332–2341.

22. Haeger SM, Yang Y, Schmidt EP. Heparan sulfate in the developing, healthy, and injured lung. Am. J. Respir. Cell Mol. Biol. 2016. p. 5–11.

23. Sarrazin S, Lamanna WC, Esko JD. Heparan sulfate proteoglycans. Cold Spring Harb. Perspect. Biol. 2011; 3: 1–33.

24. Lu J, Auduong L, White ES, Yue X. Up-regulation of heparan sulfate 6-O-sulfation in idiopathic pulmonary fibrosis. Am. J. Respir. Cell Mol. Biol. 2014; 50: 106–114.

25. Li Q, Park PW, Wilson CL, Parks WC. Matrilysin shedding of syndecan-1 regulates chemokine mobilization and transepithelial efflux of neutrophils in acute lung injury. Cell 2002; 111: 635–646.

26. Li ZY, Hirayoshi K, Suzuki Y. Expression of N-deacetylase/sulfotransferase and 3-O-sulfotransferase in rat alveolar type II cells. Am J Physiol Lung Cell Mol Physiol 2000; 279: L292-301.

27. Kai Y, Tomoda K, Yoneyama H, Yoshikawa M, Kimura H. RNA interference targeting carbohydrate sulfotransferase 3 diminishes macrophage accumulation, inhibits MMP-9 expression and promotes lung recovery in murine pulmonary emphysema. Respir. Res. 2015; 16: 146.

28. Zcharia E, Metzger S, Chajek-Shaul T, Aingorn H, Elkin M, Friedmann Y, Weinstein T, Li J-P, Lindahl U, Vlodavsky I. Transgenic expression of mammalian heparanase uncovers physiological functions of heparan sulfate in tissue morphogenesis, vascularization, and feeding behavior. FASEB J. 2004; 18: 252–263.

29. van den Heuvel LP, van den Born J, van de Velden TJ, Veerkamp JH, Monnens LA, Schroder CH, Berden JH. Isolation and partial characterization of heparan sulphate proteoglycan from the human glomerular basement membrane. Biochem J 1989; 264: 457–465.

30. van den Born J, van den Heuvel LP, Bakker MA, Veerkamp JH, Assmann KJ, Berden JH. Monoclonal antibodies against the protein core and glycosaminoglycan side chain of glomerular basement membrane heparan sulfate proteoglycan: characterization and immunohistological application in human tissues. J Histochem Cytochem 1994; 42: 89–102.

31. van den Born J, van den Heuvel LP, Bakker MA, Veerkamp JH, Assmann KJ, Berden JH. A monoclonal antibody against GBM heparan sulfate induces an acute selective proteinuria in rats. Kidney Int 1992; 41: 115–123.

32. van den Born J, Salmivirta K, Henttinen T, Östman N, Ishimaru T, Miyaura S, Yoshida K, Salmivirta M. Novel Heparan Sulfate Structures Revealed by Monoclonal Antibodies. J. Biol. Chem. 2005; 280: 20516–20523.

33. Dunnill MS. Quantitative Methods in the Study of Pulmonary Pathology. 1962; 17: 320–328.

34. Weibel ER. Principles and methods for the morphometric study of the lung and other organs. Lab Invest 1963; 12: 131–155.

35. van Kuppevelt TH, Robbesom AA, Versteeg EM, Veerkamp JE, van Herwaarden CL, Dekhuijzen PN. Restoration by vacuum inflation of original alveolar dimensions in small human lung specimens. Eur Respir J 2000; 15: 771–7.

36. Schroeder A, Mueller O, Stocker S, Salowsky R, Leiber M, Gassmann M, Lightfoot S, Menzel W, Granzow M, Ragg T. The RIN: an RNA integrity number for assigning integrity values to RNA measurements. BMC Mol. Biol. 2006; 7: 3.

37. Livak KJ, Schmittgen TD. Analysis of Relative Gene Expression Data Using Real-Time Quantitative PCR and the 2−ΔΔCT Method. Methods 2001; 25: 402–408.

38. Robbesom AA, Versteeg EM, Veerkamp JH, Van Krieken JH, Bulten HJ, Smits HT, Willems LN, Van Herwaarden CL, Dekhuijzen PN, Van Kuppevelt TH. Morphological quantification of emphysema in small human lung specimens: comparison of methods and relation with clinical data. Mod Pathol 2003; 16: 1–7.

39. Aoshiba K, Koinuma M, Yokohori N, Nagai A. Differences in the distribution of CD4+ and CD8+ T cells in emphysematous lungs. Respiration 2004; 71: 184–190.

40. Majo J, Ghezzo H, Cosio MG. Lymphocyte population and apoptosis in the lungs of smokers and their relation to emphysema. Eur Respir J 2001; 17: 946–53.

41. Lander AD. Proteoglycans: Master regulators of molecular encounter? Matrix Biol. 1998. p. 465–472.

42. Snider GL. Emphysema: the first two centuries--and beyond. A historical overview, with suggestions for future research: Part 2. Am Rev Respir Dis 1992; 146: 1615–1622.

43. Tibell LA, Sethson I, Buevich A V. Characterization of the heparin-binding domain of human extracellular superoxide dismutase. Biochim Biophys Acta 1997; 1340: 21–32.

44. Tanaka K, Tanaka Y, Miyazaki Y, Namba T, Sato K, Aoshiba K, Azuma A, Mizushima T. Therapeutic effect of lecithinized superoxide dismutase on pulmonary emphysema. J Pharmacol Exp Ther 2011; 338: 810–818.

45. Manni ML, Oury TD. Significance of polymorphisms in the superoxide dismutase-3 gene in COPD: It's all about location! COPD 2010; 7: 237–239.

46. Yao H, Arunachalam G, Hwang JW, Chung S, Sundar IK, Kinnula VL, Crapo JD, Rahman I. Extracellular superoxide dismutase protects against pulmonary emphysema by attenuating oxidative fragmentation of ECM. Proc Natl Acad Sci U S A 2010; 107: 15571–15576.

47. Aoshiba K, Nagai A, Konno K. Nicotine prevents a reduction in neutrophil filterability induced by cigarette smoke exposure. Am J Respir Crit Care Med 1994; 150: 1101–1107.

48. Adachi T, Fukushima T, Usami Y, Hirano K. Binding of human xanthine oxidase to sulphated glycosaminoglycans on the endothelial-cell surface. Biochem J 1993; 289 (Pt 2: 523–527.

49. Repine JE, Bast A, Lankhorst I. Oxidative stress in chronic obstructive pulmonary disease. Oxidative Stress Study Group. Am J Respir Crit Care Med 1997; 156: 341–57.

50. Finkelstein R, Fraser RS, Ghezzo H, Cosio MG. Alveolar inflammation and its relation to emphysema in smokers. Am J Respir Crit Care Med 1995; 152: 1666–72.

51. Bracke KR, Verhamme FM, Seys LJ, Bantsimba-Malanda C, Cunoosamy DM, Herbst R, Hammad H, Lambrecht BN, Joos GF, Brusselle GG. Role of CXCL13 in cigarette smoke-induced lymphoid follicle formation and chronic obstructive pulmonary disease. Am J Respir Crit Care Med 2013; 188: 343–355.

52. van Kuppevelt TH, van de Lest CH, Versteeg EM, Dekhuijzen PN, Veerkamp JH. Induction of emphysematous lesions in rat lung by beta-D-xyloside, an inhibitor of proteoglycan synthesis. Am J Respir Cell Mol Biol 1997; 16: 75–84.

53. van de Lest CH, Versteeg EM, Veerkamp JH, van Kuppevelt TH. Digestion of proteoglycans in porcine pancreatic elastase-induced emphysema in rats. Eur Respir J 1995; 8: 238–45.

54. Rao N V, Kennedy TP, Rao G, Ky N, Hoidal JR. Sulfated polysaccharides prevent human leukocyte elastase-induced acute lung injury and emphysema in hamsters. Am Rev Respir Dis 1990; 142: 407–412.

55. Karlinsky J, Fredette J, Davidovits G, Catanese A, Snider R, Faris B, Snider GL, Franzblau C. The balance of lung connective tissue elements in elastase-induced emphysema. J Lab Clin Med 1983; 102: 151–162.

56. Raats CJ, Bakker MA, van den Born J, Berden JH. Hydroxyl radicals depolymerize glomerular heparan sulfate in vitro and in experimental nephrotic syndrome. J Biol Chem 1997; 272: 26734–26741.

57. Kramer A, van den Hoven M, Rops A, Wijnhoven T, van den Heuvel L, Lensen J, van Kuppevelt T, van Goor H, van der Vlag J, Navis G, Berden JH. Induction of Glomerular Heparanase Expression in Rats with Adriamycin Nephropathy Is Regulated by Reactive Oxygen Species and the Renin-Angiotensin System. J Am Soc Nephrol 2006; 17: 2513–2520.

58. Latha MS, Vijayammal PL, Kurup PA. Changes in the glycosaminoglycans and glycoproteins in the tissues in rats exposed to cigarette smoke. Atherosclerosis 1991; 86: 49–54.

59. Konno K, Arai H, Motomiya M, Nagai H, Ito M, Sato H, Satoh K. A biochemical study on glycosaminoglycans (mucopolysaccharides) in emphysematous and in aged lungs. Am Rev Respir Dis 1982; 126: 797–801.

60. Lafuma C, Moczar M, Lange F, Robert L. Biosynthesis of hyaluronic acid, heparan sulfate and structural glycoproteins in hamster lung explants during elastase induced emphysema. Connect Tissue Res 1985; 13: 169–179.

61. van Straaten JF, Coers W, Noordhoek JA, Huitema S, Flipsen JT, Kauffman HF, Timens W, Postma DS. Proteoglycan changes in the extracellular matrix of lung tissue from patients with pulmonary emphysema. Mod Pathol 1999; 12: 697–705.

62. Kazemi A, Ramezanzadeh F, Esfahani MH, Saboor-Yaraghi AA, Nejat S, Rahimi-Foroshani A. Impact of environmental tobacco smoke exposure in women on oxidative stress in the antral follicle and assisted reproduction outcomes. J Res Med Sci 2013; 18: 688–694.

63. Yageta Y, Ishii Y, Morishima Y, Ano S, Ohtsuka S, Matsuyama M, Takeuchi K, Itoh K, Yamamoto M, Hizawa N. Carbocisteine reduces virus-induced pulmonary inflammation in mice exposed to cigarette smoke. Am J Respir Cell Mol Biol 2013; 50: 963–973.

64. Panasyuk A, Frati E, Ribault D, Mitrovic D. Effect of reactive oxygen species on the biosynthesis and structure of newly synthesized proteoglycans. Free Radic Biol Med 1994; 16: 157–167.

65. Klebanoff SJ, Kinsella MG, Wight TN. Degradation of endothelial cell matrix heparan sulfate proteoglycan by elastase and the myeloperoxidase-H2O2-chloride system. Am J Pathol 1993; 143: 907–917.

66. Moseley R, Waddington R, Evans P, Halliwell B, Embery G. The chemical modification of glycosaminoglycan structure by oxygen-derived species in vitro. Biochim Biophys Acta 1995; 1244: 245–252.

67. Liu Z, Perlin AS. Evidence of a selective free radical degradation of heparin, mediated by cupric ion. Carbohydr Res 1994; 255: 183–191.

68. Metcalfe DD, Thompson HL, Klebanoff SJ, Henderson Jr. WR. Oxidative degradation of rat mast-cell heparin proteoglycan. Biochem J 1990; 272: 51–57.

69. Volpi N, Mascellani G, Bianchini P. Low molecular weight heparins (5 kDa) and oligoheparins (2 kDa) produced by gel permeation enrichment or radical process: comparison of structures and physicochemical and biological properties. Anal Biochem 1992; 200: 100–107.

70. Kashihara N, Watanabe Y, Makino H, Wallner EI, Kanwar YS. Selective decreased de novo synthesis of glomerular proteoglycans under the influence of reactive oxygen species. Proc Natl Acad Sci U S A 1992; 89: 6309–6313.

71. Nagasawa K, Uchiyama H, Sato N, Hatano A. Chemical change involved in the oxidative-reductive depolymerization of heparin. Carbohydr Res 1992; 236: 165–180.

72. O'Shaughnessy TC, Ansari TW, Barnes NC, Jeffery PK. Inflammation in bronchial biopsies of subjects with chronic bronchitis: inverse relationship of CD8+ T lymphocytes with FEV1. Am J Respir Crit Care Med 1997; 155: 852–857.

73. Saetta M, Di Stefano A, Turato G, Facchini FM, Corbino L, Mapp CE, Maestrelli P, Ciaccia A, Fabbri LM. CD8+ T-lymphocytes in peripheral airways of smokers with chronic obstructive pulmonary disease. Am J Respir Crit Care Med 1998; 157: 822–826.

74. Hoonhorst SJ, Ten Hacken NH, Vonk JM, Timens W, Hiemstra PS, Lapperre TS, Sterk PJ, Postma DS. Steroid Resistance in COPD? Overlap and Differential Anti-Inflammatory Effects in Smokers and Ex-Smokers. PLoS One 2014; 9: e87443.

75. Petrovich E, Feigelson SW, Stoler-Barak L, Hatzav M, Solomon A, Bar-Shai A, Ilan N, Li JP, Engelhardt B, Vlodavsky I, Alon R. Lung ICAM-1 and ICAM-2 support spontaneous intravascular effector lymphocyte entrapment but are not required for neutrophil entrapment or emigration inside endotoxin-inflamed lungs. FASEB J. 2016; 30: 1767–1778.

76. Wang L, Fuster M, Sriramarao P, Esko JD. Endothelial heparan sulfate deficiency impairs L-selectin- and chemokine-mediated neutrophil trafficking during inflammatory responses. Nat Immunol 2005; 6: 902–910.

77. Oudijk EJ, Lammers JW, Koenderman L. Systemic inflammation in chronic obstructive pulmonary disease. Eur Respir J Suppl 2003; 46: 5s–13s.

78. Nadanaka S, Kitagawa H. EXTL2 controls liver regeneration and aortic calcification through xylose kinase-dependent regulation of glycosaminoglycan biosynthesis. Matrix Biol 2013th ed. 2014; 35: 18–24.

79. Simizu S, Ishida K, Osada H. Heparanase as a molecular target of cancer chemotherapy. Cancer Sci 2004; 95: 553–558.

80. Rivara S, Milazzo FM, Giannini G. Heparanase: a rainbow pharmacological target associated to multiple pathologies including rare diseases. Future Med. Chem. 2016; 8: 647–680.

Chapter 7

Summary, General discussion and future perspectives / Samenvatting, algemene discussie en toekomstvisie

Summary

Based on the observation that skin heals without a scar during embryonic development, we investigated the possibilities of using principles found in embryonic development to design novel constructs. Such constructs may induce embryonic-like processes, potentially, and result in scarless healing when used for the treatment of full-thickness skin wounds. Current treatments often result in scar tissue, which shows reduced functionality and elasticity in comparison to undamaged skin. The aim of the research was to elucidate effector molecules involved in skin development and to incorporate these effector molecules into a type I collagen-heparin scaffold. In addition, novel techniques and methods were developed to analyse/construct these scaffolds.

In preparation of this investigation a literature study (Chapter 1) was performed, in which the current status of various aspects involved in embryonic skin development and scarless healing was indicated. We focused on the upper two layers of skin, i.e. the epidermis and dermis, and appendages such as hair follicles. Since the construct will be used to treat skin wounds, adult wound healing was studied, which is characterized by four stages, i.e. haemostasis, inflammation, proliferation and remodeling, and compared to wound healing as found during embryonic development. This comparison revealed several points to take in account during the design of the embryonic-like scaffold. In addition, the current status of skin tissue engineering is discussed. The last part of the literature study as described in Chapter 1 reports on glycosaminoglycan (GAG) synthesis and degradation, since these extracullular matrix (ECM) components are used in the construct and are a central part of Chapter 5 and Chapter 6.

Based on the findings on skin development two time points in embryonic development, i.e. 14 days post conception (E14) and E16, and one postnatal time point, i.e. one day post birth (P1), were selected to compare gene expression with adult skin (P90) using EXON arrays. This comparison, as described in Chapter 2, resulted in a list of 20 growth factors, of which two were selected, i.e. insulin-like growth factor 2 (*Igf2*) and sonic hedgehog (*Shh*), which were successfully incorporated into a type I collagen-heparin scaffold. In addition, we created type I collagen scaffolds containing hyaluronic acid, since hyaluronic acid is found in embryonic skin and is suggested to be important during embryonic wound healing.

In Chapter 3 we present a method which allows the discrimination of newly formed collagen and implanted collagen, using a single-chain antibody GD3A12. This antibody recognizes dermatan sulfate (DS) which is strongly associated with newly synthesized collagen. This method offers a solution for the detection of newly formed collagen after construct implantation.

During embryonic development gradients of effector molecules are important. It is therefore of interest to create a type I collagen scaffold containing a gradient of effector molecules. In Chapter 4 results are presented of the development of a scaffold containing a gradient of heparin, a GAG. Subsequent incubation with fibroblast growth factor 2 resulted in a gradient of this effector molecule.

Given the importance of GAGs in the binding and gradient formation of effector molecules, we investigated the role or GAGs during skin development by studying gene expression using the EXON array data and a customly designed taqman low density array (TLDA cart) containing a large number of genes involved in GAG biology. In addition we analysed the gene expression in two mouse models, i.e. a glucuronic acid epimerase knockout mouse and a heparanase overexpression mouse. The results, as presented in Chapter 5, showed that a dynamic gene expression pattern during skin development.

The last chapter, Chapter 6, does not focus on skin, but on the lung. This chapter indicates the importance of degradation of GAGs in relation to tissue destruction. The general finding was that increase of heparanase and loss of heparan sulfate is associated with the development of lung emphysema. Gene expression data showed a number of genes differentially expressed, e.g. 3-O and 6-O sulfotransferase and an enzyme involved in GAG chain degradation.

Overall we have set the first steps in the construction of embryonic scaffolds for tissue engineering, focusing on glycosaminoglycans, effector molecules and collagen. In addition we have developed/extended methodologies for analysis and evaluation.

General discussion and future perspectives

The results presented in this thesis show that we have successfully elucidated 20 embryonic specific effector molecules involved in embryonic skin development and incorporated two, i.e. *Igf2* and *Shh* into a type I collagen-heparin construct. Although not part of this thesis, we evaluated the construct *in vivo* in a mouse wound model using 8 mm biopsy punches and results were analyzed after 7, 21 and 90 days. The results of these experiments, however, showed numerous problems with the experimental setup and various technical difficulties were encountered. We therefore decided not to include these results in this thesis.

The main problem we encountered was contraction of the wound. Murine wound healing shows more and faster contraction [1,2], which influenced the effect of the scaffold. In future research a model system must be chosen that shows wound contraction comparable to human wound healing. Alternatively the wound size could be enlarged, to prevent contraction. A porcine skin model is probably more suitable, since pig skin is more comparable to human skin than mouse skin [3,4].

In addition we tested only two effector molecules of a list of 20, i.e. insulin-like growth factor 2 (*Igf2*) and sonic hedgehog (*Shh*). It is my opinion that all discovered effector molecules should be tested on inducing embryonic-like signaling in adult epidermal and dermal cells. Initially these tests could be completed *in vitro* using keratinocytes and fibroblasts. In this more controlled environment the effect of these growth factors can be studied in more detail and the optimal concentration for activation of the signaling pathways could be determined. The most suitable candidates should subsequently be tested *in vivo* in a mouse or porcine wound model or implanted subcutaneously [2]. The effect of the scaffold should be tested using standard histology and immunohistochemistry to analyse the new tissue formation and possibly the formation of new appendages. Furthermore gene expression should be assessed to determine if the incorporated effector molecules indeed activated embryonic-like processes.

The presented research focused on a type I collagen-heparin construct. In literature on scarless healing, however, other components are presented which may be of interest for an alternative scaffold that represents the embryonic ECM more in comparison to the used scaffold [5,6]. Therefore the created type I collagen-hyaluronic acid scaffold could be of interest, since it may mimic the embryonic environment and, in combination with the embryonic effector molecules, result in embryonic-like processes. An expected problem, however, is the lack of sulfation in hyaluronic acid, which may hamper the binding of effector molecules [7]. Making a combination of hyaluronic acid and heparin could circumvent this problem.

Addition of type III collagen to the scaffold may make the scaffold more embryonic-like as well. Type I collagen is the most predominant collagen in both embryonic as adult skin, but is supplemented by type III collagen [8]. In embryonic skin, type III collagen is present at a higher percentage when compared to adult skin. The isolation of type III collagen, however, is hampered by the fact that collagen type I is the main collagen in the ECM. Recombinant produced type III collagen may offer an alternative [9], although

this option may be hampered by the lack of post-translational modifications in yeast [10].

We have shown to be able to create a gradient of effector molecules. But as described in Chapter 3, the dimension of the gradient is too large with respect to the gradients found in nature [11,12]. Alternative strategies, such as a microfluidic system as suggested in Chapter 3 or 3D printing [13], should be explored as gradients are essential for embryonic development [14,15].

The second part of this thesis predominantly deals with glycosaminoglycans (GAGs). We studied GAG biology using gene expression analysis. We started using the rationale that gene expression provides information about modification of the GAG sugar chains [7,16]. Expression data, however, suggested a more complex story. One of the possible reasons could be that expression of GAG related genes may be regulated by IRES sites [17–19], an alternative transcription method, which allows transcription during cell division. Transcription normally takes place during the G1/S-phase of cell division [19]. Another reason could be differences in enzyme activity, as was found for the different Ndst isoforms [20]. The bottom line is, that the process from DNA to functional GAGs is complex and regulated at multiple levels. Identification of specific GAG domains involved in the binding of effector molecules could be quite rewarding. Current technologies to sequence and synthesize GAGs, however, are cumbersome. Further research is therefore needed, to develop and enhance GAG analysis techniques and subsequently use them to study the role of GAGs during embryonic development, and their use in embryonic scaffolds for regenerative medicine.

Samenvatting

Gebaseerd op de observatie dat huid zonder litteken geneest tijdens de embryonale ontwikkeling, hebben we de mogelijkheid onderzocht om principes te gebruiken, zoals gevonden tijdens de embryonale ontwikkeling, voor het ontwerp van nieuwe constructen. Dergelijke constructen zouden mogelijk embryonaal-achtige processen kunnen induceren en resulteren in herstel zonder litteken als deze worden gebruikt voor de behandeling van wonden waarbij zowel de epidermis als dermis beschadigd zijn. Huidige behandelingen leiden vaak tot littekenweefsel, dat minder functionaliteit en elasticiteit laat zien als je dit vergelijkt met onbeschadigde huid. Het doel van dit onderzoek was het ophelderen van effector-moleculen betrokken bij de huid ontwikkeling en het incorporeren van deze moleculen in een type I collageen-heparine-matrix. Daarnaast zijn er nieuwe technieken en methoden ontwikkeld om deze constructen te construeren en te analyseren.

Als voorbereiding op dit onderzoek is er een literatuurstudie gedaan (Hoofdstuk 1), waarin de huidige status van verschillende aspecten betrokken bij embryonale huid ontwikkeling en genezing zonder litteken zijn aangegeven. Bij dit onderzoek is er met name gekeken naar de twee bovenste lagen van de huid, dat wil zeggen de epidermis en de dermis, en appendages zoals haarfollikels. Aangezien de constructen gebruikt zullen worden om huidwonden te behandelen, is er daarnaast gekeken naar volwassen wondgenezing, welke zich kenmerkt door vier stadia, namelijk heamostase, ontsteking, proliferatie en remodellering. De volwassen wondgenezing is vergeleken met wondgenezing zoals gevonden tijdens embryonale ontwikkeling, waarbij diverse aspecten zijn gevonden waarop gelet moet worden bij het ontwerp van de embryonaal-achtige constructen. Verder is er gekeken naar de huidige stand van zaken van huid tissue-engineering. Hoofdstuk 1 wordt afgesloten met een overzicht van de synthese en afbraak van glycosaminoglycanen (GAG), aangezien deze componenten van de extracellulaire matrix (ECM) verwerkt worden in het construct en centraal staan in Hoofdstuk 5 en Hoofdstuk 6.

Gebaseerd op de gegevens over de huid ontwikkeling zijn er twee tijdstippen tijdens de embryonale ontwikkeling, namelijk viertien dagen na conceptie (E14) en E16, en één postnataal tijdstip, namelijk één dag na geboorte (P1), geselecteerd om genexpressie te vergelijken met volwassen huid (P90), waarbij gebruik is gemaakt van EXON arrays. Deze vergelijking, zoals beschreven in Hoofdstuk 2, heeft geresulteerd in een lijst van twintig groeifactoren. Twee groeifactoren uit deze lijst zijn geselecteerd, namelijk insulin-like growth factor 2 (*Igf2*) en sonic hedgehog (*Shh*), en deze zijn succesvol geïncorporeerd in een type 1 collageen-heparine-matrix. Daarnaast hebben we type 1 collageen-matrices gemaakt waarin hyaluron zuur is verwerkt, aangezien hyaluron zuur aanwezig is in de embryonale huid en mogelijk een rol speelt tijdens embryonale wond genezing.

In Hoofdstuk 3 wordt een methode gepresenteerd die het toelaat om nieuw gevormd collageen en geïmplanteerd collageen te onderscheiden, waarbij gebruik gemaakt wordt van het single-chain antilichaam GD3A12. Een single-chain antilichaam is een heterodimeer van het variabele gedeelte van de lichte keten en het variabele gedeelte van de zware keten van een immunoglobuline molecuul. Het antilichaam herkent dermatan sulfaat (DS), die sterk verbonden is met nieuw gevormd collageen. Deze methode biedt een oplossing voor de detectie van nieuw gevormd collageen na implantatie van een type 1 collageen-construct.

Tijdens de embryonale ontwikkeling spelen gradiënten van effector moleculen een belangrijke rol. Het is daarom interessant om type 1 collageen-constructen te creëren die een gradiënt van effector moleculen bevatten. In Hoofdstuk 4 worden resultaten gepresenteerd van de ontwikkeling van een type 1 collageen-matrix met een gradiënt van heparine, een GAG. Incubatie met fibroblast growth factor 2 resulteerde in een gradiënt van dit effector molecuul.

Aangezien GAGs belangrijk zijn voor de binding en de gradiënt formatie van effector moleculen, hebben we onderzocht wat de rol van GAGs is tijdens huidontwikkeling door te kijken naar genexpressie gebruikmakend van EXON array-data en een handmatig ontworpen taqman low density array (TLDA kaart), met daarop een groot aantal genen betrokken bij GAG biologie. Daarnaast is de genexpressie geanalyseerd van twee muismodellen, namelijk een glucuron zuur epimerase knockout muis en een heparanse overexpressie muis. De resultaten, zoals gepresenteerd in Hoofdstuk 5, laten een dynamisch genexpressie patroon zien tijdens de embryonale huidontwikkeling.

Het laatste hoofdstuk, Hoofdstuk 6, richt zich niet op de huid, maar op de long. Dit hoofdstuk geeft het belang aan van GAG degradatie in relatie tot weefsel destructie. De algemene bevinding was dat de toenamen van heparanase en het verlies van heparan sulfaat verbonden is met de ontwikkeling van longemfyseem. Genexpressie data laten zien dat een aantal genen verschillend tot expressie komt, waaronder 3-O en 6-O sulfotransferases en een enzym betrokken bij GAG degradatie.

Samenvattend hebben we de eerste stappen gezet voor de constructie van embryonaal-achtige constructen voor tissue-engineering, waarbij gefocust is op glycosaminoglycanen, effector moleculen en collageen. Daarnaast hebben we methodologieën ontwikkeld voor het analyseren en evalueren van deze constructen.

Algemene discussie en Toekomstvisie

De resultaten zoals gepresenteerd in dit proefschrift laten zien dat we met succes 20 embryonaal-specifieke effector moleculen hebben opgehelderd betrokken bij de embryonale huid ontwikkeling, waarvan twee, namelijk Igf2 en Shh, geïncorporeerd zijn in een type 1 collageen-heparine-construct. Alhoewel het geen onderdeel is van dit proefschrift, hebben we het construct geëvalueerd *in vivo* in een muis wondmodel, waarbij gebruik gemaakt is van 8 mm huidstansen en de resultaten zijn geanalyseerd na 7, 21 en 90 dagen. De resultaten van de experimenten echter toonde verschillende problemen met de gekozen experimentele aanpak en er zijn verschillende technische problemen naar voren gekomen. Er is daarom gekozen deze resultaten niet op te nemen in dit proefschrift.

Het belangrijkste probleem dat naar voren kwam was de contractie van de wond. Wondgenezing bij de muis laat meer en snellere contractie zien [1,2], die het effect van het construct beïnvloedt. In toekomstig onderzoek moet een modelsysteem gekozen worden die wondcontractie heeft vergelijkbaar met wondgenezing bij de mens. Het is ook mogelijk de wondgrootte te vergroten om contractie te voorkomen. Een varkenshuidmodel is waarschijnlijk het meest geschikt, aangezien varkenshuid meer vergelijkbaar is met mensenhuid dan muizenhuid [3,4].

Verder zijn enkel twee van de lijst van twintig effector moleculen getest, namelijk insulin-like growth factor 2 (Igf2) en sonic hedgehog (Shh). Het is mijn mening dat alle ontdekte effector moleculen getest zouden moeten worden op het induceren van embryonaal-achtige signalering in adulte epidermale en dermale cellen. Initieel zouden deze test *in vitro* gedaan kunnen worden waarbij gebruik gemaakt wordt van keratinocyten en fibroblasten. In deze meer gecontroleerde omgeving is het effect van deze groeifactoren meer in detail te bestuderen en kan de optimale concentratie voor het activeren van signaleringcascades bepaald worden. De meest geschikte kandidaten zouden vervolgens getest kunnen worden *in vivo* in een muis- of varkenswondmodel of subcutaan geïmplanteerd kunnen worden [2]. Het effect van het construct zou vervolgens getest kunnen worden met behulp van standaard histologie en immunohistochemie, om te analyseren of er nieuw weefsel en mogelijk nieuwe appendages zijn gevormd. Daarnaast zou genexpressie gemeten moeten worden om te bepalen of de geïncorporeerde effector moleculen daadwerkelijk embryonaal-achtige processen heeft geactiveerd.

Het gepresenteerde onderzoek richtte zich op de ontwikkeling van een type 1 collageen-heparine-construct. In de literatuur over wondgenezing zonder litteken staan echter andere componenten die mogelijk interessant zijn voor een alternatief construct ontwerp dat beter de embryonale ECM representeert in vergelijking met het gebruikte construct [5,6]. Daarom is het ontwikkelde type 1 collageen-hyaluron zuur construct interessant, aangezien deze mogelijk de embryonale omgeving beter nabootst en kan resulteren in embryonaal-achtige processen in combinatie met de embryonale effector moleculen. Een verwacht probleem is echter het gebrek aan sulfetering van hyaluron zuur, wat de binding van effector moleculen kan bemoeilijken [7]. Het maken van een combinatie van hyaluron zuur en heparine zou dit probleem kunnen oplossen.

Het toevoegen van type 3 collageen aan de scaffold zou de scaffold ook meer embryonaal-achtig kunnen maken. Type 1 collageen is de meest voorkomende collageen in zowel de embryonale als de adulte huid, maar bevat ook type 3 collageen [8]. In embryonale huid is het percentage aanwezige type 3 collageen hoger in vergelijking met adulte huid. The isolatie van collageen type 3 wordt echter belemmerd doordat type I collageen het belangrijkste type collageen is in de ECM. Recombinant geproduceerde type III collageen zou een alternatief kunnen bieden [9], maar deze optie is beperkt door het gebrek aan post-translationele modificaties in gist [10].

We hebben getoond dat het voor ons mogelijk is om een gradiënt van effector moleculen te creëren. Maar, zoals beschreven in Hoofdstuk 3, de afmetingen van de gradiënt zijn te groot in vergelijking met de gradiënten zoals gevonden in de natuur [11,12]. Een alternatieve strategie, zoals het in Hoofdstuk 3 gesuggereerde microfluidic systeem of 3D printen [13], zou onderzocht moeten worden aangezien gradiënten essentieel zijn voor embryonale ontwikkeling [14,15].

Het tweede deel van dit proefschrift gaat voornamelijk over glycosaminoglycanen (GAGs). We hebben de GAG biologie bestudeerd met genexpressie analyse. We zijn gestart met het gebruiken van de redenering dat genexpressie informatie doorgeeft over de modificatie van de GAG suiker keten [7,16]. Expressie data suggereren echter een meer complex verhaal. Een mogelijke reden zou kunnen zijn dat expressie van GAG gerelateerde genen gereguleerd is met IRIS sites [17–19], een alternatieve transcriptie methode, die toelaat dat transcriptie plaats vindt tijdens de celdeling. Transcriptie vindt normaal gesproken alleen tijdens de G1/S-fase van de celdeling plaats [19]. Een andere reden zou verschillen in enzym activiteit kunnen zijn, zoals gevonden voor de verschillende Ndst isoformen [20]. Het komt erop neer dat het proces van DNA tot functionele GAGs complex is en gereguleerd is op meerdere niveaus. Identificatie van specifieke GAG domeinen betrokken bij het binden van effector moleculen zou zeer belonend kunnen zijn. Huidige technieken om de sequentie van GAGs te bepalen of om GAGs te synthetiseren zijn echter omslachtig. Verder onderzoek is daarom nodig om GAG analyse technieken te ontwikkelen en te verbeteren om deze vervolgens te gebruiken om de rol van GAGs tijdens de embryonale ontwikkeling en de toepassing van GAGs in embryonale constructen voor de regeneratieve geneeskunde te bestuderen.

References

[1] M.G. Jeschke, A.-R. Sadri, C. Belo, S. Amini-Nik, A Surgical Device to Study the Efficacy of Bioengineered Skin Substitutes in Mice Wound Healing Models, Tissue Eng. Part C Methods. 23 (2017) 237–242.

[2] L. Chen, R. Mirza, Y. Kwon, L.A. DiPietro, T.J. Koh, The murine excisional wound model: Contraction revisited, Wound Repair Regen. 23 (2015) 874–877.

[3] B. Godin, E. Touitou, Transdermal skin delivery: Predictions for humans from *in vivo*, ex vivo and animal models, Adv. Drug Deliv. Rev. 59 (2007) 1152–1161.

[4] A. Summerfield, F. Meurens, M.E. Ricklin, The immunology of the porcine skin and its value as a model for human skin, Mol. Immunol. 66 (2015) 14–21.

[5] M.T. Longaker, E.S. Chiu, M.R. Harrison, T.M. Crombleholme, J.C. Langer, B.W. Duncan, N.S. Adzick, E.D. Verrier, R. Stern, Studies in fetal wound healing. IV. Hyaluronic acid-stimulating activity distinguishes fetal wound fluid from adult wound fluid., Ann. Surg. 210 (1989) 667–672.

[6] P. Martin, Wound healing--aiming for perfect skin regeneration, Science (80-.). 276 (1997) 75–81.

[7] S. Sarrazin, W.C. Lamanna, J.D. Esko, Heparan sulfate proteoglycans, Cold Spring Harb. Perspect. Biol. 3 (2011) 1–33.

[8] K.M. Bullard, M.T. Longaker, H.P. Lorenz, Fetal wound healing: Current biology, World J. Surg. 27 (2003) 54–61.

[9] J. Myllyharju, M. Nokelainen, A. Vuorela, K.I. Kivirikko, Expression of recombinant human type I–III collagens in the yeast Pichia pastoris, Biochem. Soc. Trans. 28 (2000) 353.

[10] N.J. Bulleid, D.C. John, K.E. Kadler, Recombinant expression systems for the production of collagen., Biochem. Soc. Trans. 28 (2000) 350–353.

[11] H.L. Ashe, J. Briscoe, The interpretation of morphogen gradients, Development. 133 (2006) 385–394.

[12] P. Müller, K.W. Rogers, S.R. Yu, M. Brand, A.F. Schier, Morphogen transport., Development. 140 (2013) 1621–38.

[13] H.N. Chia, B.M. Wu, Recent advances in 3D printing of biomaterials, J. Biol. Eng. 9 (2015) 4.

[14] D. Yan, X. Lin, Shaping morphogen gradients by proteoglycans., Cold Spring Harb. Perspect. Biol. 1 (2009) 1–17.

[15] K.W. Rogers, A.F. Schier, Morphogen Gradients: From Generation to Interpretation, Annu. Rev. Cell Dev. Biol. 27 (2011) 377–407.

[16] J.D. Esko, S.B. Selleck, Order out of chaos: assembly of ligand binding sites in heparan sulfate, Annu. Rev. Biochem. 71 (2002) 435–471.

[17] K. Grobe, J.D. Esko, Regulated translation of heparan sulfate N-acetylglucosamine N-deacetylase/N-sulfotransferase isozymes by structured 5`-untranslated regions and internal ribosome entry sites, J. Biol. Chem. 277 (2002) 30699–30706.

[18] L. Créancier, D. Morello, P. Mercier, A.C. Prats, Fibroblast growth factor 2 internal ribosome entry site (IRES) activity ex vivo and in transgenic mice reveals a stringent tissue-specific regulation, J. Cell Biol. 150 (2000) 275–281.

[19] M. López-Lastra, A. Rivas, M.I. Barría, Protein synthesis in eukaryotes: The growing biological relevance of cap-independent translation initiation, Biol. Res. 38 (2005) 121–146.

[20] J.I. Aikawa, K. Grobe, M. Tsujimoto, J.D. Esko, Multiple isozymes of heparan sulfate/heparin GlcNAc N-deacetylase/GlcN N-sulfotransferase. Structure and activity of the fourth member, NDST4, J. Biol. Chem. 276 (2001) 5876–5882.

Chapter 8

Curriculum Vitae, List of publications, Dankwoord and Ph.D. portfolio

Curriculum Vitae (English)

Peter Uijtdewilligen was born August 5th, 1980 in Utrecht, The Netherlands, and obtained his high school diploma from the Openbare Scholengemeenschap Schoonoord in Zeist, The Netherlands, in 1999 and subsequently started his study Biotechnology at the Wageningen University. During this period, he completed three internships. The first internship was done at the Laboratory for Virology of the Wageningen University and the research done was part of the publication *"Baculovirus envelope fusion proteins F and GP64 exploit distinct receptors to gain entry into cultured insect cells"* in the *Journal of General Virology* (2007, Volume 88, pages 3302-3306). His second internship was done in Glasgow, Scotland, at the Department of Medical Oncology of the University of Glasgow on *"Telomerase regulated RNA interference"*. His final internship was done at the Hubrecht Laboratory in Utrecht on the *"Postitional cloning and characterization of Danio rerio mutant hu554a."*

After finishing his study in 2005 he started his Ph.D. research project at the Department of Biochemistry part of the Radboud Institute for Molecular Life Sciences (formerly known as Nijmegen Center for Molecular Life Sciences) of the Radboud university medical centre. His Ph.D. research was supervised by prof. dr. R.E. Brock, dr. T.H. van Kuppevelt and dr. ir. W.F. Daamen. The research presented was part of the Dutch Program for Tissue Engineering, which focused on various applications of tissue engineering. This thesis is part of the subproject, which focused on skin tissue engineering. During his Ph.D. research, Peter was involved in education of Medical and Biomedical students, and supervised a number of interns. He presented his results on several (inter)national conferences.

Peter is now working as a chemistry teacher at CSG Het Streek in Ede, The Netherlands. He obtained his teaching license in 2013 at the University of Utrecht. In addition to teaching chemistry he teaches a project-based course called "Technasium" in which students are involved in a technical-oriented assignment from local companies.

Curriculum Vitae (Nederlands)

Peter Uijtdewilligen is geboren op 5 augustus 1980 te Utrecht in Nederland. In 1999 heeft hij zijn middelbare school afgerond bij de Openbare Scholengemeenschap Schoonoord te Zeist. Vervolgens is hij Biotechnologie gaan studeren aan de Wageningen Universiteit. Tijdens zijn studie heeft hij drie stages doorlopen. De eerste stage vond plaats bij het Laboratorium voor Virologie van de Wageningen Universiteit en een deel van de resultaten is opgenomen in de publicatie getiteld *"Baculovirus envelope fusion proteins F and GP64 exploit distinct receptors to gain entry into cultured insect cells"* in het *Journal of General Virology* (2007, Volume 88, pages 3302-3306). De tweede stage vond plaats in Glasgow, Schotland, bij de afdeling Medische Oncologie van de Universiteit van Glasgow en had als onderwerp *"Telomerase regulated RNA interference"*. De laatste stage vond plaats bij het Hubrecht Laboratorium te Utrecht en betrof onderzoek naar *"Postitional cloning and characterization of Danio rerio mutant hu554a."*

Na het afronden van zijn studie in 2005, is hij gestart met zijn Ph.D.-onderzoeksproject bij de afdeling Biochemie deel van het Radboud Institute for Molecular Life Sciences (voorheen Nijmegen Center for Molecular Life Sciences) van het Radboud universiteit medisch centrum. Zijn Ph.D.-onderzoek is gedaan onder de supervisie van prof. dr. R.E. Brock, dr. T.H. van Kuppevelt en dr. ir. W.F. Daamen. Het onderzoek was deel van het Dutch Program for Tissue Engineering, welke zich richtte op de ontwikkeling van verschillende toepassingen van tissue engineering. Het onderzoek, wat gepresenteerd is in dit proefschrift, behoorde tot een deelproject dat zich richtte op tissue engineering van de huid. Tijdens zijn Ph.D.-onderzoek is Peter betrokken geweest bij het geven van onderwijs aan studenten geneeskunde en biomedische wetenschappen en hij heeft daarnaast enkele stagiaires begeleid. Tijdens (inter)nationale conferenties heeft hij de resultaten van zijn Ph.D. onderzoek gepresenteerd.

Peter werkt nu als docent scheikunde aan CSG Het Streek te Ede in Nederland. Hij heeft hiervoor zijn eerstegraads bevoegdheid behaald in 2013 aan de Universiteit van Utrecht. Naast het geven van het vak scheikunde geeft hij ook een vak gebaseerd op projectonderwijs genaamd het technasium, waarbinnen leerlingen betrokken zijn bij technische opdrachten gegeven door lokale bedrijven.

List of publication

***P.J.E. Uijtdewilligen**, E.M.M. Versteeg, C. Gilissen, S.V. van Reijmersdal, R. Schoppmeyer, R.G. Wismans, W.F. Daamen and T.H. van Kuppevelt.* **Towards embryonic-like scaffolds for skin tissue engineering: identification of effector molecules and construction of scaffolds.** *Journal of Tissue Engineering and Regenerative Medicine 2016; **10;** E34-E44*

*Corien Oostendorp[#], **Peter J.E. Uijtdewilligen[#]**, Elly M. Versteeg, Theo G. Hafmans, Ellen H. van den Bogaard, Paul K.J.D. de Jonge, Ali Pirayesh, Johannes W. Von den Hoff, Ernst Reichman, W.F. Daamen and T.H. van Kuppevelt.* **Visualisation of newly synthesised collagen in vitro and *in vivo***. *Scientific reports 2016; **6**; 18780*

(# These authors contributed equally to this work)

*Herman T.B. van Moerkerk**, Peter J.E. Uijtdewilligen**, Pauline Smits, Elly M. Versteeg, W.F. Daamen and T.H. van Kuppevelt.* **Preparation of a growth factor gradient in porous collagen scaffolds and its effect on cell proliferation**. *Journal of Controlled Release 2006;**116(2)**; e87-88*

***Peter J.E. Uijtdewilligen,** E.M. Versteeg, E.M.A. van de Westerlo, J. van der Vlag, W.F. Daamen, T.H. van Kuppevelt.* **Dynamic expression of genes involved in proteoglycan/glycosaminoglycan metabolism during skin development** *Submitted.*

Other publications

*G. Lammers, C. Gilissen, S.T. Nillesen, **P.J. Uijtdewilligen**, R.G. Wismans, J.A. Veltman, W.F. Daamen and T.H. van Kuppevelt.* **High density gene expression microarrays and gene ontology analysis for identifying processes in implanted tissue engineering constructs.** *Biomaterials 2010, 31, 8299-8312*

*M. Westenberg, **P.J. Uijtdewilligen** and J.M. Vlak.* **Baculovirus envelope fusion proteins F and GP64 exploit distinct receptors to gain entry into cultured insect cells.** *Journal of General Virology 2007, 88, 3302-3306*

Dankwoord

In dit dankwoord wil ik de mensen bedanken die direct of indirect betrokken zijn geweest bij het voltooien van mijn promotie onderzoek.

Allereerst wil ik prof. dr. Jan-Joep de Pont en prof. dr. Roland Brock bedanken voor hun rol als promotor, die het voor mij mogelijk maakte mijn promotie onderzoek te doen bij Matrix biochemie. Toen ik in 2005 startte met het Ph.D. traject was prof. dr. Jan-Joep de Pont hoofd van de afdeling en mijn promotor. Helaas is hij overleden in 2009. Per 2007 heeft prof. dr. Roland Brock het stokje overgenomen. Ik wil hen bedanken voor de gegeven kansen en hun betrokkenheid bij mijn onderzoek.

Dr. Toin van Kuppevelt en dr. ir. Willeke Daamen wil ik bedanken voor de begeleiding en het vele geduld dat jullie met mij hebben gehad. Ik wil jullie speciaal bedanken voor de mogelijkheid om mijn promotie alsnog af te kunnen ronden 7,5 jaar na het beëindigen van mijn contract bij jullie afdeling. Ik heb veel van jullie beide geleerd over de wetenschap en ook over mezelf. Toin, dank je wel en ik hoop dat ik nu voldoende 'gepokt en gemazeld' ben om mijn doctors titel te ontvangen. Willeke, dank je wel voor al je inzichten en je motiverende woorden.

Ik wil daarnaast de leden van het DPTE-programma bedanken. Ik wil mijn waardering uitspreken voor de betrokkenheid van dr. Magda Ulrich van het Rode Kruis Brandwonden centrum te Beverwijk, prof. dr. Esther Middelkoop van de Vrije Universiteit Amsterdam en prof. dr. Joost Schalkwijk en dr. Sandra Tjabringa van de afdeling Dermatologie van het Radboud universiteit medisch centrum. Ik heb diverse experimenten in Beverwijk en bij de afdeling Dermatologie kunnen doen die mijn onderzoek hebben ondersteund. Daarnaast hebben jullie inhoudelijk bijgedragen aan het project. Nogmaals dank voor alles.

I like to thank prof. dr. Jin-ping Li from the Uppsala University in Sweden for providing the epimerase knockout mouse and the heparanase overexpression mouse. The samples were important for the research described in chapter 5 of this thesis.

Een belangrijk deel van mijn onderzoek heb ik te danken aan het werk van de analisten en verzorgers werkzaam bij het Centraal Dierenlaboratorium te Nijmegen. Ik wil jullie hartelijk danken voor de samenwerking en de mogelijkheden die jullie hebben gegeven mijn onderzoek uit te voeren.

Mijn onderzoek heb ik gedaan bij het onderdeel Matrix Biochemie binnen de afdeling Biochemie. Ik wil beginnen met het bedanken van enkele analisten die cruciaal waren voor mijn promotieonderzoek. Allereerst wil ik Elly Versteeg bedanken. Jij was op het lab mijn steun en toeverlaat bij experimenten en bij de frustraties die gepaard gaan bij het doen van wetenschappelijk onderzoek. Je meedenken tijdens mijn onderzoek heeft mij erg geholpen. Daarnaast wil ik je bedanken voor al de experimenten die je samen met mij en voor mij hebt uitgevoerd. Zo was er de grote IFA en de TLDA-kaart. Dat brengt mij bij de volgende analist die ik wil bedanken, Els van de Westerlo. Ik wil jou ook bedanken voor experimenten die je samen met mij en voor mij hebt uitgevoerd.

Voor advies omtrent de histologie en immunohistochemie binnen mijn onderzoek klopte ik vaak bij Ronnie Wismans. Dankjewel voor je hulp. Theo Hafmans, ik wil jou bedanken voor de gesprekken, de motiverende woorden en vooral je technische ondersteuning tijdens mijn promotie. Je woorden hebben mij geregeld uit een dip gehaald en mij weer op de rails gezet. Ik weet nog goed dat we elkaar spraken eind 2014. Dat gesprek heeft er toe geleid dat dit boek je er toch is gekomen.

Daarnaast wil ik ook de andere analisten, Arie, Marianne, Cindy en Herman, bedanken voor hun hulp en betrokkenheid. Helaas is Herman overleden, maar ik herinner hem als de man die mij geholpen heeft de basis methoden voor het maken van collageen scaffolds te beheersen.

Ik wil Gerdy, Guido en Kaius bedanken voor hun advies en betrokkenheid als post-doc op de afdeling in de tijd dat ik mijn promotie onderzoek deed. Daarnaast wil ik mijn collega junior onderzoekers (Joost, Nicole, Suzan, Tessa, Paul, Mieke, Martin, Gerwen, Xander, Etienne, Katrien en Myrtille) bedanken voor de samenwerking. De meeste van jullie zijn inmiddels al gepromoveerd. Nu is het eindelijk mijn beurt.

Ik wil de volgende junior onderzoekers speciaal bedanken. Gerwen, dankjewel voor de samenwerking op het gebied van gen expressie en huid tissue engineering. Onze projecten lagen in dezelfde lijn en ik ben dankbaar voor je advies. Corien, wij hebben samen gewerkt aan een artikel "*Visualisation of newly synthesised collagen in vitro and in vivo"* (hoofdstuk 3 van dit proefschrift). Ik was al een aantal jaar weg van de afdeling en jij zat midden in je promotie traject. Met behulp van een cloud opslag dienst hebben we samen kunnen werken aan een prachtig artikel dat in een tijdschrift bij de Nature Publishing Group is gepubliceerd. Ik wens jou ook succes met het afronden van je promotie.

Mijn onderzoek was niet zo ver gekomen zonder de hulp van enkele stagiaires. Astrid, jij was mijn eerste student die ik mocht begeleiden. Je werk aan de gradiënt is zeer belangrijk geweest voor hoofdstuk 4 van dit boekje. Het gradiënt onderzoek is voortgezet door Petra en Ralph. Het was een avontuur om twee studenten tegelijk te begeleiden. Uiteindelijk zijn de concepten die jullie hebben getest niet succesvol geweest, maar dat neemt niet weg dat ik jullie zeer dankbaar ben voor jullie werk. Rouven, jij was mijn laatste student. Jouw werk aan de type I collagen-hyaluron zuur matrices is opgenomen in het artikel "*Towards embryonic-like scaffolds for skin tissue engineering: identification of effector molecules and construction of scaffolds"* (hoofdstuk 2). Ik wens al mijn studenten een succesvolle carrière toe.

Verder wil ik andere ondersteunde krachten bedanken. Lisette Brocatus, ik wil jou bedanken voor al het administratieve werk dat een promotie traject met zich mee brengt. Zeker toen ik op afstand werkte was je hulp zeer belangrijk. Paul Jap, jij bent als expert diverse malen ingevlogen om naar mijn coupes te kijken. Ik wil je hartelijk danken voor het delen van je wijsheid.

Ik heb mijn promotie afgemaakt tijdens mijn werk op CSG Het Streek. Ik heb daar mijn passie voor onderwijs mogen vinden en mag dit uitleven in mijn lessen scheikunde en onderzoeken&ontwerpen (technasium). Een aantal van jullie heeft geluisterd naar mijn verhalen over mijn promotie onderzoek en hoe het allemaal ging. Ik wil Nelly Trapman speciaal bedanken voor het nakijken van de Nederlandse teksten in mijn boekje.

Ik wil hier ook mijn vrienden bedanken. Kasper en Lineke, jullie hebben mij altijd gesteund in de keuzes die ik heb gemaakt en maak, ook al begrepen en begrijpen jullie ze soms niet. Ik ben jullie dankbaar voor jullie ondersteuning. Mark van Geffen, wij hebben samen vele uren geklets over onze frustraties rond het promoveren. Onder het genot van een biertje of een whisky, soms ondersteund met een sigaar, hebben we vele bomen opgezet. Ik ben je dankbaar voor je steun en betrokkenheid.

Ik wil als één na laatste mijn familie bedanken. Pa, ook al begreep je soms weinig van wat ik deed, je interesse in mijn werk heeft mij altijd goed gedaan, dankjewel. Nore, als goede vriendin van mijn overleden moeder, ben je betrokken gebleven bij mijn leven. Ook in mijn promotie traject heb je mij ondersteund met interesse en betrokkenheid. Ik dank je hier hartelijk voor. Na het trouwen in 2009 met mijn lieve vrouw Kirsten, kreeg ik er een familie bij. Sanne, Ilse en Koert, dank jullie wel voor jullie interesse in mijn promotie. Joop en Carlie, jullie wil ik speciaal bedanken. We hebben het in de gesprekken bij jullie thuis, op vakantie en bij ons thuis vaak gehad over mijn promotie. Ik wil jullie bedanken voor jullie steun en betrokkenheid.

En als laatste wil ik mijn lieve vrouw Kirsten bedanken. Mijn wens om mijn promotie af te maken vond je niet altijd makkelijk. Soms hing het als een zwaard van Damocles boven vrije dagen en vakanties. Maar als we spraken over mijn promotie, gaf je mij steun en motivatie om door te gaan. Dank je wel daarvoor. Nu is het klaar en kunnen we samen meer leuke dingen doen. Ik kijk daar erg naar uit. Ik hou ontzettend veel van je.

Peter

Ph.D. portfolio

Institute for Molecular Life Sciences
Radboudumc

Name PhD candidate: P.J.E. Uijtdewilligen	**PhD period:** ***01-09-2005 – 19-02-2018***
Department: Biochemie	***Promotor(s): Prof. R. Brock***
Graduate School: Radboud Institute for Molecular Life Sciences	***Co-promotor(s): Dr. T. van Kuppevelt, Dr. W. Daamen***

	Year(s)	ECTS
TRAINING ACTIVITIES		
a) Courses & Workshops		
- *NCMLS Graduate course (C01 Orientation course)*	2005	*3*
- *NCMLS PhD retreat - 2006-2009 Poster presentation, 2010 Oral presentation*	2006-2010	*4*
- *Laboratory Animal Science – Article 9*	2006	*3*
- *Academic writing*	2007	*3*
- *Didaktiek in de praktijk*	2008	*3*
b) Seminars & lectures		
- *NCMLS forum evenings – 28 attended, 1.5 hour each*	2005-2010	1.5
- *NCMLS workshops – 13 attended, 2 hours each*	2005-2009	1
- *NCMLS seminars – 18 attended, 1 hour each*	2005-2010	1
c) Symposia & congresses		
- *National conference NBTE te Lunteren – Poster presentation, poster price awarded.*	2005	1
- *DPTE symposium – 2006-2008 Poster presentation, 2009 Oral presentation*	2006-2009	4
- *Keystone symposium in Salt Lake City (VS) – Poster presentation*	2007	1
- *NVMB symposium in Munster (DE) – Poster presentation*	2007	1
- *ETRS conference in Malta – Oral presentation*	2008	1
d) Other		
- *Organization of NCMLS workshop*	2007	0.5
TEACHING ACTIVITIES		
e) Lecturing		
- *Lecture on Skin healing by tissue engineered templates for Master students Biology (part of Didaktijk in de praktijk*	2008	0.5
f) Supervision of internships / other		
- *Supervision bachelor student, Astrid Swinkels*	2006	1.5
- *Supervision practical course Tissue engineering P004*	2006-2009	1
- *Supervision practical course Biochemistry for first years students*	2006-2009	1
- *Supervision of master student, Petra Lücker*	2008	1.5
- *Co-supervision of master student, Ralph Jaspers*	2008	0.5
- *Supervision of bachelor student (HAN), Rouven Schoppmeer*	2010	1.5
TOTAL		**34**

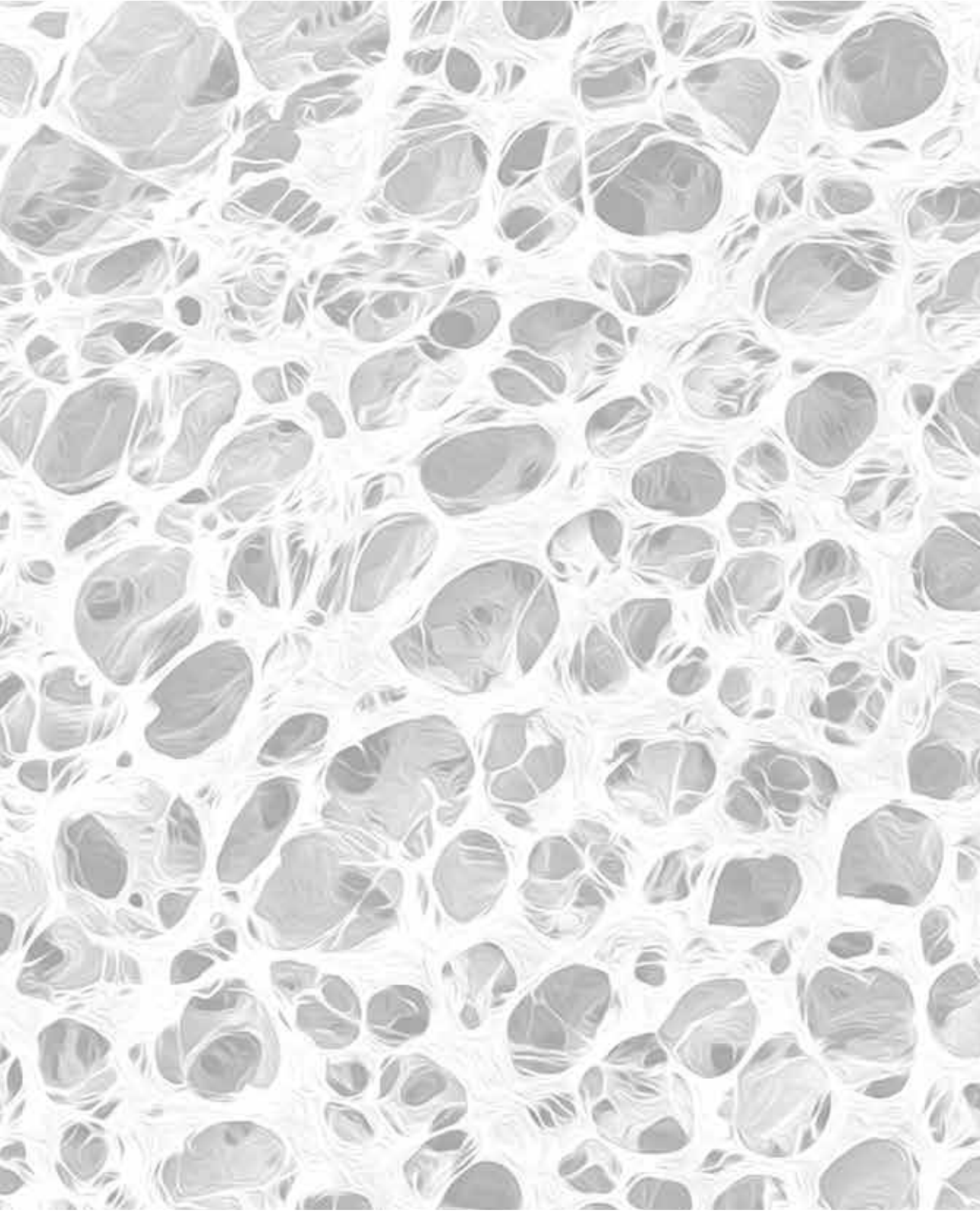

Institute for Molecular Life Sciences
Radboudumc